UNIVERSITY OF CALIFORNIA,
IRVINE

Robust Symbol Level Precoding Designs in Multiuser MIMO Systems

DISSERTATION

submitted in partial satisfaction of the requirements
for the degree of

DOCTOR OF PHILOSOPHY

in Electrical and Computer Engineering

by

Lu Liu

Dissertation Committee:
Professor A. Lee Swindlehurst, Chair
Professor Ender Ayanoglu
Professor Syed Jafar

2024

DEDICATION

To Jialei and my family.

TABLE OF CONTENTS

LIST OF FIGURES

LIST OF TABLES

LIST OF ALGORITHMS

ACKNOWLEDGMENTS

I would like to express the sincerest appreciation to my advisor Prof. A. Lee Swindlehurst for his invaluable guidance and support throughout these years. Prof. Swindlehurst not only provided me the opportunity to pursue a doctorate degree under his mentorship, but also enriched my academic experience in ways I could have never imagined. It was a precious experience working with Prof. Swindlehurst in the past six years. His profound dedication to research and contagious enthusiasm for teaching serves as a role model for me in the work. During the challenges posted by the Covid-19 pandemic, Prof. Swindlehurst's commitment to my development remained resolute through his weekly online meeting with me, where he guided me through every detail in our research. His prompt feedback and thorough comments consistently steered me in the right direction. His patience, kindness and encouragement have been my guiding lights, especially during the most arduous times of this academic adventure. Without his guidance and persistent help, this dissertation would not have been possible.

I would like to thank my other committee members, Prof. Ender Ayanoglu and Prof. Syed Jafar for their time and help during my study in UCI. Thank Prof. Marco Levorato and Tryphone Georgious for being committee members of my qualifying exam. I am honored to have the opportunity to work with Prof. Chirstos Masouros in University of College London. I am grateful for his invaluable contribution in our first published journal paper. Thank Prof. Paniz Ebrahimi for having me as her teaching assistant. I would like to thank my internship mentor Peter Molnar for hiring me and his generosity to share me a great amount of knowledge as well as experience. It was a happy and fruitful summer in North Carolina.

I extend my sincere gratitude to the National Science Foundation (NSF) Grants CCF-2008714 and CCF-222557 for sponsoring my research. Many thanks to IEEE for permission to include Chapter 4 in this dissertation. I am grateful to Prof. A. Lee Swindlehurst and Prof. Chirstos Masouros for coauthoring these publications. Additionally, I would like to thank the High Performance Computing (HPC) team at University of California, Irvine for their excellent management of computing server resources. I am grateful to all staff in EECS department and Gil Cho in the international center for their kind help during my study in UCI.

The journey toward a Ph.D. degree is not solitary. I would like to thank other members and scholars in our research group over these years. Many thanks to Qian Xu, Fangzhou Wang, Prof. Li Sun, Prof. Gonzalo Seco-Granados and Prof. Junil Choi for their invaluable suggestions to my research. Thank Qian Yang for helping me learn how to use HPC. Thank Van Ly Nguyen for coauthoring and discussion. His depth of knowledge and strong work ethic have a profound influence on me. Thank Rang Liu for many help and emotional support. She is always there whenever I faced problems. I only wish we had met each other sooner. I also would like to thank Haoyu Wang, Jiaqi Xu, Kunchao Xu, Cheng Yang and Junwen Wang for introducing their interesting topics in the group meeting. Thank Hessam Pirzadeh for his kind help when I first joined the group and for his invaluable suggestions during my job search.

I would like to thank Shipa Rao, a dear friend and colleague, with thoughtful gestures, kindness and sweetness. She made my first few years in UCI so much happier, especially with our double dates, board games, and shared cooking adventures. Talking with her over the phone is always a great source of relaxation and enjoyment. I would also like to thank Didi, my roommate and wonderful friend, who has been a constant source of companionship throughout these years. Thank her for these countless memorable moments, from our fun shopping weekends to our online gaming sessions during the pandemic. Our discussion over various topics and study time together have truly enriched my life. Many thanks to my other friends in UCI, including Xun, Xiao, Wei, Ruirui, Kefan, QiAn, for our gathering and holiday celebrations. I am grateful for Yijia and two lovely girls Cece and Annie, who always warm my heart. I also want to thank Yunmu, Cui, Juan, Yishu, Linky, Xin and Hui for their friendship, even though some of them are in China, and I've missed many of their significant moments during these year.

I would like to thank my parents for their endless love, support and sacrifices. Thank you, Dad and Mom, for trying your best to provide me with a great education and for letting me stand on your shoulders to see a wider world. Dad, thank you for instilling in me the values of independence, perseverance and the consistent pursuit of high standards. Mom, thank you for taking such great care of me, from preparing early breakfasts to ensuring every aspect of my will-being. You are the best mom I could ever ask for, and your unlimited support and love have been invaluable in my life. Your diligence and kindness to everyone are a model to me. I also want to thank my grandmother, who gave me a happy and carefree childhood. I am the apple of her eye, and her love has been a constant source of confidence for me. Her affection and support have greatly contributed to the person I am today. My brother deserves special thanks for his company throughout our childhood and for every cherished moment we shared. It has been five years since my last reunion with them, and I am grateful for their understanding during this long journey. Furthermore, I want to extend my heartfelt gratitude to my parents-in-law for their love, support, and for embracing me as their daughter. Thank you for respecting every decision I make, which has brought me immense courage and bravery to face difficulties.

Last but certainly not least, I would like to express my deepest gratitude to my husband, the love of my life, Jialei, for his unwavering support and encouragement throughout these years. His presence in my life has been a blessing beyond measure. His knowledge, talent, and passion are qualities I admire and strive to emulate. From Beijing to Seattle, from Irvine to Phoenix, no matter where we were or whether we were in long-distance, his steadfast love has been my greatest motivation and my rock, even during the most challenging times. I am deeply grateful for his patience and belief in me. His love and dedication have been a continuous source of inspiration and strength, completing my second half. I could not have walked this far without him.

VITA

Lu Liu

EDUCATION

Doctor of Philosophy in Electrical and Computer Engineering **2024**
University of California Irvine *Irvine, California*

Master of Information and Communication Engineering **2018**
Beihang University *Beijing, China*

Bachelor of Electronic and Information Engineering **2015**
Beihang University *Beijing, China*

RESEARCH EXPERIENCE

Graduate Research Assistant **2018–2024**
University of California, Irvine *Irvine, California*

Advanced Cellular Group Intern **Summer 2023**
Qorvo *Greensboro, North Carolina*

TEACHING EXPERIENCE

Teaching Assistant: EECS152B DSP Design and Lab **Winter 2024/2023/2021**
University of California, Irvine *Irvine, California*

Teaching Assistant: EECS250P Digital Signal Processing **Spring 2021**
University of California, Irvine *Irvine, California*

Teaching Assistant: EECS01 Intro to Electrical Engineering **Fall 2020**
University of California, Irvine *Irvine, California*

REFEREED JOURNAL PUBLICATIONS

Robust Symbol Level Precoding for Overlay Cognitive Radio Networks **2023**
IEEE Transactions on Wireless Communications

Symbol Level Precoding for Systems with Improper Gaussian Interference **2024**
Journal under preparation

REFEREED CONFERENCE PUBLICATIONS

Overlay Cognitive Radio Using Symbol Level Precoding With Quantized CSI **Jun 2023**
IEEE International Conference on Acoustics, Speech and Signal Processing (ICASSP)

ABSTRACT OF THE DISSERTATION

Robust Symbol Level Precoding Designs in Multiuser MIMO Systems

By

Lu Liu

Doctor of Philosophy in Electrical and Computer Engineering

University of California, Irvine, 2024

Professor A. Lee Swindlehurst, Chair

Multiple-user (MU) multiple-input multiple-output (MIMO) technology, which involves using multiple antennas to simultaneously serve multiple users or devices, is a cornerstone of both 5G and 6G. The use of MIMO in ultra-dense networks with smaller cell sizes and more antennas will result in a proportional increase in both inter- and intra-cell interference. To manage the interference, precoding or beamforming is needed to steer the transmit signals towards intended users and mitigate interference.

Symbol level precoding (SLP) techniques exploit information about the symbols to be transmitted in addition to the channel state information (CSI), which can significantly improve performance at the expense of increased complexity at the transmitter. The additional degrees of freedom (DoF) provided by the symbol-level information make it possible to exploit the constructive component of the interference, converting it into constructive interference (CI) that can move the received signals further from the decision thresholds of the constellation points. CI-based SLP recasts the traditional viewpoint of interference as a source of degradation to one where interference is a potential resource that can be exploited.

In this dissertation, we firstly study the use of SLP in the downlink of a multiuser multiple-input-single-output (MU-MISO) cognitive radio (CR) network, where a primary base station (PBS) serving primary users (PUs) and a cognitive base station (CBS) serving cognitive users

(CUs) share the same frequency band. The SLP approach is designed using the symbol-wise Maximum Safety Margin (MSM) criterion, which exploits the constructive multiuser interference present in such a network. We adapt the non-linear MSM precoder to both underlay and overlay CR scenarios, depending on whether or not the primary system shares its information with the cognitive system. Secondly, we investigate robust SLP designs in an overlay CR network, where the primary and secondary networks transmit signals concurrently, however, the PBS shares imperfect CSI with the CBS. We propose robust SLP schemes in this scenario and consider two different CSI error models. For the norm-bounded CSI error model, we adopt a max-min philosophy to conservatively achieve robust SLP constraints; for the additive quantization noise model (AQNM), we employ a stochastic constraint to formulate the problem. Simulation results show that, rather than simply trying to eliminate the network's cross-interference, the proposed robust SLP schemes enable the primary and secondary networks to aid each other in meeting their quality of service constraints.

Moreover, we propose precoding design in multi-antenna systems with improper Gaussian interference (IGI), characterized by correlated real and imaginary parts. We first study block level precoding (BLP) and SLP assuming the receivers apply a pre-whitening filter to decorrelate and normalize the IGI. We then shift to the scenario where the base station (BS) incorporates the IGI statistics in the SLP design, which allows the receivers to employ a standard detection algorithm without pre-whitenting. Finally we address the case where the non-circularity of the IGI is unknown, and we formulate robust BLP and SLP designs that minimize the worst case performance in such settings. Interestingly, we show that for BLP, the worst-case IGI is in fact proper, while for SLP the worst case occurs when the interference signal is maximally improper, with fully correlated real and imaginary parts. The numerical results reveal the superior performance of SLP in terms of symbol error rate (SER) and energy efficiency (EE), especially for the case where there is uncertainty in the non-circularity of the jammer.

Chapter 1

Introduction

The evolution from 5G to 6G represents a transformative leap in wireless communication technology, promising unprecedented advancements in speed, capacity, and connectivity. Building upon the foundation of 5G's innovations, the development of 6G aims to provide the services including ubiquitous mobile ultra broadband (uMUB), ultra-high-speed-with-low-latency communications (uHSLLC), and ultra-high data density (uHDD) [1,2]. Multiple-user (MU) multiple-input multiple-output (MIMO) technology, which involves using multiple antennas to simultaneously serve multiple users or devices, is a cornerstone of both 5G and 6G.

1.1 Background and Prior Work

In the MU-MIMO scenario, beamforming or precoding at the multi-antenna transmitter can be employed to mitigate the multiuser interference (MUI) and compensate for its adverse affect on the received signals [3, 4]. Existing precoding schemes can be classified as either block-level precoding (BLP) or symbol-level precoding (SLP). In recent decades, a number

of sophisticated algorithms have been proposed to implement block-level precoders that only depend on the current channel state information (CSI), such as maximum ratio transmission (MRT), zero-forcing (ZF), regularized ZF and optimum interference-constrained or power constrained precoding [5–10]. These papers all treat the MUI as a detrimental effect that is suppressed as much as possible.

Unlike BLP, SLP techniques exploit information about the symbols to be transmitted in addition to the CSI, which can significantly improve performance at the expense of increased complexity at the transmitter [11, 12]. The additional degrees of freedom (DoFs) provided by the symbol-level information make it possible to exploit the constructive component of the MUI, converting it into constructive interference (CI) that can move the received signals further from the decision thresholds of the constellation points [13–15]. CI-based SLP recasts the standard viewpoint of interference as a source of degradation to one where interference is a potential resource that can be exploited. The classification of MUI into constructive and destructive components was first introduced in [16], where a CI-based precoder was proposed for DS/CDMA systems. The authors then applied this idea to the downlink of MIMO systems, preserving CI and eliminating destructive interference (DI) by means of channel inversion precoding [13]. This early work showed that SLP enhances the effective signal-to-interference and noise ratio (SINR) at the receivers without investing additional power at the base station. To further improve this design, the SLP technique in [14] strictly aligns DI with the users' desired symbols so that the DI is converted to CI through a symbol-based correlation rotation matrix that depends on the combined data and channel information. Later, in [17], the phase alignment constraints were relaxed in order to extend the feasible region of the optimal precoding and achieve additional power savings. All of the above work was developed for either phase-shift keying (PSK) or quadrature-amplitude modulation (QAM) constellations.

As the number of wireless devices and their applications grow explosively, the availability of unoccupied radio spectrum is becoming increasingly scarce and occupied bands are increasingly congested. Over the past two decades, cognitive radio (CR) technology has been extensively studied as a means to alleviate this problem through more efficient, flexible and comprehensive use of the spectrum [18–22]. Compared with conventional radios, CRs have the ability to sense for available spectrum and rapidly adjust transmission parameters in order to co-exist with incumbent or primary users (PUs). Generally speaking, CR systems can interweave, overlay or underlay their transmissions with those in existing primary systems. In this dissertation, we focus on the last two categories where the primary and cognitive systems transmit concurrently. In standard underlay CR, the cognitive base station (CBS) can transmit simultaneously with the primary base station (PBS) as long as the average interference from the CR transmission to the PUs does not exceed a certain predefined limit, commonly known as the interference temperature constraint [23, 24]. In overlay CR, the PBS shares information with the CR, which allows the CR to not only transmit simultaneously, but to also facilitate the primary transmission. For example, by using a fraction of its power to relay the PUs' signals in exchange for transmitting at any power level, the CR can compensate for its interference to the PUs and also achieve optimal performance for its own network [25, 26]. The fundamental challenge for CR lies in balancing the interference it generates at the PUs with the quality of service (QoS) of the cognitive users (CUs). To address this issue, both the inter-system and inter-user interference need to be successfully managed.

To date there has been limited research on SLP for CR applications. The authors of [27] further formulated the CI-based precoder design in the underlay CR scenario to minimize the worst-case CU symbol error probability, but this work is limited to the Z-channel where the interference from the PBS to SUs is assumed to be negligible. It has been demonstrated that interference-driven precoding outperforms conventional precoding for CR networks when the cross-interference between the primary and cognitive systems is manipulated to be mutually

constructive, such as in [28] for a relay-assisted CR and [29] for an overlay scenario with the CBS transmitting the primary message. However, the phase alignment linear precoder (PALP) in [28] and [29] was derived from the sub-optimal CI correlation rotation (CICR) algorithm in [14] initially designed for conventional broadcast systems, and was applied with the MMSE criterion. A related approach for underlay CR is the CI-based SLP algorithm CCIPM in [30], which minimizes the transmit power at the CBS with interference temperature constraints as well as strict phase constraints for the CI. While this technique can achieve a desired SNR at each CU with much less power than conventional methods, the phase alignment constraint is sub-optimal and does not fully exploit the available DoFs in solving the problem. Even though the authors extended the aligned phase to a relaxed region to design the CCIMPM precoder in [31], they gave the phase constraint of the CI for QAM symbols, while in our work we will formulate the constructive interference region (CIR) in a more general form.

		[27]	[28]	[29]	[30]	[31]
Algorithm		WSUSEP	PARP	PALP	CCIPM	CCIMPM
Cognitive Radio	Underlay	✓	✓		✓	✓
	Overlay			✓		
	W/ relay		✓	✓		
Channel	X Channel		✓	✓	✓	✓
	Z Channel	✓				
Constructive Interference	Strict Phase Alignment		✓	✓	✓	
	General Relaxed Detection Region	✓				✓
Precoder	Linear		✓	✓		
	Nonlinear	✓			✓	✓
Objective	Min Power				✓	✓
	Max QoS	✓				
Power Constraint	Average		✓	✓		
	Instantaneous	✓			✓	✓
Interference Constraint	Average					
	Instantaneous	✓			✓	✓

Table 1.1: Related Work of SLP in CR

The performance of both BLP and SLP are sensitive to channel uncertainties due for example to channel estimation errors, quantization noise or latency-related effects [32–34]. To mitigate the impact of such errors, robust designs are needed that properly model the errors and account for their effect in the optimization of the precoders. Two general approaches for doing so include assuming worst-case bounded error models or exploiting known statistical properties of the CSI error. The former case involves the use of deterministic CSI error bounds that assume the error is confined to a convex uncertainty region (typically an ellipsoid) surrounding the true CSI [35]. In these approaches, robustness is achieved by constraining the users' QoS or other design objectives to be satisfied for all channel realizations in the convex uncertainty region, effectively minimizing the impact of the worst-case channel within the given error bound [33, 36]. This max-min philosophy can lead to a relatively conservative design depending on the tightness of *a priori* error bound. In the second case, a particular distribution (e.g., Gaussian) is assumed for the error, and Bayesian or other probabilistic approaches [35] are employed to optimize the QoS or transmit power under certain stochastic SINR or rate-outage probability constraints [37, 38]. In this case, the probability-constraint formulation is typically not deterministic and various techniques must be used to obtain a tractable problem [39, 40]. In either of the two cases described above, the penalty paid for increasing the robustness to imperfect CSI is increased transmit power.

In overlay or cooperative CR systems, CSI errors beyond those due to channel estimation are anticipated due to the limited cooperation between the PBS and CBS. While robust BLP designs for traditional MIMO or CR scenarios have been widely investigated [36, 41–43], robust SLP algorithms for general CR scenarios have not been considered. Prior work on robust designs for SLP includes [44], which derived a robust SLP algorithm suitable for imperfect CSI with bounded CSI errors, but it is based on a multicast formulation without fully taking advantage of CI. The work described in [45] considered a linear channel distortion model with bounded additive noise and Gaussian-distributed channel uncertainties. They designed robust SLP schemes to minimize transmission power subject to CI constraints as

well as QoS or SINR requirements. While not focused on CR applications, this prior work demonstrates that robust SLP designs can be formulated to improve and achieve a better balance between QoS and power consumption.

In this dissertation, we propose robust CR SLP algorithms for each of two different CSI error models that account for the quantization error in the CSI shared by the PBS with the CBS. In particular, we focus on overlay CR downlink channels [20, 46] where the PBS shares with the CBS its CSI to the PUs and CUs, as well as its data intended for the PUs. The shared CSI is assumed to be quantized, which is known to often make achieving the desired user QoS constraints infeasible without introducing robustness into the problem formulation [47,48]. In addition, the imperfect CSI also means that the PBS precoding is not precisely known at the CBS, and thus the CBS has an imperfect estimate of the transmitted PBS signal, even if the PBS data symbols are perfectly known. This makes finding a robust solution in the cognitive radio case more complicated than in prior SLP-related work, where the transmitted signals are assumed to be perfectly known. If left unaddressed, the combination of these effects will almost certainly cause the noise-free received symbols at both the PUs and CUs to fall outside the desired CIR. To derive a robust SLP formulation for CR systems, we formulate the problem as one of minimizing the transmit power at the CBS while simultaneously satisfying the safety margin (SM) constraints at both the PUs and CUs to guarantee the worst-case user's QoS.

We first derive a power-minimizing SLP approach for overlay CR with SM constraints at both the PUs and CUs assuming perfect CSI, leading to a quadratic optimization problem with linear constraints that can be efficiently solved. We then derive the SM at each user for two different imperfect CSI models, including the effect of the imprecisely known PBS transmit signal. We first consider the case where the quantization error is norm-bounded as in [35], and we derive a robust SLP algorithm based on maximizing the worst case SM. This leads to a conservative design that trades transmit power for increased protection of

the PUs from the CR interference due to the quantized CSI. Then we study a stochastic approach based on the additive quantization noise model (AQNM) [49,50] that is sufficiently accurate to approximate the quantization error at low and medium signal-to-noise ratios (SNR) and has been widely used in the analysis of quantized MIMO systems [51–53]. In this case, the SM of the PUs and CUs are constrained to meet a preset threshold with a certain probability. We then apply the *Safe Approximation I* method in [45] to reformulate the intractable probabilistic constraints as deterministic constraints and finally construct an optimization problem to obtain the robust SLP solution.

The use of SLP for overlay CR has not been considered previously in the literature. The work in [29] is the most related prior effort, but it requires that the CBS directly transmits the PBS data together with its own data, which is not as energy efficient as our proposed approach. In addition, unlike our proposed approaches, [29] does not consider the impact of the PBS interference at the cognitive users, it does not assume imprecise knowledge of the PBS waveform, it uses a less effective SLP technique, and it does not take into account the fact that the PBS CSI exploited at the CBS may be imperfect due to quantization or other effects. Most notably, our proposed SLP algorithms enable the PUs to exploit constructive interference as well as the CUs, and thus we can demonstrate that the presence of the cognitive network can actually *improve* the PU network performance rather than degrade it. This result is unique to the literature on CR, which focuses on not impairing the PU QoS.

We conduct a number of simulations assuming the PBS channel is quantized using the scalar Lloyd Max algorithm that minimizes the average quantization noise power [54, 55]. These simulations demonstrate the flexibility of the proposed robust SLP algorithms in trading transmit power for improved performance when quantized CSI is present. They further demonstrate the ability of the proposed methods to improve the performance of both the primary and cognitive networks. Furthermore, inspired by the results of [56], we study the problem of allocating bits to the CSI of the PBS to the PUs and CUs, and demonstrate that

the bit allocation strategy in our robust SLP algorithm is not as important as that in the non-robust methods. Note that a subset of the results presented in this dissertation were previously reported in [57].

In communication systems, random noise and interference are often modeled as zero-mean Gaussian processes whose real and imaginary parts are uncorrelated and of equal variance [58]. Such signals are referred to as "circular" or "proper," and are generally more convenient to deal with in transceiver design [59]. However, proper Gaussian signals are not always justified in practice, and the transceiver design must be correspondingly adjusted [60]. For example, improper signals arise due to hardware impairments (HWI) that result from phase noise, imperfections in power amplifier manufacturing, non-linearities and I/Q imbalances in RF front ends, etc. [61, 62]. Such factors are more severe in 5G-and-beyond communication systems due to higher carrier frequencies, and thus deserve more attention. Another source of non-circular signals arises from improper complex interference, self-interference, and asymmetric noise [63–65].

There are relatively few studies about improper Gaussian interference (IGI) in MIMO downlink communication systems. In [66], a maximum likelihood sequence estimation receiver is proposed when the data is corrupted by non-circular zero-mean Gaussian noise in single-input multiple-output (SIMO) systems. In [67], the authors investigated the effects of IGI on quadrature spatial modulation where the constellation symbols are expanded to in-phase and quadrature dimensions separately transmitting the real and imaginary parts of an amplitude/phase modulated data symbol. Besides taking IGI as an destructive effect, some studies exploited the non-circularity feature of the improper Gaussian signaling (IGS) to get better achievable rates and energy efficiency in the interference channel, which has been shown to be better than the traditional circular Gaussian signaling [68–70]. In [71], IGS was designed to managing interference in order to maximize the users' minimum rate subject to transmit power constraints. The widely linear precoding has been commonly used to tackle

the non-circularity, considering the IGS is a linear transformation of transmit signals and noise, which requires a joint design of transmitter and precoder [72–75]. However, to the best of our knowledge, there is no research about SLP designs in systems with IGI.

In this dissertation, we focus on precoding design at the transmitter for scenarios involving a jammer transmitting IGI. Assuming the non-circular covariance of the jammer is available at both the base station (BS) and the users, we first study the application of individual pre-whitening filters at each of the users in order to account for the IGI, and develop modified BLP and SLP approaches. We then study a modification to the SLP design that enables the precoding to be implemented solely by the BS without any receiver preprocessing. The non-circular IGI requires the definition of both an "upper" and "lower" SM for PSK signals defined by a bounding box that contains a confidence ellipse for the non-circular noisy observations [76, 77]. The confidence ellipse is centered at the noise-free received signal, and is defined as the region in which the noisy received signal will lie with a certain probability. Finally, we consider scenarios where the degree of non-circularity of the jammer is unknown, and the BS must design a precoder that is robust to this uncertainty. In particular, we take the conservative approach of designing the BLP and SLP approaches to maximize performance for the worst case IGI, and demonstrate that BLP and SLP lead to fundamentally different robust solutions.

1.2 Summary of Contributions

For the first part, the SLP designs are proposed in CR. Below we summarize the main contributions of this part:

1) We design an optimum interference-constrained CI-based precoder for underlay CR scenarios, which solves the dual problem of that addressed by CCIMPM in [31], but

we formulate the phase constraint in a more general and concise form. We refer to this approach as Underlay Constructive Interference SINR Balancing (UCISB).

2) We develop a precoder based on maximum SM (MSM) for the underlay CR system, referred to as Underlay Cognitive Maximum Safety Margin (UCMSM), and show that it outperforms traditional precoding algorithms based on ZF.

3) We generalize the MSE-based ZF and PALP precoders in [29] to overlay CR scenarios with separate scaling factors for the primay and cognitive systems. This improves the methods in [29] since it guarantees that the PUs' QoS is not degraded. The generalized algorithms are called Overlay Cognitive Radio Zero Forcing (OCZF) and Overlay Phase Alignment Linear Precoding (OPALP).

4) We adapt the MSM-based precoder to overlay CR scenarios and show that it is able to exploit additional CI from the cross-system transmission. The free power gleaned from CI generally improves the QoS of both the PUs and CUs without investing additional power at either the PBS or CBS. Moreover, in our approach it is not necessary for the CBS to relay the PUs' signals to compensate for the loss of QoS due to the cognitive transmission as in [28, 29]. This new algorithm is referred to as Overlay Cognitive Maximum Safety Margin (OCMSM).

5) We further amplify the conclusion in [31] and [78] that SLP has the capability to perform effectively in situations where the number of concurrently active PUs and CUs is more than the number of CBS antennas, which is not possible for conventional BLP.

6) We explore the robustness of our proposed MSM-based precoder to imperfect CSI and compare it with the state-of-the-art techniques in overlay CR scenarios. We show empirically that the loss due to CSI errors at the PUs is largely offset by the gain in CI from the cognitive system.

In the second part, we propose robust SLP designs in overlay cognitive radio systems for two different CSI error models that account for the quantization error in the CSI shared by the PBS with the CBS. Below we summarize the main contributions of this part:

1) We apply the SLP idea to the overlay CR problem where the PBS shares (possibly imperfect) information with the CBS to facilitate the co-existence of the two networks. This problem has not been addressed previously in the literature. The work in [29] is the most related prior effort, but it requires that the CBS directly transmit the PBS data together with its own data, which is not as energy efficient as our proposed approach. In addition, [29] does not consider the impact of the PBS interference at the cognitive users, it uses a less effective SLP approach, and it does not take into account the fact that the PBS CSI exploited at the CBS may be imperfect due to quantization or other effects. Our proposed SLP approach enables the PUs to exploit constructive interference as well as the CUs, and thus we can demonstrate that the presence of the cognitive network can actually *improve* the PU network performance rather than degrade it. This result is unique to the literature on CR.

2) We first derive a power-minimizing SLP approach for overlay CR with SM constraints at both the PUs and CUs assuming perfect CSI, leading to a quadratic optimization problem with linear constraints that can be efficienty solved.

3) Assuming a norm-bounded quantization error in the shared CSI from the PBS to the CBS, we derive a robust SLP algorithm based on maximizing the worst case SM. This leads to a conservative design that trades transmit power for increased protection of the PUs from PBS interference due to the quantized CSI.

4) As an alternative approach, we employ AQNM to approximate the quantized CSI from the PBS. In this case, the SM of the PUs and CUs are constrained to meet a preset threshold with a certain probability. We then apply the *Safe Approximation I*

method in [45] to reformulate the intractable probabilistic constraints as deterministic constraints and finally construct an optimization problem to obtain the robust SLP solution [57].

5) To validate the effectiveness of our proposed robust precoders, we conduct simulations assuming the PBS channel is quantized using the scalar Lloyd Max algorithm which minimizes the average quantization noise power [54, 55]. Our simulations demonstrate the flexibility of the proposed robust SLP algorithms in trading transmit power for improved performance when quantized CSI is present. Furthermore, inspired by the results of [56], we study the problem of allocating bits to the CSI of the PBS to the PUs and CUs, and demonstrate that the bit allocation strategy in our robust SLP algorithm is not as important as that in the non-robust methods.

In the third part, we mainly focus on the SLP designs for systems with IGI, especially the robust designs when the non-circularity is unknown at the BS. Our main contribution in this topic is summarized as follows:

1) We have shown how to modify the BLP approach based on the minimum mean square error (MMSE) for IGI using pre-whitening at each user, assuming that the non-circular covariance of interference is known. We have further shown that when the non-circularity of the jamming is unknown, the MMSE BLP should assume a circular covariance in order to minimize the worst case mean-squared error (MSE).

2) We have shown how to modify SLP-based designs for IGI using both pre-whitening at each user, and also using transmit-only processing where the receivers do not perform a pre-whitening step.

3) We have further investigated the case when the non-circularity of the jamming is unknown, and shown that, unlike MMSE BLP, the worst case for SLP always occurs with

maximally improper interference, where the real and imaginary parts of the jammer signal are fully correlated. We then show how to modify the SM-based SLP algorithm to find the worst-case design.

4) Finally, we provide comprehensive numerical results to compare MMSE BLP with SLP in various settings, particularly in the case where the non-circularity of the IGI is unknown. We also illustrate our theoretical conclusions regarding the worst-case jammer covariances via some graphical examples.

1.3 Outline of Dissertation

The rest of this dissertation is organized as follows.

In Chapter. 2, the symbol level precoding, constructive interference region and safety margin are introduced, which are fundamental of this dissertation.

In Chapter. 3, the SLP is applied in cognitive radio systems. We take a more fundamental approach and formulate optimal MSM precoder designs that maximize the QoS of the CUs without significantly impairing the *instantaneous* performance of the PUs. Both underlay and overlay scenarios are considered.

In Chapter. 4, the robust SLP designs are proposed in overly CR systems, where the primary and secondary networks transmit signals concurrently. When the primary base station (PBS) shares imperfect CSI to the CBS, we propose robust SLP schemes for a norm-bounded CSI error model as well as the additive quantization noise model (AQNM).

In Chapter. 5, the SLP designs are proposed in MUI systems with IGI characterized by correlated real and imaginary parts. Additionally, in scenarios where covariance of the non-

circular interference is not accessible at the base station (BS), we introduced a robust SLP design and simplified the search strategy for the optimum solution.

In Chapter. 6, we introduce an user selection strategy for SLP designs. Moreover, a possible closed-form SLP is proposed.

In Chapter. 7, we concludes the dissertation and provide some insights for the future work.

1.4 Notations

Bold lower case and upper case letters indicate vectors and matrices, and non-bold letters express scalars. The $N \times N$ identity (zero) matrix is denoted by $\mathbf{I}_N$ ($\mathbf{0}_{N\times N}$). The N dimensional vector of ones (zeroes) is denoted by $\mathbf{1}_N$ ($\mathbf{0}_N$). $\mathbf{A}_{mn}$ denotes the (m,n)-th element in the matrix $\mathbf{A}$ and a_m denotes the m-th element in the vector $\mathbf{a}$. The operators $(\cdot)^*$, $(\cdot)^{-1}$, $(\cdot)^{\mathrm{T}}$ and $(\cdot)^{\mathrm{H}}$ stand for the conjugation, the inverse, the transpose and the Hermitian transpose operations, respectively. $\mathbb{C}^{m\times n}$ represents the space of complex matrices of dimension $m \times n$. $\mathbb{E}(\cdot)$ and $\|\cdot\|$ respectively represent the expectation operator and the Euclidean norm. $|(a)|$ denotes the absolute value of a scalar a, whereas $|(\mathcal{A})|$ denotes the size of a set $\mathcal{A}$. $\mathcal{CN}(\mu, \sigma^2)$ denotes the complex normal distribution with mean μ and variance σ^2. The functions $\mathrm{Tr}\{\cdot\}$ and $\mathrm{diag}\{\cdot\}$ respectively indicate the trace of a matrix and a vector composed of the diagonal elements of a square matrix, while $\mathrm{diag}\{\mathbf{a}\}$ denotes a square diagonal matrix with the elements of vector $\mathbf{a}$ on the main diagonal. $\mathrm{blockdiag}\{\mathbf{H}_1, \cdots, \mathbf{H}_K\}$ represents the block diagonal matrix with diagonal blocks $\mathbf{H}_k, k \in \{1, \cdots, K\}$. $\mathcal{R}\{\cdot\}$ and $\mathcal{I}\{\cdot\}$ denote the real and imaginary parts of a complex number, respectively. For matrices and vectors, $\geq$ and $\leq$ denote element-wise inequalities, and $\mathbf{A} \succeq 0$ denotes that the matrix $\mathbf{A}$ is semi-definite positive. $\circ$ is the Hadamard product which is the element-wise product. $a \triangleq b$ represents a is defined as b.

Chapter 2

Symbol Level Precoding

SLP techniques exploit information about both CSI and transmitted symbols [11, 12, 79], and generally result in a nonlinear design. Although SLP requires significantly increased complexity, it enables the precoder to take advantage of the MUI and convert it to CI [13–15], thus increasing the DoFs available for the precoder design.

A number of SLP approaches have been proposed in recent years. The authors of [13] applied SLP using channel inversion precoding, and showed that it enhances the effective SINR at the receivers without investing additional power at the base station. To further improve this design, the technique in [14] strictly aligns the MUI with the users' desired symbols so that it is converted to CI through a symbol-based correlation rotation matrix that depends on the combined data and channel information. Later, in [17], the phase alignment constraints were relaxed in order to extend the feasible region of the optimal precoding and achieve additional power savings. All of the above work was developed for either phase-shift keying (PSK) or quadrature-amplitude modulation (QAM) constellations. To tackle the complexity of SLP, an optimal "closed-form" SLP solution has been introduced in [80] to make the design

more practical for PSK modulation. Recently, [81] proposed an end-to-end learning based approach to optimize the modulation orders for SLP communication systems.

A key strength of SLP is that the received signals can be moved further from the symbol decision boundaries using CI, which provides robustness against noise and interference. In the literature, CIRs have been defined to describe the degree to which the received symbols will be robust to noise and unmodeled perturbations. Recent SLP approaches have been designed to maximize the distance of the received signals to the decision boundaries, also referred to as the *safety margin* (SM) [79, 82, 83], for a given maximum transmit power. The methods described in [84, 85] introduce Maximum Safety Margin (MSM) precoder designs that are able to minimize an upper bound on the symbol error rate (SER). The MSM approach can be contrasted with algorithms based on MMSE between the desired and received symbols [15, 44]. MSM precoders generally guarantee a better QoS for the same level of transmit power, or equivalently the same QoS with less power consumption. CI-based SLP recasts the traditional viewpoint of interference as a source of degradation to one where interference is a potential resource that can be exploited.

2.1 Constructive Interference Region

Constructive inteference regions (CIRs), which define the degree to which the received symbols will be robust to noise and unmodeled perturbations, are fundamental to SLP designs. While early CI-based SLP approaches were intended to increase the distance of the CIRs from the symbol decision boundaries, they did not directly optimize the CIR. More recent techniques have focused on designing the precoder to directly optimize this distance [17, 44, 79, 80, 83, 84, 86–89], which has been referred to as the *safety margin*. Optimal Maximum Safety Margin (MSM) precoders generally result in a non-linear mapping between the symbols and the transmitted waveform, and can be shown to minimize an upper bound

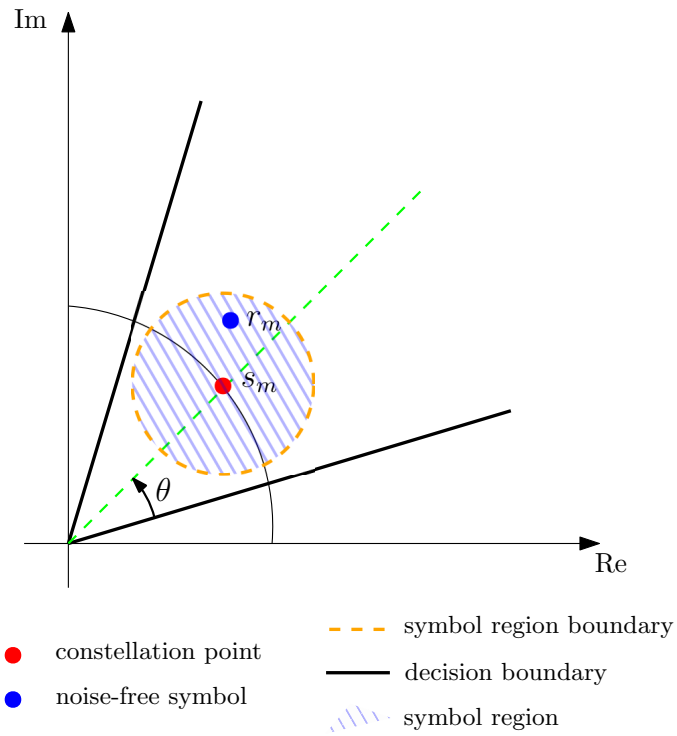

Figure 2.1: Symbol region for conventional precoding

on the SER [84]. This is contrasted with algorithms that minimize the mean squared-error between the transmitted and received symbols, which do not offer the same guarantee [15,44]. MSM precoders are in general able to achieve a better QoS for the same level of transmit power, or equivalently the same QoS with less power consumption.

2.2 Safety Margin for PSK Signaling

Conventional precoding methods such as MMSE, ZF and maximum-SINR beamforming are designed with the objective of minimizing the inter-user interference so that the received symbols lie as close as possible to the nominal constellation points (or scaled versions thereof in the case of PSK). In particular, to limit the effect of interference from other data streams, the transmit vector after precoding is chosen such that every user's received noise-free symbol is contained within a circle centered at its corresponding constellation point [44]. This is

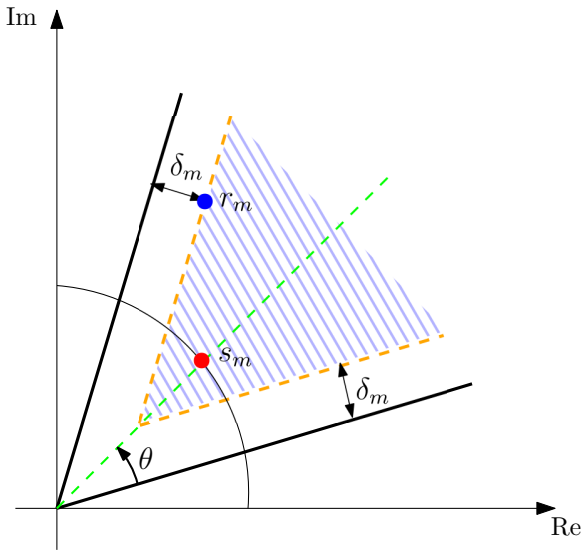

Figure 2.2: Symbol region for CI-Based SLP

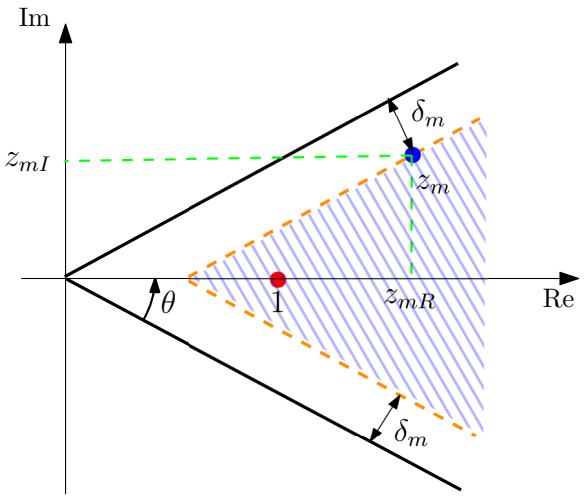

Figure 2.3: Symbol region and safety margin in a modified coordinate ststem

illustrated in Fig. 2.1, where the noise-free signal for user m given by $r_m \triangleq \mathbf{h}_m\mathbf{x}$ lies within a certain distance of the desired symbol s_m, where $\mathbf{h}_m$ is the channel of user m, $\mathbf{x}$ is the transmitted symbol after precoding, and s_m is drawn from a D-PSK constellation with unit magnitude, i.e., $s_m \in \{s|s = \exp(j\pi(2d+1))/D,\ d \in \{0, \cdots, D-1\}\}$. The idea of CI precoding can in principle be applied to any constellation design [79], e.g., QAM or otherwise, but is most easily formulated for the case of PSK signals. The shaded area inside the circle is referred to as the symbol region (SR), a downscaled version of the decision region for s_m.

For PSK constellations, it is not necessary that r_m be close to s_m in order to be decoded correctly, as long as it lies in the correct decision region with a given target SER. Thus, it is not necessary that all of the inter-user interference be eliminated, since some interference components could add constructively and push the received symbol further into the decision region, making it more robust to noise and interference external to the system. We can thus redefine the SR as, for example, in Fig. 2.2, where the SR becomes the sector of a circle sector with infinite radius and an angular extent of 2θ, where $\theta = \pi/D$. For CI-based SLP, we refer to this region as the constructive interference region. For user m, the distance from the CIR boundary to the decision boundary is defined as the safety margin and denoted as δ_m [82].

In order to mathematically interpret the CIR and SM in a unified way, we rotate the original coordinate system by the phase of the desired constellation symbol, i.e., $\measuredangle s_m$, to obtain the modified coordinate system in Fig. 2.3. After rotation, s_m is placed at 1 on the real axis, and r_m is relocated to

$$z_m = r_m s_m^* \ . \tag{2.1}$$

Then we can easily calculate the SM of the noise-free symbol at user m as

$$\delta_m = \mathcal{R}\{z_m\} \sin\theta - |\mathcal{I}\{z_m\}| \cos\theta. \tag{2.2}$$

The SM should be maximized to reduce the probability that noise or other impairments will push the noise-free signal outside the desired detection region; the larger the SM, the smaller the SER. A typical CI-based SLP optimization problem involves maximizing the worst case safety margin over all the users, under the given transmit signal constraints:

$$\delta = \arg \max_{\mathbf{x} \in \mathcal{X}} \min_{m \in \mathcal{M}} \delta_m \tag{2.3}$$

where $\mathcal{M} = \{1, \cdots, M\}$ indexes the users and $\mathcal{X}$ denotes the set of allowable transmit signal vectors. For example, the instantaneous power constraint mentioned above results in $\mathcal{X} = \{\mathbf{x} | \|\mathbf{x}\|^2 \leq P\}$ for some value P.

Chapter 3

SLP in CR Systems

3.1 Introduction

As the number of wireless devices and their applications grow exponentially, the availability of unoccupied radio spectrum is becoming increasingly scarce and occupied bands are increasingly congested. Over the past two decades, CR technology has been extensively studied as a means to alleviate this problem through more efficient, flexible and comprehensive use of the spectrum [18, 20, 90].

This chapter focuses on the use of SLP in the downlink of a MIMO CR network, where a PBS serving PUs and a CBS serving CUs share the same frequency band. The proposed precoding scheme is based on the symbol-wise MSM criterion that exploits the constructive multiuser interference present in such a network. We adapt the non-linear MSM precoder to both underlay and overlay CR scenarios, depending on whether or not the primary system shares its information with the cognitive system. We also take into account the fact that the CSI shared by the PBS may be imprecise. Simulation results show that the proposed MSM precoding method offers significant improvements in the CUs' QoS compared to conventional

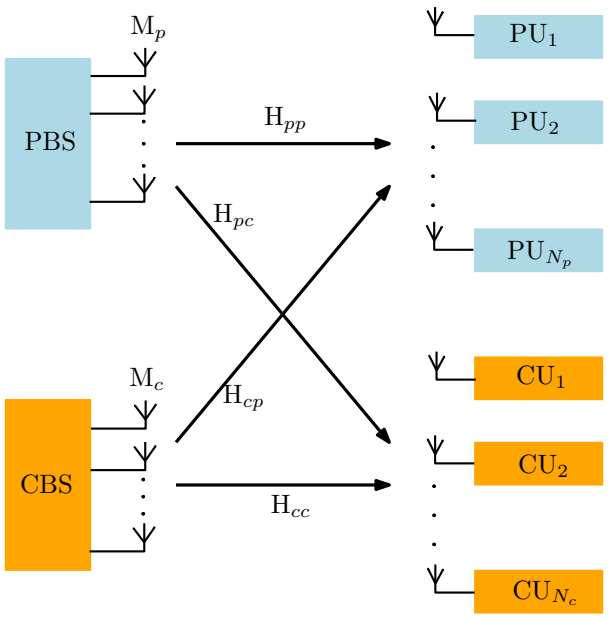

Figure 3.1: Cognitive Radio System Model

methods, and simultaneously provides constructive interference that improves the QoS of the PUs. We show that the constructive interference gain at the PUs can offset much of the loss due to imprecise channel state information.

3.2 System Model

We consider a downlink CR network with an M_c-antenna CBS serving N_c single-antenna CUs. The CR network is granted access to share the primary system spectrum in which an M_p-antenna PBS is communicating with N_p single-antenna PUs. The system model is depicted in Fig. 3.1. The direct primary and cognitive channels are respectively denoted by

$$\mathbf{H}_{pp} = \left[\mathbf{h}_{pp,1}^{\mathrm{T}} \quad \cdots \quad \mathbf{h}_{pp,N_p}^{\mathrm{T}}\right]^{\mathrm{T}} \in \mathbb{C}^{N_p \times M_p} \tag{3.1}$$

$$\mathbf{H}_{cc} = \left[\mathbf{h}_{cc,1}^{\mathrm{T}} \quad \cdots \quad \mathbf{h}_{cc,N_p}^{\mathrm{T}}\right]^{\mathrm{T}} \in \mathbb{C}^{N_c \times M_c} \tag{3.2}$$

The corresponding interference channels are defined as

$$\mathbf{H}_{pc} = \begin{bmatrix} \mathbf{h}_{pc,1}^{\mathrm{T}} & \cdots & \mathbf{h}_{pc,N_p}^{\mathrm{T}} \end{bmatrix}^{\mathrm{T}} \in \mathbb{C}^{N_c \times M_p} \tag{3.3}$$

$$\mathbf{H}_{cp} = \begin{bmatrix} \mathbf{h}_{cp,1}^{\mathrm{T}} & \cdots & \mathbf{h}_{cp,N_p}^{\mathrm{T}} \end{bmatrix}^{\mathrm{T}} \in \mathbb{C}^{N_p \times M_c} \tag{3.4}$$

from the PBS to CUs and the CBS to PUs, respectively. We assume that all channels experience frequency flat fading, but we do not assume any particular channel distribution. The vectors $\mathbf{s}_p(t) = [s_{p,1}(t), s_{p,2}(t), \cdots, s_{p,N_p}(t)]^T$ and $\mathbf{s}_c(t) = [s_{c,1}(t), s_{c,2}(t), \cdots, s_{c,N_c}(t)]^T$ contain the modulated signals to be transmitted to the individual PUs and CUs.

In this work we assume for simplicity that all transmitted symbols are uncorrelated and drawn from a D-PSK constellation with unit magnitude, i.e., $s_{l,m}(t) \in \{s | s = \exp(j\pi(2d + 1))/D,\ d \in \{0, \cdots, D-1\}\}$ where $l \in \{p, c\}$ denotes the primary or cognitive system, and m denotes the user index in the corresponding system. The sets $\mathcal{K} = \{1, \cdots, N_p\}$ and $\mathcal{J} = \{1, \cdots, N_c\}$ enumerate the PUs and CUs, respectively. The idea of CI precoding can in principle be applied to any constellation design [79], e.g., QAM or otherwise, but is most easily formulated for the case of PSK signals.

At time slot t, the received signals at the PUs and CUs can be respectively written as

$$\mathbf{y}_p(t) = \mathbf{H}_{pp}\mathbf{x}_p(t) + \mathbf{H}_{cp}\mathbf{x}_c(t) + \mathbf{n}_p(t) \tag{3.5}$$

$$\mathbf{y}_c(t) = \mathbf{H}_{cc}\mathbf{x}_c(t) + \mathbf{H}_{pc}\mathbf{x}_p(t) + \mathbf{n}_c(t) \tag{3.6}$$

where $\mathbf{x}_p(t) \in \mathbb{C}^{M_p \times 1}$ and $\mathbf{x}_c(t) \in \mathbb{C}^{M_c \times 1}$ are the transmitted signals at the PBS and CBS after precoding and power loading, and $\mathbf{n}_p(t) \sim \mathcal{CN}(0, \sigma_p^2)$ and $\mathbf{n}_c(t) \sim \mathcal{CN}(0, \sigma_c^2)$ are additive white Gaussian noise (AWGN) vectors. In order to simplify the notation, in what follows we drop the time index t.

Conventional methods for CR networks assume an average power constraint at the CBS expressed as $\mathbb{E}\{\|\mathbf{x}_c\|^2\} \leq P_c$. When block-level linear precoding is employed, the transmitted symbol can be expressed as $\mathbf{x}_c = \mathbf{W}_c\mathbf{s}_c$, where $\mathbf{W}_c = \begin{bmatrix} \mathbf{w}_{c,1} & \cdots & \mathbf{w}_{c,N_c} \end{bmatrix}$ is the linear precoding matrix, and the power constraint can be rewritten as $\mathbb{E}\{\|\mathbf{x}_c\|^2\} = \mathbb{E}\{\mathrm{Tr}\{\mathbf{W}_c\mathbf{s}_c\mathbf{s}_c^{\mathrm{H}}\mathbf{W}_c^{\mathrm{H}}\}\} = \mathrm{Tr}\left\{\mathbf{W}_c\mathbb{E}\left\{\mathbf{s}_c\mathbf{s}_c^{\mathrm{H}}\right\}\mathbf{W}_c^{\mathrm{H}}\right\} = \mathrm{Tr}\left\{\mathbf{W}_c\mathbf{W}_c^{\mathrm{H}}\right\} \leq P_c$, where $\mathbb{E}\left\{\mathbf{s}_c\mathbf{s}_c^{\mathrm{H}}\right\} = \mathbf{I}$ due to the assumption of unit-power uncorrelated symbols. On the other hand, non-linear symbol-level precoding can naturally enforce instantaneous constraints on the transmitted signal, most commonly in terms of instantaneous power $\|\mathbf{x}_c\|^2 \leq P_c$ [17], although instantaneous amplitude or quantization-related constraints can be formulated as well [12, 80, 82, 84].

3.3 Underlay Cognitive Networks

In an underlay CR network, the CBS exploits knowledge of the channel $\mathbf{H}_{cp}$ to limit interference at the PUs while achieving some precoding objective for the CUs. In this section, we present three methods: a standard block-precoding approach based on zero-forcing, the SLP method of [31] that also uses zero-forcing for the PUs but employs constellation rotation-based precoding for the CUs to exploit CI, and our proposed approach which maximizes the SM subject to PU interference constraints. We will assume that the PBS employs ZF precoding to cancel the co-channel interference in the primary network, i.e.,

$$\mathbf{W}_p = \mathbf{H}_{pp}^{\mathrm{H}}(\mathbf{H}_{pp}\mathbf{H}_{pp}^{\mathrm{H}})^{-1}\ , \tag{3.7}$$

although this assumption is not critical for our proposed methods.

3.3.1 Underlay CR Zero Forcing (UCZF)

If the CBS has a sufficient number of antennas, then it can perform zero-forcing to eliminate all MUI for both the PUs and CUs. This Underlay CR Zero Forcing (UCZF) method will be a baseline approach for comparison with the CI-based precoders, and can be implemented by forcing the CBS precoder to lie in the nullspace of the cross-channel $\mathbf{H}_{cp}$ [91, 92]. Assuming that $L_{cp} = \text{rank}(\mathbf{H}_{cp}) < M_c$, we define the singular value decomposition (SVD) of the cross channel as

$$\mathbf{H}_{cp} = \mathbf{U}_{cp}\mathbf{\Sigma}_{cp}\begin{bmatrix}\mathbf{V}_{cp}^{(1)} & \mathbf{V}_{cp}^{(0)}\end{bmatrix}^{\text{H}} \tag{3.8}$$

where $\mathbf{V}_{cp}^{(1)}$ holds the first L_{cp} and $\mathbf{V}_{cp}^{(0)}$ the last $(M_c - L_{cp})$ right singular vectors. The effective channel from the CBS to the CUs can then be expressed as

$$\widehat{\mathbf{H}}_{cc} \triangleq \mathbf{H}_{cc}\mathbf{V}_{cp}^{(0)}. \tag{3.9}$$

As long as the effective channel is full rank and $L_{cp} + N_c < M_c$, the CBS can employ ZF precoding to cancel the interference among the CUs:

$$\mathbf{W}_c = \mathbf{V}_{cp}^{(0)} \cdot \widehat{\mathbf{H}}_{cc}^{\text{H}} \cdot (\widehat{\mathbf{H}}_{cc}\widehat{\mathbf{H}}_{cc}^{\text{H}})^{-1}. \tag{3.10}$$

The transmitted signal is thus

$$\mathbf{x}_c = f_c\mathbf{W}_c\mathbf{s}_c = f_c\mathbf{V}_{cp}^{(0)} \cdot \widehat{\mathbf{H}}_{cc}^{\text{H}} \cdot (\widehat{\mathbf{H}}_{cc}\widehat{\mathbf{H}}_{cc}^{\text{H}})^{-1}\mathbf{s}_c \tag{3.11}$$

where f_c is chosen to meet the instantaneous power constraint:

$$f_c = \sqrt{\frac{P_c}{\text{Tr}\{\mathbf{W}_c\mathbf{s}_c\mathbf{s}_c^{\text{H}}\mathbf{W}_c^{\text{H}}\}}}. \tag{3.12}$$

3.3.2 Underlay Constructive Interference SINR Balancing (UCISB)

In [30] and [31], the authors proposed an SLP scheme using CI among the CUs in order to minimize the CBS transmission power. In contrast, our objective is to optimize the QoS of the CUs with fixed transmission power and also not impair the QoS of the PUs. A block-level SINR balancing (SB) approach to solving this problem is to maximize the minimum achievable SINR over all the CUs under an average power constraint without violating the interference temperature constraints imposed by the primary system, as follows [93]:

$$\max_{\mathbf{w}_{c,j}} \quad \beta \tag{3.13}$$

$$\text{subject to} \quad \text{SINR}_{c,j} \geq \beta \quad \forall j \in \mathcal{J} \tag{3.14}$$

$$\sum_{j=1}^{N_c} |\mathbf{h}_{cp,k}\mathbf{w}_{c,j}|^2 \leq \eta_k \quad \forall k \in \mathcal{K} \tag{3.15}$$

$$\mathbb{E}\left\{\sum_{j=1}^{N_c} \|\mathbf{w}_{c,j}\|^2\right\} \leq P_c \tag{3.16}$$

where η_k is the interference constraint at PU k and $\text{SINR}_{c,j}$ is the SINR of the j-th CU, expressed as

$$\text{SINR}_{c,j} = \frac{\|\mathbf{h}_{cc,j}\mathbf{w}_{c,j}\|^2}{\sum_{m=1,m\neq j}^{N_c} \|\mathbf{h}_{cc,m}\mathbf{w}_{c,m}\|^2 + \|\mathbf{h}_{pc,k}\mathbf{x}_p\|^2 + \sigma_c^2} \tag{3.17}$$

assuming $\mathbb{E}\{\mathbf{s}_c\mathbf{s}_c^{\text{H}}\} = \mathbf{I}$. This SB problem is non-convex and generally difficult to solve.

To apply CI-based SLP to the SB problem, we use a non-linear precoder that directly optimizes the precoded signal vector $\mathbf{x}_c$ to guarantee that the received noiseless signal, $r_{c,j} = \mathbf{h}_{cc,j}\mathbf{x}_c$, lies in the CIR. Using the method in [31] to construct the CIR, the problem can be

formulated as

$$\max_{\mathbf{x}_c} \quad \gamma \tag{P1}$$

$$\text{subject to} \quad \measuredangle s_{c,j} - \theta \leq \measuredangle r_{c,j} \leq \measuredangle s_{c,j} + \theta \quad \forall j \in \mathcal{J} \tag{C1-1}$$

$$\|\mathbf{h}_{cc,j}\mathbf{x}_c\|^2 \geq \gamma \quad \forall j \in \mathcal{J} \tag{C1-2}$$

$$\|\mathbf{h}_{cp,k}\mathbf{x}_c\|^2 \leq \eta_k \quad \forall k \in \mathcal{K} \tag{C1-3}$$

$$\|\mathbf{x}_c\|^2 \leq P_c \tag{C1-4}$$

where P_c is the instantaneous power budget. The second constraint C1-2 is used to ensure that the desired CU SINR is high enough given the background noise and the interference from the PBS. For PSK constellations, the region defined by constraints C1-1 and C1-2 consists of points with magnitude greater than γ in the 2θ-angular sector centered at the origin with infinite radius, as shown by the non-convex pink shaded region in Fig. 3.2. To achieve a convex region, we propose an alternative constraint which yields the 2θ-angular sector centered at $\gamma s_{c,j}$ with infinite radius shown with blue shading in Fig. 3.2 and denoted as $\mathcal{D}_j$. The boundaries of $\mathcal{D}_j$ are parallel to the decision boundaries of the constellation point $s_{c,j}$.

To express $\mathcal{D}_j$ in a concise mathematical form, we adopt the method in [89]. We define the two neighboring constellation points of $s_{c,j}$ as $x_{l,j} = s_{c,j}\exp\{j2\theta\}$ and $x_{r,j} = s_{c,j}\exp\{-j2\theta\}$, and we denote each constellation point by an equivalent real-valued vector:

$$\mathbf{s}_{c,j} = \begin{bmatrix} \mathcal{R}\{s_{c,j}\} & \mathcal{I}\{s_{c,j}\} \end{bmatrix}^T, \tag{3.18}$$

$$\mathbf{x}_{l,j} = \begin{bmatrix} \mathcal{R}\{x_{l,j}\} & \mathcal{I}\{x_{l,j}\} \end{bmatrix}^T, \tag{3.19}$$

$$\mathbf{x}_{r,j} = \begin{bmatrix} \mathcal{R}\{x_{r,j}\} & \mathcal{I}\{x_{r,j}\} \end{bmatrix}^T. \tag{3.20}$$

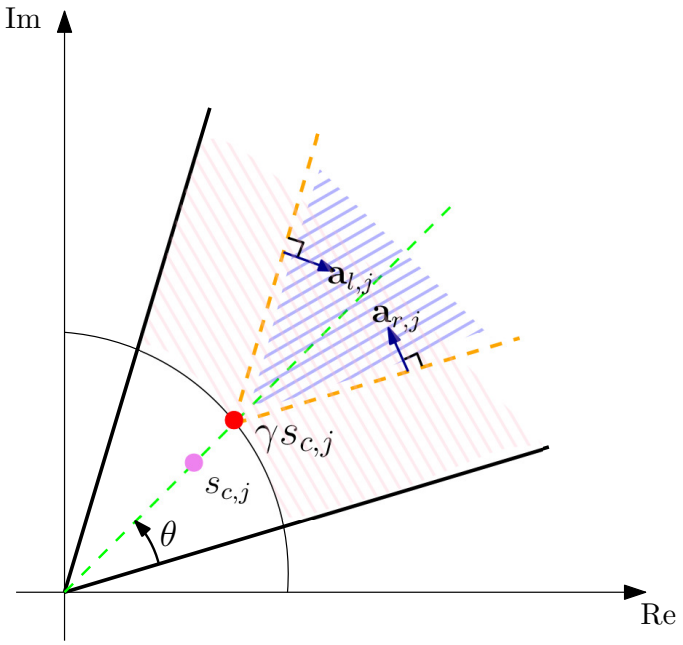

Figure 3.2: Symbol Region for UCISB precoding

Thus, we have

$$\mathcal{D}_j = \{\mathbf{x} \mid (\mathbf{a}_{l,j}^T \mathbf{x} \geq b_{l,j}) \cap (\mathbf{a}_{r,j}^T \mathbf{x} \geq b_{r,j}),\ \mathbf{x} \in \mathbb{R}^2\}, \tag{3.21}$$

where $\mathbf{a}_{l,j} \in \mathbb{R}^2$ and $\mathbf{a}_{r,j} \in \mathbb{R}^2$ represent normal vectors of the boundaries and point inwards to the symbol region, and $b_{l,j}$ and $b_{r,j}$ determine the offset of the corresponding hyperplane from the origin. The normal vector $\mathbf{a}_{l,j}$ is orthogonal to the decision boundary shared by $\mathbf{s}_{c,j}$ and $\mathbf{x}_{l,j}$, and thus can be expressed as $\mathbf{a}_{l,j} = \mathbf{s}_{c,j} - \mathbf{x}_{l,j}$. The boundary of the symbol region (orange dashed line in Fig. 3.2) crosses the point $\gamma \mathbf{s}_{c,j}$ which is the vertex of the symbol region, so $b_{l,j} = \gamma \mathbf{a}_{l,j}^T \mathbf{s}_{c,j}$. The method to obtain $\mathbf{a}_{r,j}$ and $b_{r,j}$ is similar. The compact form of Eq. (3.21) then becomes

$$\mathcal{D}_j = \{\mathbf{x} \mid \mathbf{A}_j \mathbf{x} \geq \mathbf{b}_j\}, \tag{3.22}$$

where $\mathbf{A}_j = \begin{bmatrix} \mathbf{a}_{l,j} & \mathbf{a}_{r,j} \end{bmatrix}^T$ and $\mathbf{b}_j = \gamma \begin{bmatrix} \mathbf{a}_{l,j} & \mathbf{a}_{r,j} \end{bmatrix}^T \mathbf{s}_{c,j}$.

Finally, problem (P1) can be rewritten as:

$$\max_{\mathbf{x}_c} \ \gamma \tag{P2}$$

$$\text{subject to} \ \begin{bmatrix} \mathbf{a}_{l,j}^T \\ \mathbf{a}_{r,j}^T \end{bmatrix} \begin{bmatrix} \mathcal{R}\{\mathbf{h}_{cc,j}\mathbf{x}_c\} \\ \mathcal{I}\{\mathbf{h}_{cc,j}\mathbf{x}_c\} \end{bmatrix} \geq \gamma \begin{bmatrix} \mathbf{a}_{l,j}^T \\ \mathbf{a}_{r,j}^T \end{bmatrix} \mathbf{s}_{c,j} \ , \ \forall j \in \mathcal{J} \tag{C2-1}$$

$$\|\mathbf{h}_{cp,k}\mathbf{x}_c\|^2 \leq \eta_k \ , \ \forall k \in \mathcal{K} \tag{C2-2}$$

$$\|\mathbf{x}_c\|^2 \leq P_c \tag{C2-3}$$

which is a convex optimization problem and can be solved by standard algorithms. This algorithm will be referred to as Underlay Constructive Interference SINR Balancing (UCISB).

3.3.3 Underlay Cognitive Maximum Safety Margin (UCMSM)

In this section, we introduce an optimal CI-based precoding method for the underlay case that maximizes the worst-case SM of the cognitive users without violating interference temperature constraints at the PUs. These constraints guarantee that the power of the interference from the CR at each PU is less than the given value η_k:

$$\|\mathbf{h}_{cp,k}\mathbf{x}_c\|^2 \leq \eta_k \quad \forall k \in \mathcal{K}. \tag{3.23}$$

Since the CBS does not have information about $\mathbf{H}_{pc}$ and $\mathbf{s}_p$, it will simply treat the interference from the PBS as noise.

The vector of noiseless signals at the CUs is given by

$$\mathbf{r}_c = \mathbf{H}_{cc}\mathbf{x}_c. \tag{3.24}$$

After modifying the coordinate system as in Fig. 2.3, we have

$$\mathbf{z}_c = \widetilde{\mathbf{H}}_{cc}\mathbf{x}_c \tag{3.25}$$

where $\mathbf{S}_c = \mathrm{diag}(\mathbf{s}_c)$ and $\widetilde{\mathbf{H}}_{cc} = \mathbf{S}_c^{\mathrm{H}}\mathbf{H}_{cc}$. As in Eq. (2.2), the safety margin for each CU is given by

$$\delta_{c,j} = \mathcal{R}\{z_{c,j}\}\sin\theta - |\mathcal{I}\{z_{c,j}\}|\cos\theta. \tag{3.26}$$

The guarantee that $z_{c,j}$ lies in the CIR defined by δ_c can be expressed mathematically as

$$\mathcal{R}\{\mathbf{z}_c\} \geq \delta_c \mathbf{1}_{N_c}, \tag{3.27}$$

for BPSK signals, and more generally for DPSK ($D > 2$) as

$$-\mathcal{R}\{\mathbf{z}_c\}\tan\theta + \frac{\delta_c}{\cos\theta}\mathbf{1}_{N_c} \leq \mathcal{I}\{\mathbf{z}_c\} \leq \mathcal{R}\{\mathbf{z}_c\}\tan\theta - \frac{\delta_c}{\cos\theta}\mathbf{1}_{N_c}. \tag{3.28}$$

To formulate the desired MSM optimization problem, we write the constraints using real-valued notation by defining

$$\mathbf{u} = \begin{bmatrix} \mathcal{R}\{\mathbf{x}_c\} \\ \mathcal{I}\{\mathbf{x}_c\} \end{bmatrix}, \tag{3.29}$$

so that

$$\mathcal{R}\{\mathbf{z}_c\} = \mathcal{R}\{\widetilde{\mathbf{H}}_{cc}\mathbf{x}_c\} \tag{3.30}$$

$$= \begin{bmatrix} \mathcal{R}\{\widetilde{\mathbf{H}}_{cc}\} & -\mathcal{I}\{\widetilde{\mathbf{H}}_{cc}\} \end{bmatrix} \begin{bmatrix} \mathcal{R}\{\mathbf{x}_c\} \\ \mathcal{I}\{\mathbf{x}_c\} \end{bmatrix} \tag{3.31}$$

$$= \mathbf{C}\mathbf{u} \tag{3.32}$$

$$\mathcal{I}\{\mathbf{z}_c\} = \mathcal{I}\{\widetilde{\mathbf{H}}_{cc}\mathbf{x}_c\} \tag{3.33}$$

$$= \begin{bmatrix} \mathcal{I}\{\widetilde{\mathbf{H}}_{cc}\} & \mathcal{R}\{\widetilde{\mathbf{H}}_{cc}\} \end{bmatrix} \begin{bmatrix} \mathcal{R}\{\mathbf{x}_c\} \\ \mathcal{I}\{\mathbf{x}_c\} \end{bmatrix} \tag{3.34}$$

$$= \mathbf{D}\mathbf{u}\ . \tag{3.35}$$

Then, the CIR constraints in Eqs. (3.27) and (3.28) can be rewritten as

$$\begin{bmatrix} -\mathbf{C} & \mathbf{1}_{N_c} \end{bmatrix} \begin{bmatrix} \mathbf{u} \\ \delta_c \end{bmatrix} \leq \mathbf{0}_{N_c} \quad \text{(BPSK)} \tag{3.36}$$

$$\begin{bmatrix} -\mathbf{C}\tan\theta + \mathbf{D} & \frac{1}{\cos\theta}\mathbf{1}_{N_c} \\ -\mathbf{C}\tan\theta - \mathbf{D} & \frac{1}{\cos\theta}\mathbf{1}_{N_c} \end{bmatrix} \begin{bmatrix} \mathbf{u} \\ \delta_c \end{bmatrix} \leq \mathbf{0}_{2N_c}\ (D\text{PSK},\ D > 2) \tag{3.37}$$

With an instantaneous power budget P_c at the CBS, the precoded symbols should satisfy

$$\|\mathbf{x}_c\|^2 = \mathbf{u}^{\mathrm{H}}\mathbf{u} \leq P_c. \tag{3.38}$$

Thus, we can formulate the optimal MSM problem for the underlay CR scenario for D-PSK ($D > 2$) signaling as

$$\max_{\mathbf{u},\delta_c} \quad \begin{bmatrix} \mathbf{0}_{2M_c}^{\mathrm{T}} & 1 \end{bmatrix} \begin{bmatrix} \mathbf{u} \\ \delta_c \end{bmatrix} \tag{P3}$$

$$\text{subject to} \quad \|\mathbf{h}_{cp,k}\mathbf{x}_c\|^2 \leq \eta_k \quad \forall k \in \mathcal{K} \tag{C3-1}$$

$$\begin{bmatrix} -\mathbf{C}\tan\theta + \mathbf{D} & \frac{1}{\cos\theta}\mathbf{1}_{N_c} \\ -\mathbf{C}\tan\theta - \mathbf{D} & \frac{1}{\cos\theta}\mathbf{1}_{N_c} \end{bmatrix} \begin{bmatrix} \mathbf{u} \\ \delta_c \end{bmatrix} \leq \mathbf{0}_{2N_c} \tag{C3-2}$$

$$\mathbf{u}^{\mathrm{H}}\mathbf{u} \leq P_c \,, \tag{C3-3}$$

where the first constraint guarantees the desired PU interference temperature, the second constraint defines the CIR for δ_c, and the third constraint addresses the instantaneous power constraint. For BPSK signaling, the constraint in (C3-2) is replaced by (3.36). The resulting optimization problem is convex, and can be easily solved. This approach is referred to as Underlay Cognitive Maximum Safety Margin (UCMSM).

In Section 3.5, we will see that this method provides the same performance as UCISB since the CIRs are the same and the objective variable γ in UCISB is linear in the safety margin δ_c when information about the PBS signal is not available at the CBS. However, in the overlay CR scenarios developed in the next section, the advantage of the MSM criterion compared with SB will be revealed.

3.4 Overlay Cognitive Radios

In an overlay CR network, the PBS cooperates with the CBS and provides information that enables the cognitive and primary networks to better co-exist. In this section, we assume the PBS shares with the CBS its CSI for both the PUs and CUs as well as the data it transmits

to the PUs. This leads to several important benefits. First, the CBS can employ SLP to counteract the effect of the PBS interference at the CUs, and ensure that the combination of the MUI and the primary network interference is constructive for the CUs. Second, the CBS can simultaneously tune its SLP to not only avoid interference at the PUs, but in fact to potentially improve the safety margin of the PUs and hence their QoS as well. This provides performance well beyond what is achievable with prior underlay CR approaches. In the following sections, we present two linear precoders derived from [29] as baselines and two new proposed nonlinear precoders for the CBS. As before, we assume the PBS still employs conventional ZF precoding to remove the multiuser interference among the PUs.

3.4.1 Overlay CR Zero Forcing (OCZF)

In [29], a ZF linear precoder is proposed for the overlay CR scenario in which the CBS uses knowledge of the primary data and CSI of all links. Moreover, to compensate for the potential loss in PU QoS due to the concurrent CBS transmissions, the CBS is also tasked with relaying the PUs' signals in addition to its own messages. The method in [29] used an equal power scaling for both the PU and CU symbols, and as a result the presence of the cognitive system can degrade the PU performance in certain scenarios. The approach we present in this subsection, Overlay CR Zero Forcing (OCZF), generalizes the algorithm of [29] by allowing separate primary and cognitive power scaling factors, and consequently can guarantee no impact on the QoS of the PUs.

For OCZF, the precoded symbol vectors transmitted by the PBS and CBS are respectively given by

$$\mathbf{x}_p = f_p \mathbf{W}_p \mathbf{s}_p, \ \mathbf{x}_c = f_c \mathbf{W}_c \mathbf{s} \tag{3.39}$$

$$f_p = \sqrt{\frac{P_p}{\mathrm{Tr}\{\mathbf{W}_p \mathbf{W}_p^H\}}}, \ f_c = \sqrt{\frac{P_c}{\mathrm{Tr}\{\mathbf{W}_c \mathbf{W}_c^H\}}} \tag{3.40}$$

where f_p and f_c are the average transmitted power scaling factors, $\mathbf{W}_p$ and $\mathbf{W}_c$ denote precoding matrices at the PBS and CBS, and $\mathbf{s} = \begin{bmatrix} \mathbf{s}_p^T & \mathbf{s}_c^T \end{bmatrix}^T$ denotes the symbol vector transmitted by the CBS, which includes both the CU and PU data. Excluding the power scaling factor, the precoder at the CBS using the ZF criterion can be expressed as

$$\mathbf{W}_c = \mathbf{H}^H(\mathbf{H}\mathbf{H}^H)^{-1}(\mathbf{I} - \mathbf{V}_p) \tag{3.41}$$

where

$$\mathbf{H} = \begin{bmatrix} \mathbf{H}_{cp} \\ \mathbf{H}_{cc} \end{bmatrix}, \quad \mathbf{V}_p = \begin{bmatrix} \mathbf{H}_{pp}\mathbf{W}_p & \mathbf{0}_{N_p \times N_c} \\ \mathbf{H}_{pc}\mathbf{W}_p & \mathbf{0}_{N_c \times N_c} \end{bmatrix}. \tag{3.42}$$

Therefore, the received signals at the PUs and CUs are

$$\mathbf{y}_p = f_p\mathbf{s}_p + \mathbf{n}_p \tag{3.43}$$

$$\mathbf{y}_c = (f_p - f_c)\mathbf{H}_{pc}\mathbf{W}_p\mathbf{s}_p + f_c\mathbf{s}_c + \mathbf{n}_c. \tag{3.44}$$

Forcing $f_p = f_c$ as in [29] to eliminate PBS interference at the CUs can result in a significant loss of SNR for the PUs compared to the case without the cognitive system. Thus, the price paid for maintaining the QoS of the PUs with different power normalizations is increased interference at the CUs, particularly at high SNRs.

3.4.2 Overlay Phase Alignment Linear Precoding (OPALP)

An alternative linear precoder proposed in [29] for the overlay case is based on the use of CI that rotates the phase of the MUI such that is aligned with the signal of interest and thus constructive. As before, we generalize the approach in [29] to allow differsent power scaling factors, so that the PU performance is not impacted and some PBS interference is leaked to

the CUs. The generalized MSE criterion is thus

$$\epsilon = \mathbb{E}\{\|\mathbf{V}_p\mathbf{s} + \mathbf{H}\mathbf{W}_c\mathbf{s} - (\mathbf{A} + \mathbf{B}\mathbf{Q}^{\phi})\mathbf{s}\|^2\} \tag{3.45}$$

where $\mathbf{A} = \text{diag}\{[1, \cdots, 1, 0, \cdots, 0]\}$ is a diagonal matrix whose first N_p diagonal elements equal 1, $\mathbf{B} = \text{diag}\{[0, \cdots, 0, 1, \cdots, 1]\}$ is a diagonal matrix whose last N_c elements equal 1, and $\mathbf{Q}^{\phi} = \text{diag}(\mathbf{s}) \cdot |\mathbf{H}\mathbf{H}^H| \cdot \text{diag}(\mathbf{s})^H$ contains the phase-corrected correlation elements. The precoding matrix at the CBS in this case is given by

$$\mathbf{W}_c = \mathbf{H}^H(\mathbf{H}\mathbf{H}^H)^{-1}(\mathbf{A} + \mathbf{B}\mathbf{Q}^{\phi} - \mathbf{V}_p), \tag{3.46}$$

and the received signals at the PUs and CUs are

$$\mathbf{y}_p = f_p\mathbf{s}_p + \mathbf{n}_p \tag{3.47}$$

$$\mathbf{y}_c = (f_p - f_c)\mathbf{H}_{pc}\mathbf{W}_p\mathbf{s}_p + f_c\mathbf{Q}_c^{\phi}\mathbf{s}_c + \mathbf{n}_c \tag{3.48}$$

where

$$\mathbf{Q}_c^{\phi} = \text{diag}\left\{\left[\sum_{j=1}^{N_p+N_c} |\rho_{(N_p+1)j}|, \cdots, \sum_{j=1}^{N_p+N_c} |\rho_{(N_p+N_c)j}|\right]\right\} \tag{3.49}$$

and ρ_{ij} is the (i, j)th element in the cross correlation matrix $\mathbf{Q} = \mathbf{H}\mathbf{H}^H$. This algorithm, referred to as Overlay Phase Alignment Linear Precoding (OPALP), allows the CUs to benefit from the inter-user constructive interference in the cognitive system, but in general will not entirely eliminate interference from the PBS.

3.4.3 Overlay Constructive Interference SINR Balancing (OCISB)

To overcome the need of for the CBS to spare power for relaying the PU messages as in the above approaches, in this section we present a new algorithm, Overlay Constructive Interference SINR Balancing (OCISB), that applies the SB idea of UCISB to the overlay scenario, where knowledge of the data and CSI from the primary system is exploited. In this approach, the CBS transmission is designed such that all interference terms make constructive contributions to the signal power, and each CU's SINR can be expressed as:

$$\mathrm{SINR}_{c,j} = \frac{\|\mathbf{h}_{cc,j}\mathbf{x}_c + \mathbf{h}_{pc,j}\mathbf{x}_p\|^2}{\sigma_c^2} \ . \tag{3.50}$$

To achieve this goal, the noiseless received signal at each CU, i.e., $r_{c,j} = \mathbf{h}_{cc,j}\mathbf{x}_c + \mathbf{h}_{pc,j}\mathbf{x}_p$, should be located inside the target decision region. Therefore, the SINR balancing approach for exploiting CI in the overlay scanario can be written as the following convex optimization problem:

$$\max_{\mathbf{x}_c} \ \gamma \tag{P4}$$

$$\text{subject to} \ \begin{bmatrix} \mathbf{a}_{l,j}^T \\ \mathbf{a}_{r,j}^T \end{bmatrix} \begin{bmatrix} \mathcal{R}\{\mathbf{h}_{cc,j}\mathbf{x}_c + \mathbf{h}_{pc,j}\mathbf{x}_p\} \\ \mathcal{I}\{\mathbf{h}_{cc,j}\mathbf{x}_c + \mathbf{h}_{pc,j}\mathbf{x}_p\} \end{bmatrix} \geq \gamma \begin{bmatrix} \mathbf{a}_{l,j}^T \\ \mathbf{a}_{r,j}^T \end{bmatrix} \mathbf{s}_{c,j} \ , \ \forall j \in \mathcal{J} \tag{C4-1}$$

$$\|\mathbf{h}_{cp,k}\mathbf{x}_c\|^2 \leq \eta_k \ , \ \forall k \in \mathcal{K} \tag{C4-2}$$

$$\|\mathbf{x}_c\|^2 \leq P_c \tag{C4-3}$$

where $\mathbf{a}_{l,j}$ and $\mathbf{a}_{r,j}$ are defined as in Section 3.3.2.

3.4.4 Overlay Cognitive Maximum Safety Margin (OCMSM)

Our second proposed CI-based nonlinear precoder for overlay systems is designed using the MSM criterion. Rather than using an interference temperature constraint or simply eliminating all CBS interference to the primary system, in this approach we maximize the SM of the CUs while ensuring that the SM of the PUs is no smaller than what it would be in the primary-only scenario. Most importantly, even though the CBS does not directly use part of its power for relaying the primary transmission, the PUs can still achieve an improvement in their QoS due to the energy harvested from the CI produced by the cognitive transmission.

3.4.4.1 Primary System

In the primary-only scenario, the noiseless received signal for user k is given by

$$r_{p,k}^{0} = \mathbf{h}_{pp,k}\mathbf{x}_{p} \ , \tag{3.51}$$

which in the modified coordinate system is

$$z_{p,k}^{0} = s_{p,k}^{*} r_{p,k}^{0} = s_{p,k}^{*}\mathbf{h}_{pp,k}\mathbf{x}_{p}. \tag{3.52}$$

The vector form of this equation for all users is

$$\mathbf{z}_{p}^{0} = \mathbf{S}_{p}^{\mathrm{H}}\mathbf{H}_{pp}\mathbf{x}_{p} \tag{3.53}$$

where $\mathbf{S}_{p} = \mathrm{diag}(\mathbf{s}_{p})$. Then the original SM for each PU can be expressed as

$$\delta_{p,k}^{0} = \mathcal{R}\{z_{p,k}^{0}\}\sin\theta - |\mathcal{I}\{z_{p,k}^{0}\}|\cos\theta. \tag{3.54}$$

The worst-case SM in this case is

$$\delta_p^0 = \min_{k \in \mathcal{K}} \quad \delta_{p,k}^0 \ , \tag{3.55}$$

and we design the CBS transmission such that this value is not reduced by the existence of the CR network.

When the secondary system is active, the noiseless signal in the modified coordinate system at kth PU becomes

$$z_{p,k} = s_{p,k}^* r_{p,k} = s_{p,k}^* (\mathbf{h}_{pp,k} \mathbf{x}_p + \mathbf{h}_{cp,k} \mathbf{x}_c) \ . \tag{3.56}$$

To keep the secondary transmission from reducing the worst-case SM, the following constraint must be satisfied:

$$\delta_{p,k} = \mathcal{R}\{z_{p,k}\} \sin\theta - |\mathcal{I}\{z_{p,k}\}| \cos\theta \geq \delta_p^0 \ , \ \forall k \in \mathcal{K}. \tag{3.57}$$

Stacking the N_p constraints in matrix form, for BPSK we have

$$\mathcal{R}\{\mathbf{z}_p\} \geq \delta_p^0 \mathbf{1}_{N_p} \tag{3.58}$$

and for DPSK ($D > 2$):

$$-\mathcal{R}\{\mathbf{z}_p\} \tan\theta + \frac{\delta_p^0}{\cos\theta} \mathbf{1}_{N_p} \leq \mathcal{I}\{\mathbf{z}_p\} \leq \mathcal{R}\{\mathbf{z}_p\} \tan\theta - \frac{\delta_p^0}{\cos\theta} \mathbf{1}_{N_p} \tag{3.59}$$

where

$$\mathbf{z}_p = \mathbf{S}_p^{\mathrm{H}} (\mathbf{H}_{pp} \mathbf{x}_p + \mathbf{H}_{cp} \mathbf{x}_c) = \mathbf{z}_p^0 + \mathbf{S}_p^{\mathrm{H}} \mathbf{H}_{cp} \mathbf{x}_c \ . \tag{3.60}$$

If we define $\widetilde{\mathbf{H}}_{cp} = \mathbf{S}_p^{\mathrm{H}} \mathbf{H}_{cp}$, the real and imaginary parts of $\mathbf{z}_p$ can be written as

$$\mathcal{R}\{\mathbf{z}_p\} = \mathcal{R}\{\mathbf{z}_p^0\} + \mathcal{R}\{\widetilde{\mathbf{H}}_{cp}\mathbf{x}_c\} \tag{3.61}$$

$$= \begin{bmatrix} \mathcal{R}\{\mathbf{z}_p^0\} & \mathcal{R}\{\widetilde{\mathbf{H}}_{cp}\} & -\mathcal{I}\{\widetilde{\mathbf{H}}_{cp}\} \end{bmatrix} \begin{bmatrix} 1 \\ \mathcal{R}\{\mathbf{x}_c\} \\ \mathcal{I}\{\mathbf{x}_c\} \end{bmatrix} \tag{3.62}$$

$$= \mathbf{E}\mathbf{v} \tag{3.63}$$

$$\mathcal{I}\{\mathbf{z}_p\} = \mathcal{I}\{\mathbf{z}_p^0\} + \mathcal{I}\{\widetilde{\mathbf{H}}_{cp}\mathbf{x}_c\} \tag{3.64}$$

$$= \begin{bmatrix} \mathcal{I}\{\mathbf{z}_p^0\} & \mathcal{I}\{\widetilde{\mathbf{H}}_{cp}\} & \mathcal{R}\{\widetilde{\mathbf{H}}_{cp}\} \end{bmatrix} \begin{bmatrix} 1 \\ \mathcal{R}\{\mathbf{x}_c\} \\ \mathcal{I}\{\mathbf{x}_c\} \end{bmatrix} \tag{3.65}$$

$$= \mathbf{F}\mathbf{v}. \tag{3.66}$$

Then, the constraint in (3.59) can be rewritten as

$$\begin{bmatrix} -\mathbf{E} & \mathbf{1}_{N_p} \end{bmatrix} \begin{bmatrix} \mathbf{v} \\ \delta_p^0 \end{bmatrix} \leq \mathbf{0}_{N_p} \quad \text{(BPSK)} \tag{3.67}$$

$$\begin{bmatrix} -\mathbf{E}\tan\theta + \mathbf{F} & \frac{1}{\cos\theta}\mathbf{1}_{N_p} \\ -\mathbf{E}\tan\theta - \mathbf{F} & \frac{1}{\cos\theta}\mathbf{1}_{N_p} \end{bmatrix} \begin{bmatrix} \mathbf{v} \\ \delta_p^0 \end{bmatrix} \leq \mathbf{0}_{2N_p} \ (D\text{PSK},\ D > 2) \tag{3.68}$$

3.4.4.2 Cognitive System

For the jth CU, the noiseless received symbol in the modified coordinate system is

$$z_{c,j} = s_{c,j}^{*} r_{c,j} = s_{c,j}^{*}(\mathbf{h}_{cc,j}\mathbf{x}_c + \mathbf{h}_{pc,j}\mathbf{x}_p) \tag{3.69}$$

which in vector form for all CUs becomes

$$\mathbf{z}_c = \mathbf{S}_c^{\mathrm{H}}\mathbf{H}_{cc}\mathbf{x}_c + \mathbf{S}_c^{\mathrm{H}}\mathbf{H}_{pc}\mathbf{x}_p = \widetilde{\mathbf{H}}_{cc}\mathbf{x}_c + \mathbf{g} \tag{3.70}$$

where $\mathbf{g} = \mathbf{S}_c^{\mathrm{H}}\mathbf{H}_{pc}\mathbf{x}_p$ is known due to the data shared by the PBS. The safety margin for each CU is

$$\delta_{c,j} = \mathcal{R}\{z_{c,j}\}\sin\theta - |\mathcal{I}\{z_{c,j}\}|\cos\theta. \tag{3.71}$$

Denote the worst SM of all CUs as

$$\delta_c = \min_{j\in\mathcal{J}} \quad \delta_{c,j}, \tag{3.72}$$

so that

$$\mathcal{R}\{z_{c,j}\}\sin\theta - |\mathcal{I}\{z_{c,j}\}|\cos\theta \geq \delta_c \quad \forall j \in \mathcal{J} \tag{3.73}$$

The CBS designs the transmit signal vector $\mathbf{x}_c$ to maximize δ_c. Similar to Eq. (3.28), the constraint can be formulated in matrix form as follows, for BPSK:

$$\mathcal{R}\{\mathbf{z}_c\} \geq \delta_c \mathbf{1}_{N_c} \tag{3.74}$$

and for DPSK ($D > 2$):

$$-\mathcal{R}\{\mathbf{z}_c\}\tan\theta + \frac{\delta_c}{\cos\theta}\mathbf{1}_{N_c} \leq \mathcal{I}\{\mathbf{z}_c\} \leq \mathcal{R}\{\mathbf{z}_c\}\tan\theta - \frac{\delta_c}{\cos\theta}\mathbf{1}_{N_c} \tag{3.75}$$

Using the real-valued matrix representation,

$$\mathcal{R}\{\mathbf{z}_c\} = \mathcal{R}\{\mathbf{g}\} + \mathcal{R}\{\widetilde{\mathbf{H}}_{cc}\mathbf{x}_c\} \tag{3.76}$$

$$= \begin{bmatrix} \mathcal{R}\{\mathbf{g}\} & \mathcal{R}\{\widetilde{\mathbf{H}}_{cc}\} & -\mathcal{I}\{\widetilde{\mathbf{H}}_{cc}\} \end{bmatrix} \begin{bmatrix} 1 \\ \mathcal{R}\{\mathbf{x}_c\} \\ \mathcal{I}\{\mathbf{x}_c\} \end{bmatrix} \tag{3.77}$$

$$= \mathbf{G}\mathbf{v} \tag{3.78}$$

$$\mathcal{I}\{\mathbf{z}_c\} = \mathcal{I}\{\mathbf{g}\} + \mathcal{I}\{\widetilde{\mathbf{H}}_{cc}\mathbf{x}_c\} \tag{3.79}$$

$$= \begin{bmatrix} \mathcal{I}\{\mathbf{g}\} & \mathcal{I}\{\widetilde{\mathbf{H}}_{cc}\} & \mathcal{R}\{\widetilde{\mathbf{H}}_{cc}\} \end{bmatrix} \begin{bmatrix} 1 \\ \mathcal{R}\{\mathbf{x}_c\} \\ \mathcal{I}\{\mathbf{x}_c\} \end{bmatrix} \tag{3.80}$$

$$= \mathbf{Q}\mathbf{v}, \tag{3.81}$$

the constraints in (3.74) and (3.75) can be rewritten as

$$\begin{bmatrix} -\mathbf{G} & \mathbf{1}_{N_c} \end{bmatrix} \begin{bmatrix} \mathbf{v} \\ \delta_c \end{bmatrix} \leq \mathbf{0}_{N_c} \quad \text{(BPSK)} \tag{3.82}$$

$$\begin{bmatrix} -\mathbf{G}\tan\theta + \mathbf{Q} & \frac{1}{\cos\theta}\mathbf{1}_{N_c} \\ -\mathbf{G}\tan\theta - \mathbf{Q} & \frac{1}{\cos\theta}\mathbf{1}_{N_c} \end{bmatrix} \begin{bmatrix} \mathbf{v} \\ \delta_c \end{bmatrix} \leq \mathbf{0}_{2N_c} \ (D\text{PSK},\ D > 2). \tag{3.83}$$

In the overlay CR system, the objective is to maximize the worst case SM of the CUs without degrading the worst-case SM of the PUs. For the case of DPSK with $D > 2$, the resulting SLP optimization problem is obtained by combining Eq. (2.3), (3.68) and (3.83), as follows:

$$\underset{\mathbf{u},\delta_c}{\text{maximize}} \quad \delta_c \tag{P5}$$

$$\text{subject to} \quad \begin{bmatrix} -\mathbf{E}\tan\theta + \mathbf{F} & \frac{1}{\cos\theta}\mathbf{1}_{N_p} & \mathbf{0}_{N_p} \\ -\mathbf{E}\tan\theta - \mathbf{F} & \frac{1}{\cos\theta}\mathbf{1}_{N_p} & \mathbf{0}_{N_p} \\ -\mathbf{G}\tan\theta + \mathbf{Q} & \mathbf{0}_{N_c} & \frac{1}{\cos\theta}\mathbf{1}_{N_c} \\ -\mathbf{G}\tan\theta - \mathbf{Q} & \mathbf{0}_{N_c} & \frac{1}{\cos\theta}\mathbf{1}_{N_c} \end{bmatrix} \begin{bmatrix} 1 \\ \mathbf{u} \\ \delta_p^0 \\ \delta_c \end{bmatrix} \leq \mathbf{0}_{2(N_c+N_p)} \tag{C5-1}$$

$$\|\mathbf{u}\|^2 \leq P_c, \tag{C5-2}$$

where the last constraint is to limit the instantaneous transmit power. For BPSK signaling, we substitute the constraint in (C5-1) with Eq. (3.67) and (3.82):

$$\begin{bmatrix} -\mathbf{E} & \mathbf{1}_{N_p} & \mathbf{0}_{N_p} \\ -\mathbf{G} & \mathbf{0}_{N_c} & \mathbf{1}_{N_c} \end{bmatrix} \begin{bmatrix} 1 \\ \mathbf{u} \\ \delta_p^0 \\ \delta_c \end{bmatrix} \leq \mathbf{0}_{N_c+N_p}. \tag{C5-1'}$$

The precoded transmit vector $\mathbf{x}_c$ is then found using (3.29). This optimization problem is convex, and is referred to as Overlay Cognitive Maximum Safety Margin (OCMSM).

3.5 Numerical Results

Table 3.1 provides a summary of the precoding algorithms presented in this chapter, together with the CR problem they address and the extent of their use of constructive interference. "Among CUs" indicates that CI is exploited among the MUI in the CU symbols, while

P $\rightarrow$ C and C $\rightarrow$ P respectively indicate that CI from the PBS benefits the CUs and CI from the CBS benefits the PUs. In this section, we assess the performance of our proposed MSM-based precoding approaches and compare them with the other techniques developed in Sections 3.3 and 3.4. Monte-Carlo simulations are conducted over 1000 independent channel realizations with a block of $T = 100$ symbols in both underlay and overlay CR scenarios. The channels $\mathbf{H}_{pp}$, $\mathbf{H}_{cp}$, $\mathbf{H}_{pc}$ and $\mathbf{H}_{cc}$ are composed of i.i.d. Gaussian random variables with zero mean and unit variance. The complex Gaussian noise is assumed to have the same power (= 1) for all PUs and CUs. The PBS transmission power is set at $P_p = 10$ dBW. Both the PBS and CBS are assumed to have 10 antennas, and unless stated otherwise, the number of PUs and CUs are both set at 4.

Table 3.1: Constructive Interference Algorithm Summary

CR type	CI / Precoder	Among CUs	P→C	C→P
Underlay	UCZF	-	-	-
	UCISB	✓	-	-
	UCMSM	✓	-	-
Overlay	OCZF	-	-	-
	OPALP	✓	-	-
	OCISB	✓	✓	-
	OCMSM	✓	✓	✓

Since for SLP we work with finite alphabet constellations, we will analyze the block transmission performance of the system using the throughput τ as calculated in [94]:

$$\tau = (1 - P_B) \times c \times T \times N, \tag{3.84}$$

where P_B is the block error rate (BLER), $c = \log_2 D$ is the number of bits per modulation symbol, T is the block length and N is the number of receivers. In each block for each user, there are $C = c \times T$ data message bits transmitted from the BS. For PSK modulation, assuming a binomial distribution of errors in each block, the probability of more than q

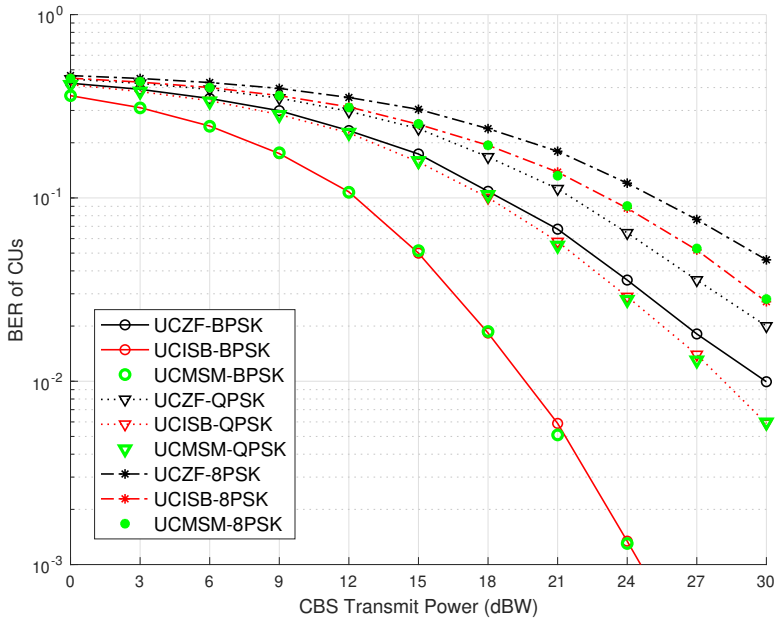

Figure 3.3: CBS Transmit Power vs. CU BER in the underlay scenario where $P_p = 10$ dBW, $M_p = M_c = 8$, $N_p = N_c = 4$, and $\sigma_c^2 = \sigma_p^2 = 1$.

errors occurring in one block of C bits is expressed as

$$P_e(q, C) = 1 - \sum_{i=0}^{q} \binom{C}{i} P_b^i (1 - P_b)^{C-i} \tag{3.85}$$

where P_b is BER. If the receiver detects errors without correction, a block is received correctly only if all C bits in the block are received correctly, and thus the BLER is $P_B = P_e(0, C)$. On the other hand, if the receiver is capable of correcting up to Q errors in each block, then the BLER is given by $P_B = P_e(Q, C)$ [95].

3.5.1 Underlay CR Scenarios

A comparison among UCZF, UCISB and UCMSM is illustrated in Fig. 3.3, which shows the BER of the CUs with respect to the CBS transmit power. For UCISB, we assume the interference temperature imposed by each PU is 0, i.e., $\eta_k = 0 \ \forall k \in \mathcal{K}$ in Eq. (3.23). In Fig. 3.3, we see that in the underlay case, UCISB and UCMSM are equivalent because

they employ the same CIR and linear optimization objective. Both precoders outperform the traditional ZF scheme, particularly when the symbols are generated with lower order modulation. For example, in the BPSK case, UCISB and UCMSM have more than a 10dBW power gain compared to UCZF. With higher transmit power, the SLP feasible region can be further enlarged and made more resistant to the impact of noise, and thus UCISB and UCMSM perform much better as the SNR increases.

3.5.2 Overlay CR Scenarios

We focus more attention on the more interesting overlay case discussed in Section 3.4. In order to protect the PUs from the CR transmission, for OCISB we assume an allowable interference temperature of zero, while for OCMSM the smallest SM of the PUs is set as the threshold δ_p^0 in the optimization problem (P5). In the following figures, the performance of OCISB and OCMSM is only plotted for the cases where the optimizations are feasible. We include plots showing the percentage of the trials that were feasible for each algorithm.

3.5.2.1 BER and Throughput

Fig. 3.4a and 3.4b show the BER performance of the CUs versus the CBS transmit power for different precoding schemes. Both OCISB and OCMSM, the two CI-based SLP approaches, significantly outperform the OCZF and OPALP precoders since they take advantage of CI not only from the CU MUI but also what is available (although not optimized) from the primary system. Similar to the result in the underlay CR scenarios, the lower the modulation order, the better the CI precoders perform. The superiority of OCMSM over OCISB results from the MSM criterion which maintains the BER lower bound of the PUs' by ensuring that the worst-case SM is not deteriorated by the CBS interference. For the OCZF precoder, when the CBS transmit power is high, the scaling factor f_c will be large, and the PBS interference

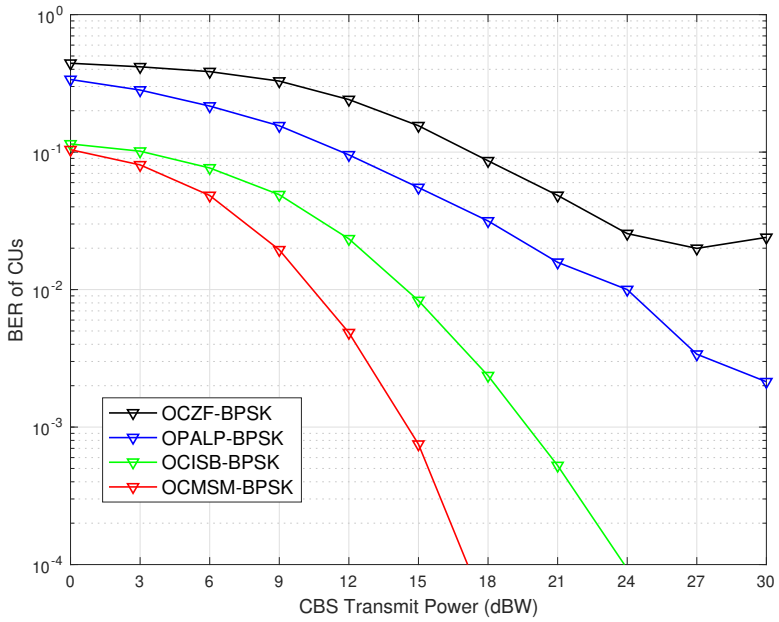

(a) BPSK

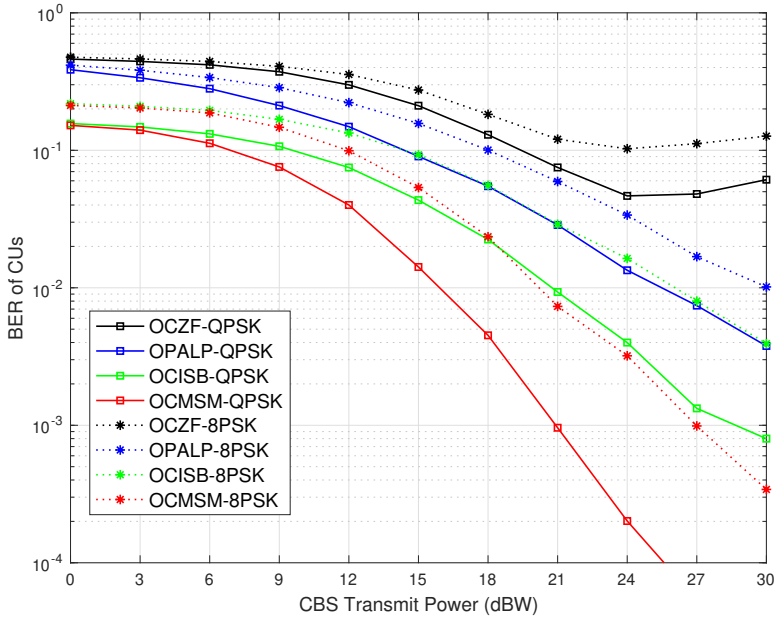

(b) QPSK and 8PSK

Figure 3.4: CBS Transmit Power vs. CU BER in the Overlay scenario where $P_p = 10$ dBW, $M_p = M_c = 8$, $N_p = N_c = 4$, $\sigma_c^2 = \sigma_p^2 = 1$, and $\eta_1 = \cdots = \eta_{N_c} = 0$.

term in Eq. (3.44) will have a significant affect, deteriorating the CU performance. On the other hand, the alternative setting where $f_p = f_c$ leads to an unacceptable degradation to the PU performance.

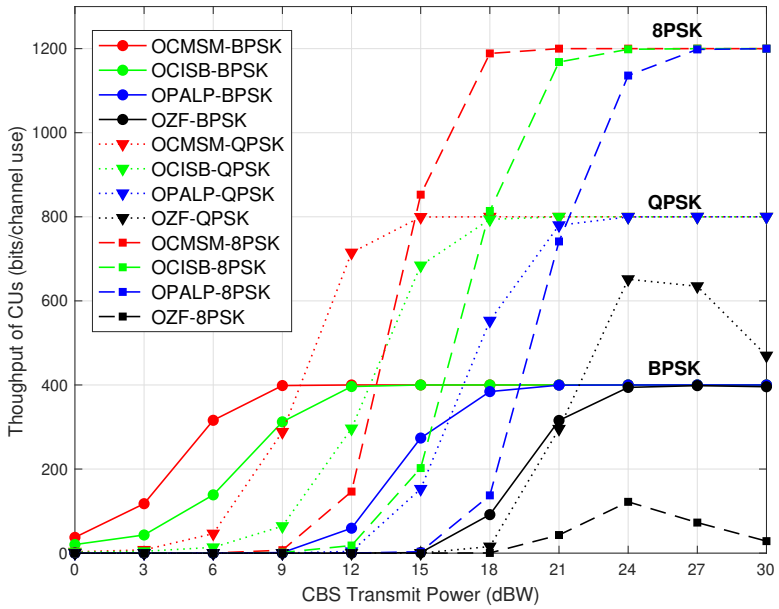

Figure 3.5: CBS Transmit Power vs. CU Throughput in the overlay scenario where $P_p = 10$ dBW, $M_p = M_c = 8$, $N_p = N_c = 4$, $\sigma_c^2 = \sigma_p^2 = 1$, and $Q = 6$

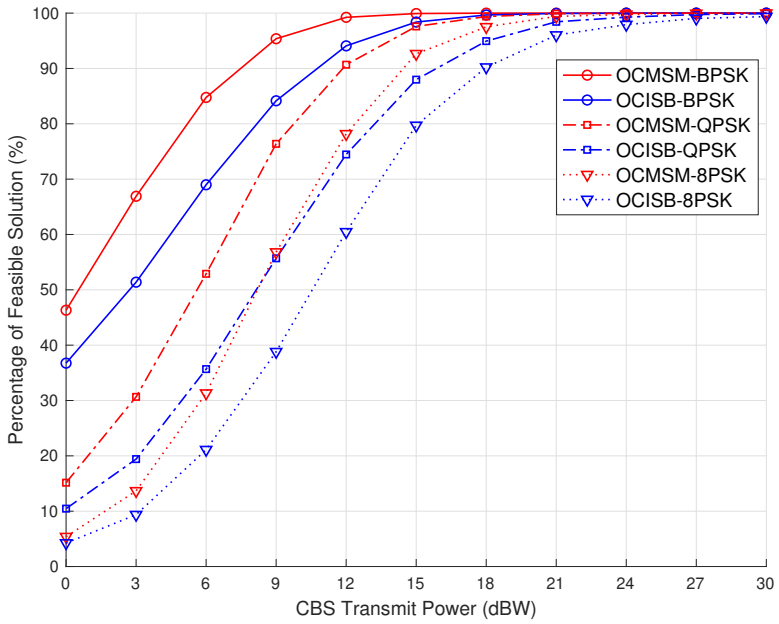

Figure 3.6: CBS Transmit Power vs. Percentage of Feasible Solutions in the overlay scenario where $P_p = 10$ dBW, $M_p = M_c = 8, N_p = N_c = 4$, $\sigma_c^2 = \sigma_p^2 = 1$ and OCMSM precoding.

We present the throughput at the CUs versus the CBS transmission power in Fig. 3.5 for different PSK modulations. We assume that the receivers have the capability of correcting up to $Q = 6$ errors in one block. It can be observed that the throughput saturates to 400,

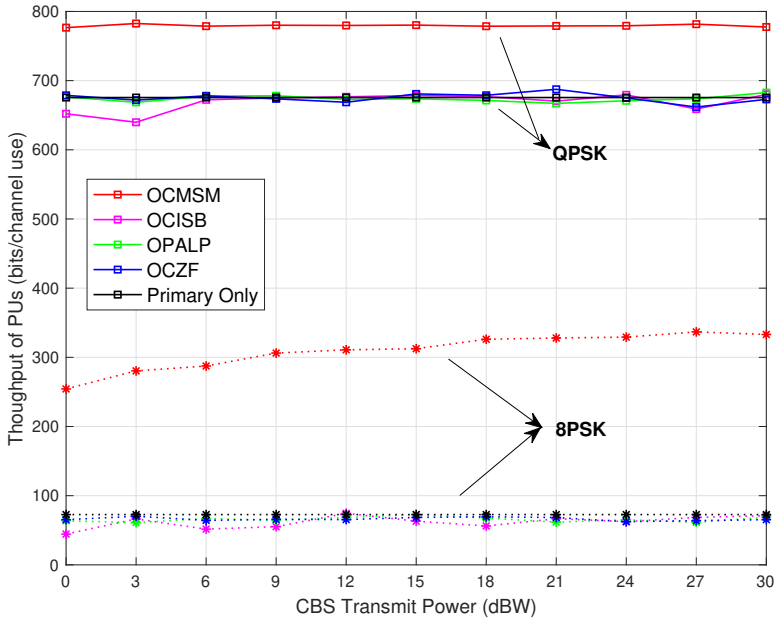

Figure 3.7: CBS Transmit Power vs. PU Throughput in the overlay scenario where $P_p = 10$ dBW, $M_p = M_c = 8$, $N_p = N_c = 4$, and $\sigma_c^2 = \sigma_p^2 = 1$

800, 1200 bits per channel use (per block) for BPSK, QPSK and 8PSK respectively, which is the maximum achievable for the given modulations. When feasible, OCMSM provides the highest throughput, and allows for switching to higher-order modulations at lower SNR when adaptive modulation is employed [96]. In Fig. 3.6, we compare OCMSM with OCISB precoding with respect to the percentage of feasible solutions. With the same modulation and transmission power, it is more likely that a feasible solution can be found with OCMSM than OCISB.

We show the PU throughput in Fig. 3.7 as the CBS power increases. Note that since the PBS is operating in a relatively low SNR regime with a transmit power of 10dBW, the lower order modulation QPSK actually outperforms 8PSK in terms of throughput. When the CBS employs OCISB, OPALP, or OCZF, the performance of the PUs will remain constant since the secondary system eliminates all CBS interference at the PUs. Note however that when OCMSM is feasible, the PU throughput actually improves significantly for both the QPSK and 8PSK cases, due to the exploitation of CI from the secondary network which is not available using the other methods. While the algorithm ensures that the worst-case

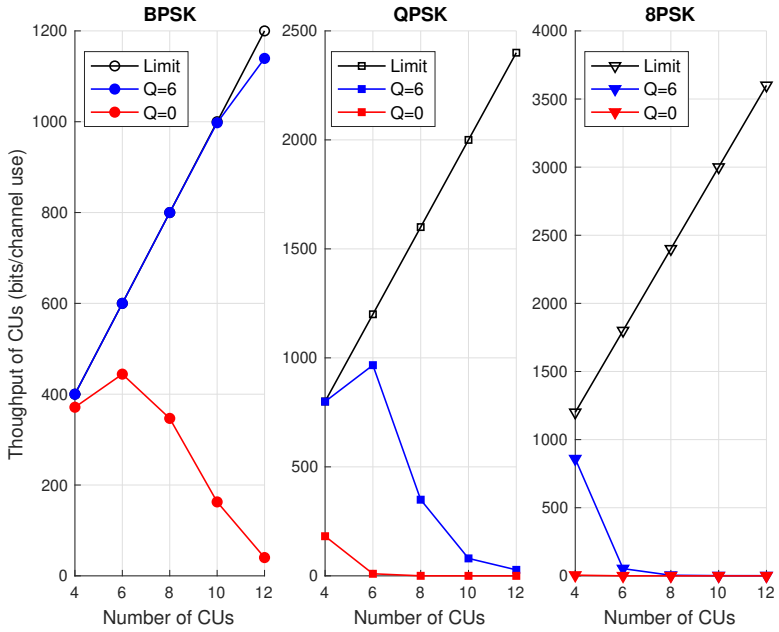

Figure 3.8: Number of CUs vs. CU Throughput in the overlay scenario where $P_p = 10$ dBW, $P_c = 15$ dBW, $M_p = M_c = 8$, $N_p = 4$, $\sigma_c^2 = \sigma_p^2 = 1$ and OCMSM precoding.

SM is not deteriorated, we see that in fact significant extra CI is available from the CBS transmissions. OCMSM is thus a relatively conservative approach; better CU performance could in principle be achieved by using a different constraint that maintained the nominal PU QoS.

3.5.2.2 Number of CUs

For the block-level precoding methods, UCZF and OCZF, the number of CUs served by the CBS and the number of PUs protected from the CBS interference cannot be greater than the number of CBS antennas. However, this restriction does not hold for CI-based symbol level precoding, due to the exploitation of CI and the extra DoFs generated at the symbol level, the transmitter can often serve more users than there are antennas [78]. Fig. 3.8 shows the throughput of the secondary network with OCMSM precoding when the number CBS antennas is 8, the number of PUs is 4, and the number of CUs increases from 4 to 12. For

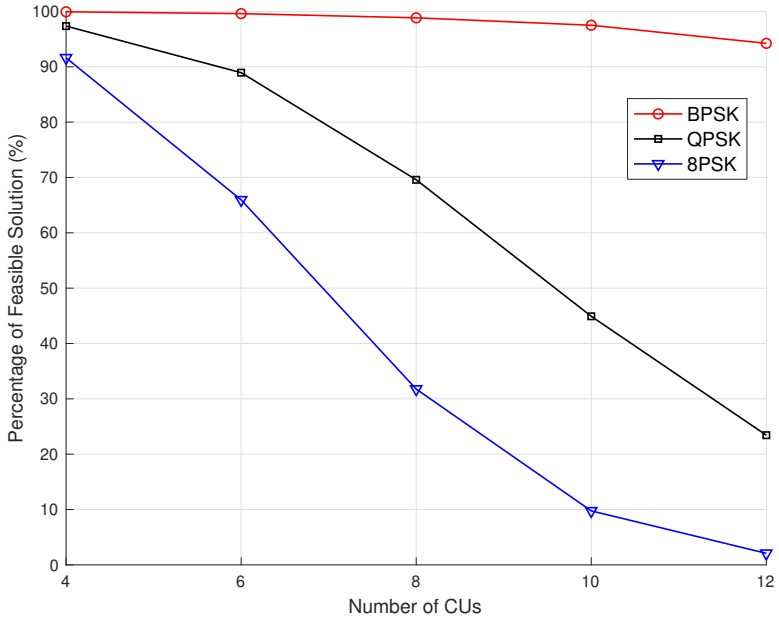

Figure 3.9: Number of CUs vs. Percentage of Feasible Solutions in the overlay scenario where $P_p = 10$ dBW, $P_c = 15$dBW, $M_p = M_c = 8$, $N_p = 4$, $\sigma_c^2 = \sigma_p^2 = 1$ and OCMSM precoding.

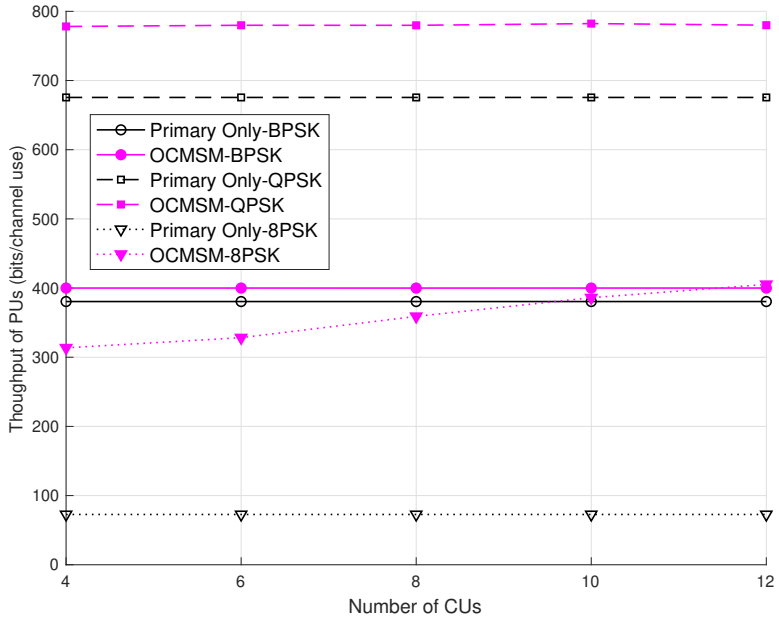

Figure 3.10: Number of CUs vs. PU Throughput in the overlay scenario where $P_p = 10$ dBW, $P_c = 15$dBW, $M_p = M_c = 8$, $N_p = 4$, and $\sigma_c^2 = \sigma_p^2 = 1$.

BPSK modulation with error correction ($Q = 6$), the CU throughput is able to maintain the maximum achievable value as the number of CUs increases, with only a slight degradation beginning with $N_c = 12$. Even without error correction, for BPSK the total CU throughput

increases up to $N_c = 6$ before beginning to decrease. QPSK also achieves an increase in total throughput with error correction when $N_c = 6$, but at this level of CBS transmit power no improvement is achieved for 8-PSK. This suggests that SLP is useful for low-rate applications where massive connectivity is required, such as in IoT networks.

The percentage of feasibile solutions for OCMSM is plotted in Fig. 3.9 when $N_p + N_c \geq M_c$. While feasible solutions are less likely for larger numbers of CUs and higher-order modulation, the degradation is gradual, unlike the block-level algorithms. In Fig. 3.10 we show the PU throughput versus the number of CUs with the primary-only cases as benchmarks. The trend of the curves is similar to that in Fig. 3.7. Regardless of the modulation order, OCMSM is always able to improve the PU throughput. With the aid of CI, the QoS of both the CUs and PUs can be increased without investing more transmission power or directly relaying the primary signals.

3.5.2.3 Robustness to Imperfect CSI

Here we compare the robustness of the overlay algorithms presented above when the CSI is not estimated perfectly. In order to reflect the CSI imperfections, we use a simple model in which the channel estimates $\hat{\mathbf{H}}$ are related to the true channels as follows:

$$\hat{\mathbf{H}} = \sqrt{1-\alpha^2}\mathbf{H} + \alpha\boldsymbol{\epsilon} \tag{3.86}$$

where the scalar $\alpha \in [0, 1]$ specifies the level of CSI inaccuracy, and $\boldsymbol{\epsilon}$ is composed of circular $\mathcal{CN}(0, 1)$ random variables representing the CSI error with each element following a circularly symmetric normal distribution [97]. A value of $\alpha = 0$ indicates that the channel is estimated perfectly while $\alpha = 1$ corresponds to no CSI. Fig. 3.11a and Fig. 3.11b respectively show the BER performance of the PUs and CUs when $\alpha = .03$ for both $\mathbf{H}_{cp}$ and $\mathbf{H}_{cc}$. The BER results for perfect CSI are repeated for comparison. Clearly, the introduction of CSI errors

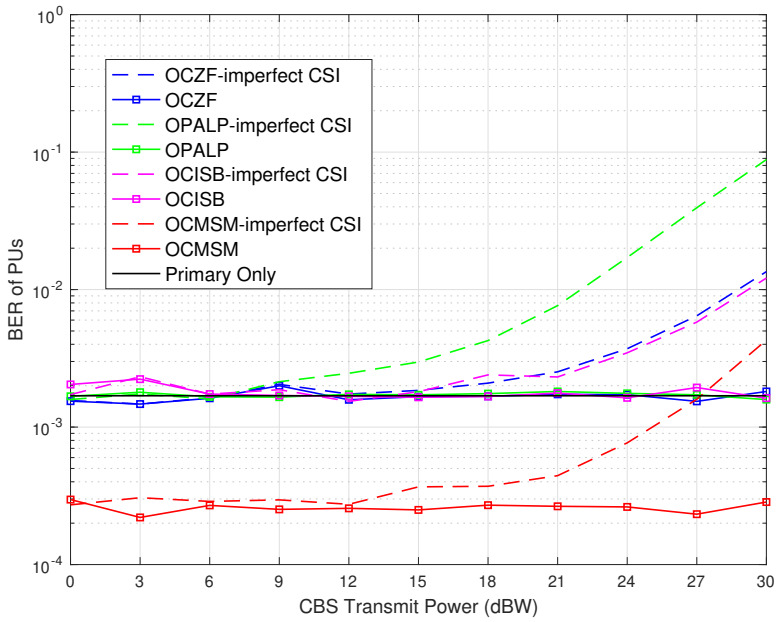

(a) Primary System

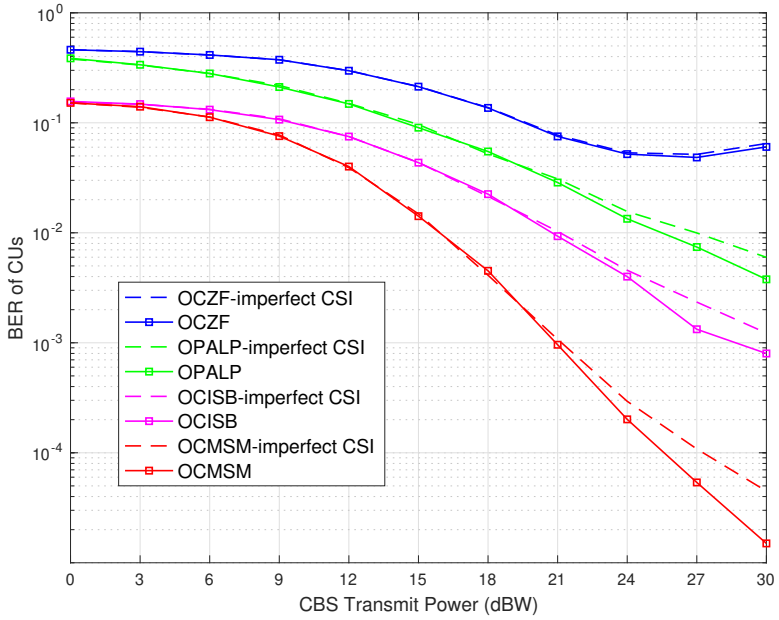

(b) Cognitive System

Figure 3.11: CBS Transmit Power vs. CU BER in the overlay scenario with imperfect CSI where $P_p = 10$ dBW, $M_p = M_c = 8$, $N_p = N_c = 4$, $\sigma_c^2 = \sigma_p^2 = 1$, $\alpha = 3\%$ and QPSK.

degrades the BER regardless of what precoder is used, especially for higher CBS power levels, but the order of performance among the algorithms remains unchanged. The impact on the PUs is clearly much greater than for the CUs, and effectively places a limit on the allowable transmit power at the CBS. However, note that the gain in BER provided by CI

in OCMSM provides some additional robustness to CSI errors. The performane of OCMSM with imperfect CSI is as good as or better than the performance of the other algorithms with perfect CSI for CBS transmit powers up to 27dBW.

3.6 Conclusion

In this chapter, we have proposed a number of different SLP algorithms for underlay and overlay CR networks that take advantage of constructive interference via symbol level precoding. For the underlay case, we reformulated the SINR balancing problem to optimize the CU performance subject to an interference temperature constraint for the PUs, and we also showed how the concept of maximum safety margin can be employed to reformulate the SLP problem. For the overlay case, we have generalized two previous approaches to the problem based on zero-forcing and interference balancing, and we have shown how to extend the SINR balancing and maximum safety margin algorithms to take advantage of the channel and data information shared by the PBS. When feasible, our proposed algorithms achieve significantly improved performance compared with prior overlay solutions since they do not require the CBS to directly relay the PU symbols, but instead allow the benefit of CI to be naturally exploited. While all algorithms are designed to have no negative impact on the performance of the primary network, the interference constraint imposed by the OCMSM algorithm was shown to actually enhance the QoS of the PUs. The SLP-based methods were further shown to allow transitions to higher-order modulation at lower transmit powers in adaptive modulation systems, and allow many more cognitive users than antennas to be served for low-order modulations. Further work is needed to make the algorithms robust to errors in the CSI estimation.

Chapter 4

Robust SLP in Overlay CR Systems

For the case of imperfect CSI from the PBS, we propose robust SLP schemes. First, with a norm-bounded CSI error model to approximate the uncertain channels, we adopt a max-min philosophy to conservatively achieve robust SLP constraints. Second, we use the additive quantization noise model (AQNM) to describe the quantized PBS CSI and employ a stochastic constraint to formulate the problem. Both robust approaches also result in a quadratic objective with linear inequality constraints. Simulation results show that, rather than simply trying to eliminate the network's cross-interference, the proposed robust SLP schemes enable the primary and secondary networks to aid each other in meeting their quality of service constraints.

4.1 System Model and Problem Formulation

We consider a downlink CR network with an M_c-antenna CBS serving N_c single-antenna CUs. The CR network is granted access to share the primary system spectrum in which an M_p-antenna PBS is communicating with N_p single-antenna PUs. The system model is depicted

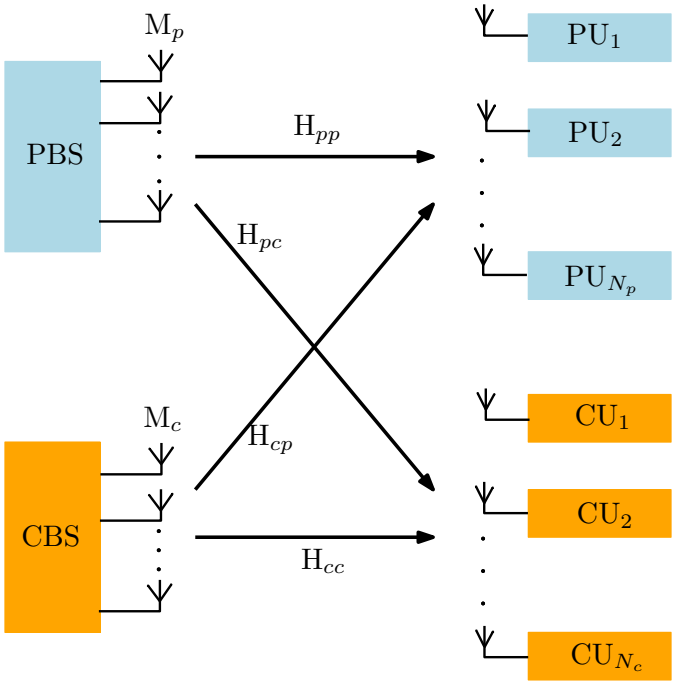

Figure 4.1: Cognitive Radio System Model

in Fig. 4.1. The direct primary and cognitive channels are assumed to be respectively denoted by the following flat-fading model:

$$\mathbf{H}_{pp} = \left[\mathbf{h}_{pp,1}^{\mathrm{T}} \quad \cdots \quad \mathbf{h}_{pp,N_p}^{\mathrm{T}}\right]^{\mathrm{T}} \in \mathbb{C}^{N_p \times M_p} , \tag{4.1}$$

$$\mathbf{H}_{cc} = \left[\mathbf{h}_{cc,1}^{\mathrm{T}} \quad \cdots \quad \mathbf{h}_{cc,N_p}^{\mathrm{T}}\right]^{\mathrm{T}} \in \mathbb{C}^{N_c \times M_c} . \tag{4.2}$$

The corresponding interference channels are defined as

$$\mathbf{H}_{pc} = \left[\mathbf{h}_{pc,1}^{\mathrm{T}} \quad \cdots \quad \mathbf{h}_{pc,N_p}^{\mathrm{T}}\right]^{\mathrm{T}} \in \mathbb{C}^{N_c \times M_p} , \tag{4.3}$$

$$\mathbf{H}_{cp} = \left[\mathbf{h}_{cp,1}^{\mathrm{T}} \quad \cdots \quad \mathbf{h}_{cp,N_p}^{\mathrm{T}}\right]^{\mathrm{T}} \in \mathbb{C}^{N_p \times M_c} \tag{4.4}$$

from the PBS to CUs and the CBS to PUs, respectively. We will leave further specification of the channel models until later.

The vectors $\mathbf{s}_p(t) = [s_{p,1}(t), s_{p,2}(t), \cdots, s_{p,N_p}(t)]^T$ and $\mathbf{s}_c(t) = [s_{c,1}(t), s_{c,2}(t), \cdots, s_{c,N_c}(t)]^T$ will be used to represent the symbols to be transmitted to the individual PUs and CUs, respectively, at time t. In this work we assume for simplicity that all transmitted symbols are uncorrelated and drawn from a D-PSK constellation with unit magnitude, i.e., $s_{l,m}(t) \in \{s|s = \exp(j\pi(2d+1)/D),\ d \in \{0, \cdots, D-1\}\}$ where $l \in \{p, c\}$ denotes the primary or cognitive system, and m denotes the user index in the corresponding system. The sets $\mathcal{K} = \{1, \cdots, N_p\}$ and $\mathcal{J} = \{1, \cdots, N_c\}$ enumerate the PUs and CUs, respectively. The idea of CI precoding can in principle be applied to any constellation design [79], e.g., QAM [84] otherwise, but is most easily formulated for the case of PSK signals. The algorithm for other constellations such as QAM is slightly more complicated since the definition of safety margin becomes dependent on whether an inner, edge, or corner constellation point is transmitted, but the basic principle of the algorithm is the same.

At time slot t, the received signals at the PUs and CUs can be respectively written as

$$\mathbf{y}_p(t) = \mathbf{H}_{pp}\mathbf{x}_p(t) + \mathbf{H}_{cp}\mathbf{x}_c(t) + \mathbf{n}_p(t)\ , \tag{4.5}$$

$$\mathbf{y}_c(t) = \mathbf{H}_{cc}\mathbf{x}_c(t) + \mathbf{H}_{pc}\mathbf{x}_p(t) + \mathbf{n}_c(t)\ , \tag{4.6}$$

where $\mathbf{x}_p(t) \in \mathbb{C}^{M_p \times 1}$ and $\mathbf{x}_c(t) \in \mathbb{C}^{M_c \times 1}$ are the transmitted signals at the PBS and CBS after precoding and power loading, and $\mathbf{n}_p(t) \sim \mathcal{CN}(0, \sigma_p^2)$ and $\mathbf{n}_c(t) \sim \mathcal{CN}(0, \sigma_c^2)$ are additive white Gaussian noise (AWGN) vectors. In order to simplify the notation, in what follows we drop the time index t.

4.1.1 Phase Alignment Linear Precoding (PALP)

Conventional precoding methods such as MMSE, ZF and maximum-SINR beamforming are designed with the objective of minimizing the inter-user interference so that the received symbols lie as close as possible to the nominal constellation points (or scaled versions thereof

in the case of PSK). This is effectively equivalent to ensuring that for each user m, the noise-free received signal $r_m = \mathbf{h}_m \mathbf{x}$ lies within a circle centered at its corresponding constellation point s_m [44], as depicted in Fig. 2.1. The shaded area inside the circle is referred to as the symbol region (SR), a down-scaled version of the decision region for s_m.

The method described in [29] is based on the MMSE criterion and the early Phase Alignment Linear Precoding (PALP) technique for SLP [14]; it is the prior approach most closely related to the algorithms we present in this chapter for cognitive radio scenarios. However, a modification to the PALP approach in [29] is necessary for a fair comparison, and to allow the algorithm to protect the PUs from the CR interference. In particular, we tailor [29] (hereafter referred to as CR-PALP) by allowing different instantaneous power scaling factors at the PBS and CBS:

$$f_p = \sqrt{\frac{P_p}{\mathrm{Tr}\{\mathbf{W}_p \mathbf{s}_p \mathbf{s}_p^H \mathbf{W}_p^H\}}} \ , \ f_c = \sqrt{\frac{P_c}{\mathrm{Tr}\{\mathbf{W}_c \mathbf{s}_c \mathbf{s}_c^H \mathbf{W}_c^H\}}}$$

where P_p and P_c respectively denote the total transmit power of the PBS and CBS, f_p and f_c are the respective instantaneous scaling factors, and $\mathbf{W}_p$ and $\mathbf{W}_c$ are the linear precoders for the primary and cognitive systems, respectively. The generalized MSE criterion for CR-PALP is given by

$$\epsilon = \mathbb{E}\{\|\mathbf{V}_p \mathbf{s} + \mathbf{H}\mathbf{W}_c \mathbf{s} - (\mathbf{A} + \mathbf{B}\mathbf{Q}^{\phi})\mathbf{s}\|^2\} \ , \tag{4.7}$$

where according to [29],

$$\mathbf{V}_p = \begin{bmatrix} \mathbf{H}_{pp}\mathbf{W}_p & \mathbf{0}_{N_p \times N_c} \\ \mathbf{H}_{pc}\mathbf{W}_p & \mathbf{0}_{N_c \times N_c} \end{bmatrix} \ , \quad \mathbf{s} = \begin{bmatrix} \mathbf{s}_p \\ \mathbf{s}_c \end{bmatrix} \ , \quad \mathbf{H} = \begin{bmatrix} \mathbf{H}_{cp} \\ \mathbf{H}_{cc} \end{bmatrix} \ ,$$

$\mathbf{A} = \mathrm{diag}\{[1, \cdots, 1, 0, \cdots, 0]\}$ is a diagonal matrix whose first N_p diagonal elements equal 1, $\mathbf{B} = \mathrm{diag}\{[0, \cdots, 0, 1, \cdots, 1]\}$ is a diagonal matrix whose last N_c elements equal 1, and

$\mathbf{Q}^{\phi} = \text{diag}(\mathbf{s}) \cdot |\mathbf{H}\mathbf{H}^H| \cdot \text{diag}(\mathbf{s})^H$ contains the phase-corrected correlation elements. The precoding matrix at the CBS derived from the MMSE criterion is given by

$$\mathbf{W}_c = \mathbf{H}^H(\mathbf{H}\mathbf{H}^H)^{-1}(\mathbf{A} + \mathbf{B}\mathbf{Q}^{\phi} - \mathbf{V}_p) \ , \tag{4.8}$$

and the received signals at the PUs and CUs are

$$\mathbf{y}_p = f_p\mathbf{s}_p + \mathbf{n}_p \ , \tag{4.9}$$

$$\mathbf{y}_c = (f_p - f_c)\mathbf{H}_{pc}\mathbf{W}_p\mathbf{s}_p + f_c\mathbf{Q}_c^{\phi}\mathbf{s}_c + \mathbf{n}_c \ . \tag{4.10}$$

The performance of the PUs in our CR scenario will not be impaired using this modified CR-PALP approach, unlike using the method of [29] directly.

4.1.2 SM-constrained SLP

For PSK constellations, it is not necessary that r_m be close to s_m in order to be decoded correctly, as long as it lies in the correct decision region with a given level of certainty. Thus, it is not necessary that all of the inter-user interference be eliminated, since some interference components could add constructively and push the received symbol further into the decision region, making it more robust to noise and interference external to the system. We can thus redefine the SR as, for example, in Fig. 2.2, where the SR becomes a displaced version of the circular sector of angular extent $2\pi/D$ centered at the origin and corresponding to s_m. This displaced sector has an infinite radius, and all points within it are at least a certain distance δ_m from the decision boundaries for s_m. This region is referred to as a constructive interference region with safety margin δ_m [82]. The larger δ_m, the more robust the received signal will be to noise, interference, modeling errors, or other impairments.

In order to mathematically interpret the CIR and SM in a unified way, we rotate the original coordinate system by the negative phase of the desired constellation symbol, i.e., $\measuredangle s_m^*$, to obtain the modified coordinate system in Fig. 2.3. After rotation, s_m is placed at 1 on the real axis, and r_m is relocated to

$$z_m = s_m^* r_m \ . \tag{4.11}$$

Then we can easily calculate the SM of the noise-free symbol at user m as [82, 84]

$$\delta_m = \mathcal{R}\{z_m\} \sin\theta - |\mathcal{I}\{z_m\}| \cos\theta. \tag{4.12}$$

Ideally, the SM should be large enough to sufficiently reduce the probability that noise or other impairments will push the noise-free signal outside the desired detection region; the larger the SM, the smaller the SER. To design the precoder, one can constrain the SM to be above a certain threshold to ensure a given target SER. The fact that the CIR in Fig. 2.3 is much larger than the SR in Fig. 2.2 means that increased flexibility is available to achieve the given performance objective. In this chapter, we will consider the following type of SLP optimization, which minimizes the transmit power to achieve a certain desired SM:

$$\min_{\mathbf{x}} \quad \|\mathbf{x}\|^2 \tag{4.13}$$

$$\text{subject to} \quad \delta_m \geq \delta_{m,0} \ , \quad \forall m \in \mathcal{M} \tag{4.14}$$

where $\delta_{m,0}$ is the desired minimum SM for user m and $\mathcal{M} = \{1, \cdots, M\}$ indexes the users.

4.2 Power Minimization SLP in CR

Before considering the robust SLP design, we first examine the simpler case where the PBS shares its data and perfect CSI with the CBS. The SM for each PU and CU is assumed to be constrained to be $\delta_{p,k}^0$ for $k \in \mathcal{K}$ and $\delta_{c,j}^0$ for $j \in \mathcal{J}$, corresponding for example to possibly different target SERs for each PU and SU. Here we focus on SLP designs that minimize the transmit power at the CBS and achieve the SM QoS constraints at both the PUs and CUs.

4.2.1 Primary System

The rotated symbols received at the PUs can be expressed as

$$z_{p,k} = s_{p,k}^* r_{p,k} = s_{p,k}^* (\mathbf{h}_{pp,k}\mathbf{x}_p + \mathbf{h}_{cp,k}\mathbf{x}_c), \tag{4.15}$$

for $k \in \mathcal{K}$. Defining

$$\tilde{\mathbf{h}}_{pp,k} \triangleq s_{p,k}^* \mathbf{h}_{pp,k}, \quad \tilde{\mathbf{h}}_{cp,k} \triangleq s_{p,k}^* \mathbf{h}_{cp,k} \ , \tag{4.16}$$

we have

$$z_{p,k} = \tilde{\mathbf{h}}_{pp,k}\mathbf{x}_p + \tilde{\mathbf{h}}_{cp,k}\mathbf{x}_c. \tag{4.17}$$

The constraints ensuring the QoS of the PUs can be expressed as

$$\delta_{p,k} = \mathcal{R}\{z_{p,k}\}\sin\theta - |\mathcal{I}\{z_{p,k}\}|\cos\theta \geq \delta_{p,k}^0 \, , \forall k \in \mathcal{K} \tag{4.18}$$

which is equivalent to

$$\begin{cases} \mathcal{R}\{\tilde{\mathbf{h}}_{pp,k}\mathbf{x}_p\}\sin\theta - \mathcal{I}\{\tilde{\mathbf{h}}_{pp,k}\mathbf{x}_p\}\cos\theta + \mathcal{R}\{\tilde{\mathbf{h}}_{cp,k}\mathbf{x}_c\}\sin\theta - \mathcal{I}\{\tilde{\mathbf{h}}_{cp,k}\mathbf{x}_c\}\cos\theta \geq \delta^0_{p,k} \ , \\ \mathcal{R}\{\tilde{\mathbf{h}}_{pp,k}\mathbf{x}_p\}\sin\theta + \mathcal{I}\{\tilde{\mathbf{h}}_{pp,k}\mathbf{x}_p\}\cos\theta + \mathcal{R}\{\tilde{\mathbf{h}}_{cp,k}\mathbf{x}_c\}\sin\theta + \mathcal{I}\{\tilde{\mathbf{h}}_{cp,k}\mathbf{x}_c\}\cos\theta \geq \delta^0_{p,k} \ . \end{cases}$$

For any given complex vector $\mathbf{x}$, we define the operator

$$\mho(\mathbf{x}) \triangleq \begin{bmatrix} \mathcal{R}\{\mathbf{x}\}\sin\theta - \mathcal{I}\{\mathbf{x}\}\cos\theta & -\mathcal{R}\{\mathbf{x}\}\cos\theta - \mathcal{I}\{\mathbf{x}\}\sin\theta \\ \mathcal{R}\{\mathbf{x}\}\sin\theta + \mathcal{I}\{\mathbf{x}\}\cos\theta & \mathcal{R}\{\mathbf{x}\}\cos\theta - \mathcal{I}\{\mathbf{x}\}\sin\theta \end{bmatrix} \tag{4.19}$$

and denote

$$\widetilde{\mathbf{H}}^{\mho}_{pp,k} = \mho(\tilde{\mathbf{h}}_{pp,k}), \quad \widetilde{\mathbf{H}}^{\mho}_{cp,k} = \mho(\tilde{\mathbf{h}}_{cp,k}). \tag{4.20}$$

Using the following real-valued notation,

$$\check{\mathbf{x}}_p = \begin{bmatrix} \mathcal{R}\{\mathbf{x}_p\} \\ \mathcal{I}\{\mathbf{x}_p\} \end{bmatrix}, \quad \check{\mathbf{x}}_c = \begin{bmatrix} \mathcal{R}\{\mathbf{x}_c\} \\ \mathcal{I}\{\mathbf{x}_c\} \end{bmatrix}, \tag{4.21}$$

the constraints in Eq. (4.18) can be simplified as

$$\widetilde{\mathbf{H}}^{\mho}_{pp,k}\check{\mathbf{x}}_p + \widetilde{\mathbf{H}}^{\mho}_{cp,k}\check{\mathbf{x}}_c \geq \delta^0_{p,k}\mathbf{1}_2 \ , \quad \forall k \in \mathcal{K} \ . \tag{4.22}$$

4.2.2 Cognitive System

Similarly, the rotated symbols at the CUs can be written as

$$z_{c,j} = s^*_{c,j} r_{c,j} = s^*_{c,j}(\mathbf{h}_{cc,j}\mathbf{x}_c + \mathbf{h}_{pc,j}\mathbf{x}_p) = \tilde{\mathbf{h}}_{cc,j}\mathbf{x}_c + \tilde{\mathbf{h}}_{pc,j}\mathbf{x}_p \ , \tag{4.23}$$

where

$$\tilde{\mathbf{h}}_{cc,j} \triangleq s^*_{c,j}\mathbf{h}_{cc,j} \ , \quad \tilde{\mathbf{h}}_{pc,j} \triangleq s^*_{c,j}\mathbf{h}_{pc,j} \ . \tag{4.24}$$

The SM constraints at the CUs can be expressed as

$$\begin{cases} \mathcal{R}\{\tilde{\mathbf{h}}_{cc,j}\mathbf{x}_c\}\sin\theta - \mathcal{I}\{\tilde{\mathbf{h}}_{cc,j}\mathbf{x}_c\}\cos\theta + \mathcal{R}\{\tilde{\mathbf{h}}_{pc,j}\mathbf{x}_p\}\sin\theta - \mathcal{I}\{\tilde{\mathbf{h}}_{pc,j}\mathbf{x}_p\}\cos\theta \geq \delta^0_{c,j} \ , \\ \mathcal{R}\{\tilde{\mathbf{h}}_{cc,j}\mathbf{x}_c\}\sin\theta + \mathcal{I}\{\tilde{\mathbf{h}}_{cc,j}\mathbf{x}_c\}\cos\theta\mathcal{R}\{\tilde{\mathbf{h}}_{pc,j}\mathbf{x}_p\}\sin\theta + \mathcal{I}\{\tilde{\mathbf{h}}_{pc,j}\mathbf{x}_p\}\cos\theta \geq \delta^0_{c,j} \ , \end{cases}$$

for $j \in \mathcal{J}$, which can again be written more compactly using the operator in Eq. (4.19):

$$\widetilde{\mathbf{H}}^{\mho}_{cc,j}\check{\mathbf{x}}_c + \widetilde{\mathbf{H}}^{\mho}_{pc,j}\check{\mathbf{x}}_p \geq \delta^0_{c,j}\mathbf{1}_2 \ , \quad \forall j \in \mathcal{J} \ . \tag{4.25}$$

Combining all of the above notation together, we can express the general power minimization SLP problem with perfect CSI as follows:

$$\min_{\check{\mathbf{x}}_c} \quad \|\check{\mathbf{x}}_c\|^2 \tag{4.26}$$

$$\text{subject to} \quad \begin{bmatrix} -\widetilde{\mathbf{H}}^{\mho}_{cp} \\ -\widetilde{\mathbf{H}}^{\mho}_{cc} \end{bmatrix} \check{\mathbf{x}}_c \leq \begin{bmatrix} \widetilde{\mathbf{H}}^{\mho}_{pp} \\ \widetilde{\mathbf{H}}^{\mho}_{pc} \end{bmatrix} \check{\mathbf{x}}_p - \begin{bmatrix} \boldsymbol{\delta}^0_p \otimes \mathbf{1}_2 \\ \boldsymbol{\delta}^0_c \otimes \mathbf{1}_2 \end{bmatrix} \tag{4.27}$$

where the inequalities are to be interpreted element-wise, $\boldsymbol{\delta}^0_p = \begin{bmatrix} \delta^0_{p,1} & \cdots & \delta^0_{p,N_p} \end{bmatrix}^T$, $\boldsymbol{\delta}^0_c = \begin{bmatrix} \delta^0_{c,1} & \cdots & \delta^0_{c,N_c} \end{bmatrix}^T$, and $\widetilde{\mathbf{H}}^{\mho}_{ab} \triangleq \mho(\text{diag}(\mathbf{s}^*_b)\mathbf{H}_{ab})$, with $a, b \in \{c, p\}$. The result is a quadratic programming problem with linear inequality constraints which can be efficiently solved using a variety of numerical methods.

4.3 Robust SLP for Norm-Bounded CSI Errors

In practice, the CSI shared by the PBS with the CBS will be imperfect due for example to quantization, or somewhat outdated due to delays required for processing and transmission. As a result, robust precoding designs are critical for overlay systems. We address such a design in this section for the case where the imperfect CSI can be described in terms of a norm-bounded error. We model the CSI shared by the PBS with the CBS as follows:

$$\mathbf{h}_{pp,k} = \hat{\mathbf{h}}_{pp,k} + \mathbf{e}_{p,k} \ , \tag{4.28}$$

$$\mathbf{h}_{pc,j} = \hat{\mathbf{h}}_{pc,j} + \mathbf{e}_{c,j} \ , \tag{4.29}$$

where the $\hat{\cdot}$ indicates the shared CSI and $\mathbf{e}_{p,k}, \mathbf{e}_{c,j}$ are norm-bounded CSI error vectors, i.e., $\|\mathbf{e}_{p,k}\|_2 \leq \epsilon_{p,k}$ and $\|\mathbf{e}_{c,j}\|_2 \leq \epsilon_{c,j}$. No other assumption regarding the channels is required. Using Eq. (4.19), it is easy to show that

$$\widetilde{\mathbf{H}}^{\mho}_{pp,k} = \mho(\tilde{\mathbf{h}}_{pp,k}) = \mho(s^*_{p,k}(\hat{\mathbf{h}}_{pp,k} + \mathbf{e}_{p,k})) = \bar{\mathbf{H}}^{\mho}_{pp,k} + \tilde{\mathbf{E}}^{\mho}_{p,k} \ , \tag{4.30}$$

$$\widetilde{\mathbf{H}}^{\mho}_{pc,j} = \mho(\tilde{\mathbf{h}}_{pc,j}) = \mho(s^*_{c,j}(\hat{\mathbf{h}}_{pc,j} + \mathbf{e}_{c,j})) = \bar{\mathbf{H}}^{\mho}_{pc,j} + \tilde{\mathbf{E}}^{\mho}_{c,j}, \tag{4.31}$$

where $\bar{\mathbf{h}}_{pp,k} \triangleq s^*_{p,k}\hat{\mathbf{h}}_{pp,k}$, $\bar{\mathbf{H}}^{\mho}_{pp,k} \triangleq \mho(\bar{\mathbf{h}}_{pp,k})$, $\tilde{\mathbf{E}}^{\mho}_{p,k} \triangleq \mho(s^*_{p,k}\mathbf{e}_{p,k})$, $\bar{\mathbf{h}}_{pc,j} \triangleq s^*_{c,j}\hat{\mathbf{h}}_{pc,j}$, $\bar{\mathbf{H}}^{\mho}_{pc,j} \triangleq \mho(\bar{\mathbf{h}}_{pc,j})$, and $\tilde{\mathbf{E}}^{\mho}_{c,j} \triangleq \mho(s^*_{c,j}\mathbf{e}_{c,j})$. Due to the uncertainty in $\mathbf{h}_{pp,k}$, the transmitted signal at the PBS, i.e., $\mathbf{x}_p$, which necessarily depends on $\mathbf{h}_{pp,k}$, is not precisely known. Assuming that the precoding method used at the PBS is known to the CBS, we will assume that an estimate of the transmitted signal, denoted by $\check{\mathbf{x}}^e_p$, can be computed by the CBS using the quantized CSI $\hat{\mathbf{h}}_{pp,k}$. With this notation, the constraints in 4.26 can be reformulated as

$$(\bar{\mathbf{H}}^{\mho}_{pp,k} + \tilde{\mathbf{E}}^{\mho}_{p,k})\check{\mathbf{x}}^e_p + \widetilde{\mathbf{H}}^{\mho}_{cp,k}\check{\mathbf{x}}_c \geq \delta^0_{p,k}\mathbf{1}_2, \ \forall k \in \mathcal{K} \ , \tag{4.32}$$

$$\widetilde{\mathbf{H}}^{\mho}_{cc,j}\check{\mathbf{x}}_c + (\bar{\mathbf{H}}^{\mho}_{pc,j} + \tilde{\mathbf{E}}^{\mho}_{c,j})\check{\mathbf{x}}^e_p \geq \delta^0_{c,j}\mathbf{1}_2, \ \forall j \in \mathcal{J}. \tag{4.33}$$

For a robust bounded-CSI-error design, we desire that the above constraints hold for every possible error realization and every user:

$$-\tilde{\mathbf{E}}_{p,k}^{\mho}\check{\mathbf{x}}_p^e \leq \bar{\mathbf{H}}_{pp,k}^{\mho}\check{\mathbf{x}}_p^e + \widetilde{\mathbf{H}}_{cp,k}^{\mho}\check{\mathbf{x}}_c - \delta_{p,k}^0\mathbf{1}_2\ ,\ \forall\|\mathbf{e}_{p,k}\|_2 \leq \epsilon_{p,k},\ \forall k \in \mathcal{K}\ , \tag{4.34}$$

$$-\tilde{\mathbf{E}}_{c,j}^{\mho}\check{\mathbf{x}}_p^e \leq \widetilde{\mathbf{H}}_{cc,j}^{\mho}\check{\mathbf{x}}_c + \bar{\mathbf{H}}_{pc,j}^{\mho}\check{\mathbf{x}}_p^e - \delta_{c,j}^0\mathbf{1}_2\ ,\ \forall\|\mathbf{e}_{c,j}\|_2 \leq \epsilon_{c,j},\ \forall j \in \mathcal{J}\ . \tag{4.35}$$

We separate the operator $\mho(\mathbf{x})$ into two parts, as follows:

$$\mho(\mathbf{x}) \triangleq \begin{bmatrix}\mho_1(\mathbf{x})\\ \mho_2(\mathbf{x})\end{bmatrix} \triangleq \begin{bmatrix}\mathbf{x}^{\mho_1}\\ \mathbf{x}^{\mho_2}\end{bmatrix}, \tag{4.36}$$

where

$$\mho_1(\mathbf{x}) = \mathbf{x}^{\mho_1} = \begin{bmatrix}\mathcal{R}\{\mathbf{x}^T\}\sin\theta - \mathcal{I}\{\mathbf{x}^T\}\cos\theta\\ -\mathcal{R}\{\mathbf{x}^T\}\cos\theta - \mathcal{I}\{\mathbf{x}^T\}\sin\theta\end{bmatrix}^T, \tag{4.37}$$

$$\mho_2(\mathbf{x}) = \mathbf{x}^{\mho_2} = \begin{bmatrix}\mathcal{R}\{\mathbf{x}^T\}\sin\theta + \mathcal{I}\{\mathbf{x}^T\}\cos\theta\\ \mathcal{R}\{\mathbf{x}^T\}\cos\theta - \mathcal{I}\{\mathbf{x}^T\}\sin\theta\end{bmatrix}^T, \tag{4.38}$$

so that constraint (4.34) can be rewritten in two parts as

$$-\tilde{\mathbf{e}}_{p,k}^{\mho_1}\check{\mathbf{x}}_p^e \leq \bar{\mathbf{h}}_{pp,k}^{\mho_1}\check{\mathbf{x}}_p^e + \widetilde{\mathbf{h}}_{cp,k}^{\mho_1}\check{\mathbf{x}}_c - \delta_{p,k}^0\ ,\ \forall\|\mathbf{e}_{p,k}\|_2 \leq \epsilon_{p,k},\ \forall k \in \mathcal{K}\ , \tag{4.39a}$$

$$-\tilde{\mathbf{e}}_{p,k}^{\mho_2}\check{\mathbf{x}}_p^e \leq \bar{\mathbf{h}}_{pp,k}^{\mho_2}\check{\mathbf{x}}_p^e + \widetilde{\mathbf{h}}_{cp,k}^{\mho_2}\check{\mathbf{x}}_c - \delta_{p,k}^0\ ,\ \forall\|\mathbf{e}_{c,j}\|_2 \leq \epsilon_{c,j},\ \forall j \in \mathcal{J}\ . \tag{4.39b}$$

Note that

$$
\begin{aligned}
&\| - \tilde{\mathbf{e}}_{p,k}^{\mho_1} \check{\mathbf{x}}_p^e \|_2 \\
\leq & \| - \tilde{\mathbf{e}}_{p,k}^{\mho_1} \|_2 \| \check{\mathbf{x}}_p^e \|_2 \\
= & \left\| \begin{bmatrix} \mathcal{R}\{\mathbf{e}_{p,k}^T\} & \mathcal{I}\{\mathbf{e}_{p,k}^T\} \end{bmatrix} \begin{bmatrix} \sin\theta & -\cos\theta \\ -\cos\theta & -\sin\theta \end{bmatrix} \right\|_F \left\| \check{\mathbf{x}}_p^e \right\|_2 \\
\leq & \left\| \begin{bmatrix} \mathcal{R}\{\mathbf{e}_{p,k}^T\} & \mathcal{I}\{\mathbf{e}_{p,k}^T\} \end{bmatrix} \right\|_F \left\| \begin{bmatrix} \sin\theta & -\cos\theta \\ -\cos\theta & -\sin\theta \end{bmatrix} \right\|_F \left\| \check{\mathbf{x}}_p^e \right\|_2 \\
\leq & \sqrt{2} \epsilon_{p,k} \| \check{\mathbf{x}}_p^e \|_2
\end{aligned}
$$

and similarly, we can show $\| - \tilde{\mathbf{e}}_{p,k}^{\mho_2} \check{\mathbf{x}}_p^e \|_2 \leq \sqrt{2} \epsilon_{p,k} \| \check{\mathbf{x}}_p^e \|_2$. Thus, if we can guarantee that the following constraints are satisfied, namely

$$
\begin{aligned}
&\bar{\mathbf{H}}_{pp,k}^{\mho} \check{\mathbf{x}}_p^e + \widetilde{\mathbf{H}}_{cp,k}^{\mho} \check{\mathbf{x}}_c \geq (\sqrt{2} \epsilon_{p,k} \| \check{\mathbf{x}}_p^e \|_2 + \delta_{p,k}^0) \mathbf{1}_2, \ \forall k \in \mathcal{K} \ , \\
&\bar{\mathbf{H}}_{pc,j}^{\mho} \check{\mathbf{x}}_p^e + \widetilde{\mathbf{H}}_{cc,j}^{\mho} \check{\mathbf{x}}_c \geq (\sqrt{2} \epsilon_{c,j} \| \check{\mathbf{x}}_p^e \|_2 + \delta_{c,j}^0) \mathbf{1}_2, \ \forall j \in \mathcal{J} \ ,
\end{aligned}
$$

then the constraints in (4.34) and (4.35) will be satisfied as well.

Using the above results, we obtain the robust precoder by solving the following optimization problem:

$$
\begin{aligned}
\min_{\check{\mathbf{x}}_c} \quad & \| \check{\mathbf{x}}_c \|^2 && (4.40) \\
\text{subject to} \quad & \bar{\mathbf{H}}_{pp,k}^{\mho} \check{\mathbf{x}}_p^e + \widetilde{\mathbf{H}}_{cp,k}^{\mho} \check{\mathbf{x}}_c \geq (\sqrt{2} \epsilon_{p,k} \| \check{\mathbf{x}}_p^e \|_2 + \delta_{p,k}^0) \mathbf{1}_2 \ , \ \forall k \in \mathcal{K} \ , && (4.41) \\
& \bar{\mathbf{H}}_{pc,j}^{\mho} \check{\mathbf{x}}_p^e + \widetilde{\mathbf{H}}_{cc,j}^{\mho} \check{\mathbf{x}}_c \geq (\sqrt{2} \epsilon_{c,j} \| \check{\mathbf{x}}_p^e \|_2 + \delta_{c,j}^0) \mathbf{1}_2 \ , \ \forall j \in \mathcal{J} \ . && (4.42)
\end{aligned}
$$

As in the case with perfect CSI, the robust SLP design can be found via a quadratic program with linear inequality constraints.

4.4 Robust SLP for Stochastic CSI Errors

The bounded error model above is a very conservative approach, given its goal of ensuring that the SM constraints are met for all possible CSI error realizations. A less conservative approach that allows constraint violations with some acceptably small probability is to assume a statistical CSI error model. As an example, in this section we consider the case where such a model for the PBS CSI error is available due to knowledge of how the channel is quantized. In particular, we assume that the channels $\mathbf{h}_{pp,k}^{Q}$ and $\mathbf{h}_{pc,j}^{Q}$ shared by the PBS are element-wise quantized, and we use the approximate additive quantization noise model (AQNM) [49, 50] to describe their resulting statistics. Other models are possible based on the specific quantization method employed.

We assume that the channels are Gaussian with zero mean and covariance given by

$$\mathbb{R}_{\mathbf{h}_{pp,k}} \triangleq \mathbb{E}\{\mathbf{h}_{pp,k}^{\mathrm{H}}\mathbf{h}_{pp,k}\} = \beta_p \mathbf{I}_{M_p} \ , \tag{4.43}$$

$$\mathbb{R}_{\mathbf{h}_{pc,j}} \triangleq \mathbb{E}\{\mathbf{h}_{pc,j}^{\mathrm{H}}\mathbf{h}_{pc,j}\} = \beta_c \mathbf{I}_{M_p} \ . \tag{4.44}$$

Using AQNM, the quantized CSI from the PBS after rotation is expressed as

$$\widetilde{\mathbf{h}}_{pp,k}^{Q} = \mathbb{Q}(\widetilde{\mathbf{h}}_{pp,k}) \approx \alpha_p \widetilde{\mathbf{h}}_{pp,k} + \widetilde{\mathbf{n}}_{pp,k}^{Q} \ , \tag{4.45}$$

$$\widetilde{\mathbf{h}}_{pc,j}^{Q} = \mathbb{Q}(\widetilde{\mathbf{h}}_{pc,j}) \approx \alpha_c \widetilde{\mathbf{h}}_{pc,j} + \widetilde{\mathbf{n}}_{pc,j}^{Q} \ , \tag{4.46}$$

where $\mathbb{Q}(\cdot)$ is a scalar quantization function applied element-wise and separately to the real and imaginary parts of the input. The vectors $\widetilde{\mathbf{n}}_{pp,k}^{Q} \triangleq s_{p,k}^{*}\mathbf{n}_{pp,k}^{Q} \in \mathbb{C}^{1\times M_p}$ and $\widetilde{\mathbf{n}}_{pc,j}^{Q} \triangleq s_{c,j}^{*}\mathbf{n}_{pc,j}^{Q} \in \mathbb{C}^{1\times M_p}$ denote the zero-mean Gaussian-distributed quantization noise vectors, and both are assumed to be uncorrelated with $\widetilde{\mathbf{h}}_{pp,k}$ and $\widetilde{\mathbf{h}}_{pc,j}$. The gains $\alpha_k = 1-\rho_k$ for $k \in \{p, c\}$

Table 4.1: Distortion Factors for Different Quantization Bit Resolutions

b	1	2	3	4	5
ρ	0.3634	0.1175	0.03454	0.009497	0.002499

are functions of the following distortion factors [51]:

$$\rho_p = \frac{\mathbb{E}\{\|\mathbf{h}_{pp,k} - \mathbf{h}_{pp,k}^Q\|^2\}}{\mathbb{E}\{\|\mathbf{h}_{pp,k}\|^2\}},\ \rho_c = \frac{\mathbb{E}\{\|\mathbf{h}_{pc,j} - \mathbf{h}_{pc,j}^Q\|^2\}}{\mathbb{E}\{\|\mathbf{h}_{pc,j}\|^2\}}\ .$$

The value of ρ is given in Table 4.1 for different bit resolutions b assuming an optimal non-uniform Lloyd-Max quantizer [54]. The phase rotation does not alter the covariance matrices of the quantization noise, which are given by [49]

$$\mathbb{R}_{\widetilde{\mathbf{n}}_{pp,k}^Q} = \alpha_p\rho_p\text{diag}\{\mathbb{R}_{\mathbf{h}_{pp,k}}\} = \alpha_p\rho_p\beta_p\mathbf{I}_{M_p},$$
$$\mathbb{R}_{\widetilde{\mathbf{n}}_{pc,j}^Q} = \alpha_c\rho_c\text{diag}\{\mathbb{R}_{\mathbf{h}_{pc,j}}\} = \alpha_c\rho_c\beta_c\mathbf{I}_{M_p}.$$

Based on Eq. (4.45) and Eq. (4.46), we can derive

$$\widetilde{\mathbf{h}}_{pp,k} = \frac{\widetilde{\mathbf{h}}_{pp,k}^Q - \widetilde{\mathbf{n}}_{pp,k}^Q}{\alpha_p} = \bar{\alpha_p}\widetilde{\mathbf{h}}_{pp,k}^Q - \bar{\alpha_p}\widetilde{\mathbf{n}}_{pp,k}^Q\ ,$$
$$\widetilde{\mathbf{h}}_{pc,j} = \frac{\widetilde{\mathbf{h}}_{pc,j}^Q - \widetilde{\mathbf{n}}_{pc,j}^Q}{\alpha_c} = \bar{\alpha_c}\widetilde{\mathbf{h}}_{pc,j}^Q - \bar{\alpha_c}\widetilde{\mathbf{n}}_{pc,j}^Q\ ,$$

where $\bar{\alpha_p} = \frac{1}{\alpha_p}$ and $\bar{\alpha_c} = \frac{1}{\alpha_c}$. Therefore,

$$\widetilde{\mathbf{H}}_{pp,k}^{\mho} = \mho(\bar{\alpha_p}\widetilde{\mathbf{h}}_{pp,k}^Q - \bar{\alpha_p}\widetilde{\mathbf{n}}_{pp,k}^Q) = \bar{\alpha_p}(\widetilde{\mathbf{H}}_{pp,k}^{Q,\mho} - \widetilde{\mathbf{N}}_{pp,k}^{Q,\mho})\ , \tag{4.47}$$
$$\widetilde{\mathbf{H}}_{pc,j}^{\mho} = \mho(\bar{\alpha_c}\widetilde{\mathbf{h}}_{pc,j}^Q - \bar{\alpha_c}\widetilde{\mathbf{n}}_{pc,j}^Q) = \bar{\alpha_c}(\widetilde{\mathbf{H}}_{pc,j}^{Q,\mho} - \widetilde{\mathbf{N}}_{pc,j}^{Q,\mho}), \tag{4.48}$$

where $\widetilde{\mathbf{H}}_{pp,k}^{Q,\mho} \triangleq \mho(\widetilde{\mathbf{h}}_{pp,k}^{Q})$, $\widetilde{\mathbf{N}}_{pp,k}^{Q,\mho} \triangleq \mho(\widetilde{\mathbf{n}}_{pp,k}^{Q})$, $\widetilde{\mathbf{H}}_{pc,j}^{Q,\mho} \triangleq \mho(\widetilde{\mathbf{h}}_{pc,j}^{Q})$, and $\widetilde{\mathbf{N}}_{pc,j}^{Q,\mho} \triangleq \mho(\widetilde{\mathbf{n}}_{pc,j}^{Q})$. Substituting Eq. (4.47) and Eq. (4.48) in (4.27), we have

$$\bar{\alpha_p}(\widetilde{\mathbf{H}}_{pp,k}^{Q,\mho} - \widetilde{\mathbf{N}}_{pp,k}^{Q,\mho})\check{\mathbf{x}}_p + \widetilde{\mathbf{H}}_{cp,k}^{\mho}\check{\mathbf{x}}_c \geq \delta_{p,k}^{0}\mathbf{1}_2, \forall k \in \mathcal{K}, \tag{4.49}$$

$$\widetilde{\mathbf{H}}_{cc,j}^{\mho}\check{\mathbf{x}}_c + \bar{\alpha_c}(\widetilde{\mathbf{H}}_{pc,j}^{Q,\mho} - \widetilde{\mathbf{N}}_{pc,j}^{Q,\mho})\check{\mathbf{x}}_p \geq \delta_{c,j}^{0}\mathbf{1}_2, \forall j \in \mathcal{J}. \tag{4.50}$$

4.4.1 Primary System

As a special case to fix the details, we assume that the PBS employs ZF precoding to cancel the interference among the PUs. Thus, the transmit symbol at the PBS can be expressed as

$$\mathbf{x}_p = f_p \mathbf{H}_{pp}^{H}(\mathbf{H}_{pp}\mathbf{H}_{pp}^{H})^{-1}\mathbf{s}_p \ , \tag{4.51}$$

where

$$f_p = \sqrt{\frac{P_p}{\mathrm{Tr}\{(\mathbf{H}_{pp}\mathbf{H}_{pp}^{H})^{-1}\}}}$$

is the scaling factor to satisfy the PBS power budget. Then we will have

$$\begin{aligned}
&(\widetilde{\mathbf{H}}_{pp,k}^{Q,\mho} - \widetilde{\mathbf{N}}_{pp,k}^{Q,\mho})\check{\mathbf{x}}_p \\
=&\alpha_p \widetilde{\mathbf{H}}_{pp,k}^{\mho}\check{\mathbf{x}}_p \\
=&\alpha_p \begin{bmatrix} \mathcal{R}\{\tilde{\mathbf{h}}_{pp,k}\mathbf{x}_p\}\sin\theta - \mathcal{I}\{\tilde{\mathbf{h}}_{pp,k}\mathbf{x}_p\}\cos\theta \\ \mathcal{R}\{\tilde{\mathbf{h}}_{pp,k}\mathbf{x}_p\}\sin\theta + \mathcal{I}\{\tilde{\mathbf{h}}_{pp,k}\mathbf{x}_p\}\cos\theta \end{bmatrix} \\
=&\alpha_p f_p \sin\theta \mathbf{1}_2
\end{aligned}$$

due to $\tilde{\mathbf{h}}_{pp,k}\mathbf{x}_p = s_{p,k}^{*} f_p s_{p,k} = f_p$, which is not surprising, since even with imperfect CSI, the CBS can assume the ZF precoding at the PBS is successful in delivering the desired symbols

to the users. The exact value of the scaling factor f_p depends on the true channel $\mathbf{H}_{pp}$, but the CBS can employ an estimate based on its quantized approximation:

$$f_p^Q = \sqrt{\frac{P_p}{\mathrm{Tr}\{(\mathbf{H}_{pp}^Q(\mathbf{H}_{pp}^Q)^H)^{-1}\}}} \ ,$$

where $\mathbf{H}_{pp}^Q = \left[(\mathbf{h}_{pp,1}^Q)^{\mathrm{T}} \ \ \cdots \ \ (\mathbf{h}_{pp,N_p}^Q)^{\mathrm{T}}\right]^{\mathrm{T}}$, and P_p is assumed to be known. Using a similar argument, we can obtain the following deterministic form of the constraint in Eq. (4.49) as follows:

$$\widetilde{\mathbf{H}}_{cp,k}^{\mho}\check{\mathbf{x}}_c \geq (\delta_{p,k}^0 - f_p^Q \sin\theta)\mathbf{1}_2 \ . \tag{4.52}$$

4.4.2 Cognitive System

For the cognitive system, the constraint (4.50) above is expressed in terms of the unknown random quantization noise, and thus cannot be directly enforced. Instead, we choose to pose the problem such that the constraint is achieved with a certain probability. In particular, considering that $\check{\mathbf{x}}_p$ relies on $\mathbf{H}_{pp,k}$ and thus is also uncertain, we rewrite (4.50) as follows:

$$\mathbb{P}\{\alpha_c(\widetilde{\mathbf{H}}_{cc,j}^{\mho}\check{\mathbf{x}}_c - \delta_{c,j}^0\mathbf{1}_2) \geq (\widetilde{\mathbf{N}}_{pc,j}^{Q,\mho} - \widetilde{\mathbf{H}}_{pc,j}^{Q,\mho})\check{\mathbf{x}}_p\} \geq v_c \ , \tag{4.53}$$

where $\mathbb{P}\{A\}$ denotes the probability of event A, and $v_c \in (0.5, 1]$ represent the probability threshold. In the following, we find expressions for the probabilities in (4.53).

First, we get

$$\mathbb{E}\{\widetilde{\mathbf{N}}_{pc,j}^{Q,\mho}\} = \mathbf{0}_{2\times 2M_p} \ ,$$

$$\mathbb{E}\{\widetilde{\mathbf{N}}_{pc,j}^{Q,\mho}(\widetilde{\mathbf{N}}_{pc,j}^{Q,\mho})^{\mathrm{H}}\} = M_p\alpha_c\rho_c\beta_c \begin{bmatrix} 1 & -\cos 2\theta \\ -\cos 2\theta & 1 \end{bmatrix} \ ,$$

$$\mathbb{E}\{\widetilde{\mathbf{H}}_{pc,j}^{Q,\mho}(\widetilde{\mathbf{H}}_{pc,j}^{Q,\mho})^{H}\} = M_p\alpha_c\beta_c \begin{bmatrix} 1 & -\cos 2\theta \\ -\cos 2\theta & 1 \end{bmatrix} \ ,$$

and we define

$$\mathbf{q}_{c,j} \triangleq (\widetilde{\mathbf{N}}_{pc,j}^{Q,\mho} - \widetilde{\mathbf{H}}_{pc,j}^{Q,\mho})\check{\mathbf{x}}_p \triangleq \begin{bmatrix} q_{c,j}^1 \\ q_{c,j}^2 \end{bmatrix} \ . \tag{4.54}$$

We can show that $\mathbf{q}_{c,j}$ is a bivariate correlated Gaussian random variable with mean

$$\mathbb{E}\{\mathbf{q}_{c,j}\} = \mathbf{0}_{2\times 1} \tag{4.55}$$

and covariance

$$\mathbb{R}_{\mathbf{q}_{c,j}} = \mathbb{E}\{(\widetilde{\mathbf{N}}_{pc,j}^{Q,\mho} - \widetilde{\mathbf{H}}_{pc,j}^{Q,\mho})\check{\mathbf{x}}_p\check{\mathbf{x}}_p^H(\widetilde{\mathbf{N}}_{pc,j}^{Q,\mho} - \widetilde{\mathbf{H}}_{pc,j}^{Q,\mho})^H\} \tag{4.56}$$

$$= \frac{P_p}{2M_p}\left\{\mathbb{E}\{\widetilde{\mathbf{N}}_{pc,j}^{Q,\mho}(\widetilde{\mathbf{N}}_{pc,j}^{Q,\mho})^H\} + \mathbb{E}\{\widetilde{\mathbf{H}}_{pc,j}^{Q,\mho}(\widetilde{\mathbf{H}}_{pc,j}^{Q,\mho})^H\}\right\} \tag{4.57}$$

$$= \frac{P_p\beta_c\alpha_c(2-\alpha_c)}{2} \begin{bmatrix} 1 & -\cos 2\theta \\ -\cos 2\theta & 1 \end{bmatrix} \ . \tag{4.58}$$

Furthermore, we define

$$\mathbf{w}_{c,j}(\check{\mathbf{x}}_c) \triangleq \alpha_c\widetilde{\mathbf{H}}_{cc,j}^{\mho}\check{\mathbf{x}}_c - \alpha_c\delta_{c,j}^0\mathbf{1}_2 \triangleq \begin{bmatrix} w_{c,j}^1 \\ w_{c,j}^2 \end{bmatrix} \tag{4.59}$$

which is affine in $\check{\mathbf{x}}_c$. Using the new notation, the chance constraint (4.53) can be rewritten as

$$\mathbb{P}\{\mathbf{w}_{c,j}(\check{\mathbf{x}}_c) \geq \mathbf{q}_{c,j}\} \geq v_c \, . \tag{4.60}$$

For ease of notation, we define $\bar{\mathbf{w}}_{c,j}(\check{\mathbf{x}}_c) \triangleq \mathbb{R}_{\mathbf{q}_{c,j}}^{-\frac{1}{2}} \mathbf{w}_{c,j}(\check{\mathbf{x}}_c)$ and $\bar{\mathbf{q}}_{c,j} \triangleq \mathbb{R}_{\mathbf{q}_{c,j}}^{-\frac{1}{2}} \mathbf{q}_{c,j}$, and we obtain the following lemma.

Lemma 4.1. *$\mathbb{P}\{\bar{\mathbf{w}}_{c,j}(\check{\mathbf{x}}_c) \geq \bar{\mathbf{q}}_{c,j}\} \geq v_c$ can be approximated by the inequality*

$$\widetilde{\mathbf{H}}_{cc,j}^{\mho} \check{\mathbf{x}}_c \geq \bar{\alpha_c} \eta_c \mathbb{R}_{\mathbf{q}_{c,j}}^{\frac{1}{2}} \mathbf{1}_2 + \delta_{c,j}^0 \mathbf{1}_2, \tag{4.61}$$

where $\eta_c = \sqrt{2}\,\mathrm{erf}^{-1}\left(2\sqrt{v_c} - 1\right)$ is a preset constant.

Proof. See Appendix. □

With this lemma, knowledge of the precise value for $\mathbf{x}_p$ is not necessary in the design of the precoder at the CBS, which is important under the assumption of a finite capacity channel for information sharing.

4.4.3 Optimization Problem for Stochastic CSI Error Model

We can now formulate the robust SLP design with probabilistic constraints by replacing (4.49) and (4.50) with (4.52) and (4.61), as follows:

$$\min_{\check{\mathbf{x}}_c} \quad \|\check{\mathbf{x}}_c\|^2 \tag{4.62}$$

$$\text{subject to} \quad \widetilde{\mathbf{H}}_{cp,k}^{\mho} \check{\mathbf{x}}_c \geq (\delta_{p,k}^0 - f_p^Q \sin\theta)\mathbf{1}_2, \ \forall k \in \mathcal{K}, \tag{4.63}$$

$$\widetilde{\mathbf{H}}_{cc,j}^{\mho} \check{\mathbf{x}}_c \geq \bar{\alpha_c} \eta_c \mathbb{R}_{\mathbf{q}_{c,j}}^{\frac{1}{2}} \mathbf{1}_2 + \delta_{c,j}^0 \mathbf{1}_2, \ \forall j \in \mathcal{J}. \tag{4.64}$$

As with the previous problem studied above, the result is a quadratic program with linear inequality constraints which is robust to imperfect CSI shared from the PBS.

4.5 Numerical Results

In this section, we assess the performance of our proposed power-minimizing SLP (PMSLP) approaches. Monte-Carlo simulations are conducted over 1000 independent channel realizations, each employing a block of $T = 100$ symbols. The channels $\mathbf{H}_{pp}$, $\mathbf{H}_{cp}$, $\mathbf{H}_{pc}$ and $\mathbf{H}_{cc}$ are composed of i.i.d. Gaussian random variables with zero mean and unit variance. The complex Gaussian noise is assumed to have the same power ($\sigma_p = \sigma_c = 1$) for all PUs and CUs. The PBS transmission power is set at $P_p = 10$. We employ the same threshold for all users within a given network, i.e., $\delta^0_{p,1} = \cdots = \delta^0_{p,N_p} = \delta^0_p$ for the PUs and $\delta^0_{c,1} = \cdots = \delta^0_{c,N_c} = \delta^0_c$ for the CUs, ensuring the same worst-case SER for the users in each network.

Since for SLP we work with finite alphabet constellations, we will analyze the block transmission performance of the system using the throughput τ as calculated in [94]:

$$\tau = (1 - P_B) \times c \times T \times N, \tag{4.65}$$

where P_B is the block error rate (BLER), $c = \log_2 D$ is the number of bits per modulation symbol, T is the block length and N is the number of receivers. In each block for each user, there are $C = c \times T$ data message bits transmitted from the BS. For PSK modulation, assuming a binomial distribution of errors in each block, the probability of more than q errors occurring in one block of C bits is expressed as

$$P_e(q, C) = 1 - \sum_{i=0}^{q} \binom{C}{i} P_b^i (1 - P_b)^{C-i}\,, \tag{4.66}$$

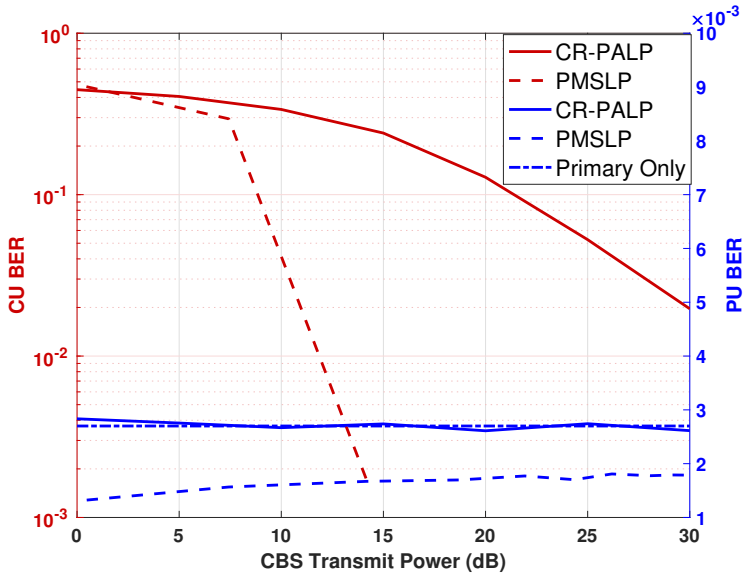

Figure 4.2: BER of CU (left) or PU (right) vs. CBS transmit power where $P_p = 10$, QPSK.

where P_b is the BER. If the receiver detects errors without correction, a block is received correctly only if all C bits in the block are received correctly, and thus the BLER is $P_B = P_e(0, C)$. On the other hand, if the receiver is capable of correcting up to Q errors in each block, then the BLER is given by $P_B = P_e(Q, C)$ [95].

We begin in Fig. 4.2 assuming perfect CSI, plotting the average BER of the users versus the CBS transmission power, and comparing PMSLP assuming a minimum safety margin $\delta_p^0 = 1.9$ with the performance of the CR-PALP algorithm described in Section 4.1.1. Both the PBS and CBS are assumed to have $M_p = M_c = 8$ antennas and the number of PUs and CUs are both set at $N_p = N_c = 4$. With these settings, even when the CBS increases its transmit power to better serve the CUs, it can still avoid any negative impact on the PUs such that the BER of PUs is not greater than that in the primary-only case as shown in Fig. 4.2. Moreover, the BER of the PUs remains nearly unchanged for both types of precoders, although the PUs actually enjoy some benefit with PMSLP since it exploits CI from the CBS signals which can further improve the SM for the PUs. Meanwhile, PMSLP provides a much lower BER for the CUs; the CBS can save more than 15dB of power to achieve an uncoded BER of 10^{-2}, compared to the CR-PALP method which allows only

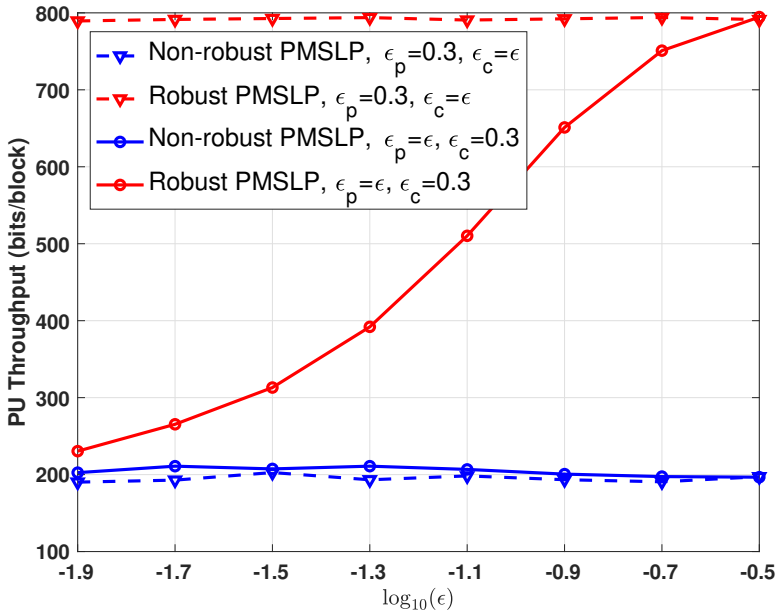

Figure 4.3: Throughput of PU vs. error norm bound where $P_p = 10$, $\delta_p^0 = \delta_c^0 = 1.5$, QPSK.

the CUs to benefit from the inter-user CI in the cognitive system, but in general will not entirely eliminate the destructive interference from the PBS. On the contrary, our proposed PMSLP precoder can take advantage of CI not only from the CU MUI but also what is available (although not optimized) from the primary system. Moreover, the PUs can also benefit from the CI produced by the cognitive system. CR-PALP requires that the CBS act as a relay transmitting not only the CUs' but also the PUs' signals, which is unnecessary in our PMSLP design.

Next we consider the norm-bounded CSI error model discussed in Section 4.3. With the SM threshold for the PUs and CUs set to 1.5, we plot the throughput of the PUs and CUs as the norm of one error ($\epsilon_{p,k}$ or $\epsilon_{c,j}$) changes as $\log_{10}\epsilon$ while the norm of the other is fixed to 0.3 [44]. For simplicity, we assume that the CSI error bounds are the same for all users: $\epsilon_{p,k} = \epsilon_p$ and $\epsilon_{c,j} = \epsilon_c$. Fig. 4.3 and Fig. 4.4 respectively show the throughput for the PUs and CUs as a function of the error bound, and demonstrate that the proposed robust precoder can mitigate the CSI uncertainty and provide a much higher throughput compared to the non-robust precoder. With the robustness introduced, the throughput of the PUs and CUs

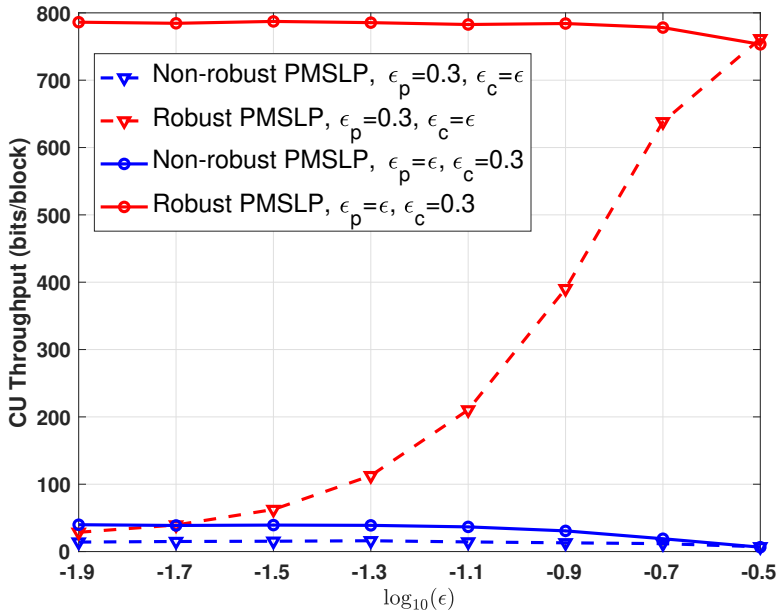

Figure 4.4: Throughput of CU vs. error norm bound where $P_p = 10$, $\delta_p^0 = \delta_c^0 = 1.5$, QPSK.

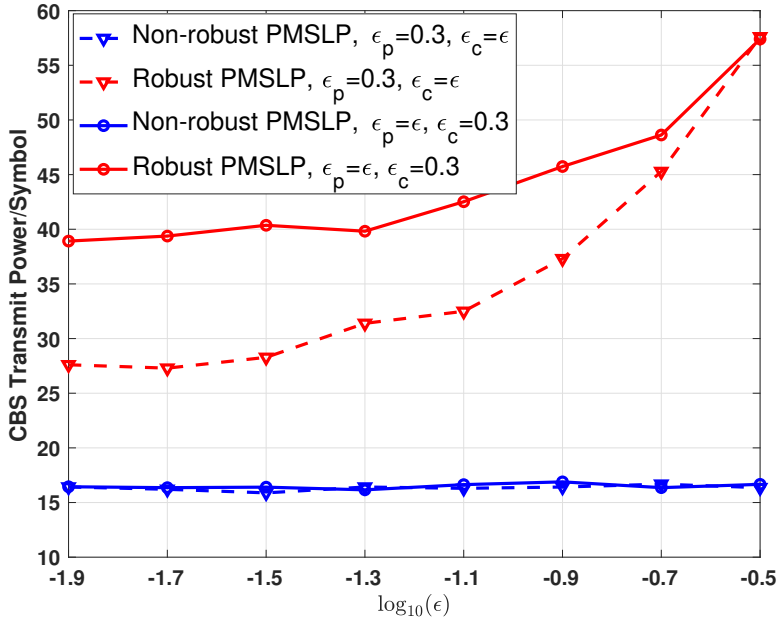

Figure 4.5: Transmit power vs. error norm bound where $P_p = 10$, $\delta_p^0 = \delta_c^0 = 1.5$, QPSK.

actually increases as the norm of the corresponding error increases. This can be explained by examining (4.41) and (4.42), where we see that a larger error bound creates a larger effective SM in the constraint, which provides the robustness necessary to account for the imperfect channel and also imperfect knowledge of $\mathbf{x}_p$ and f_p. There is however a price to be paid for this robustness, as clearly seen in Fig. 4.5, which shows that the robust schemes require the

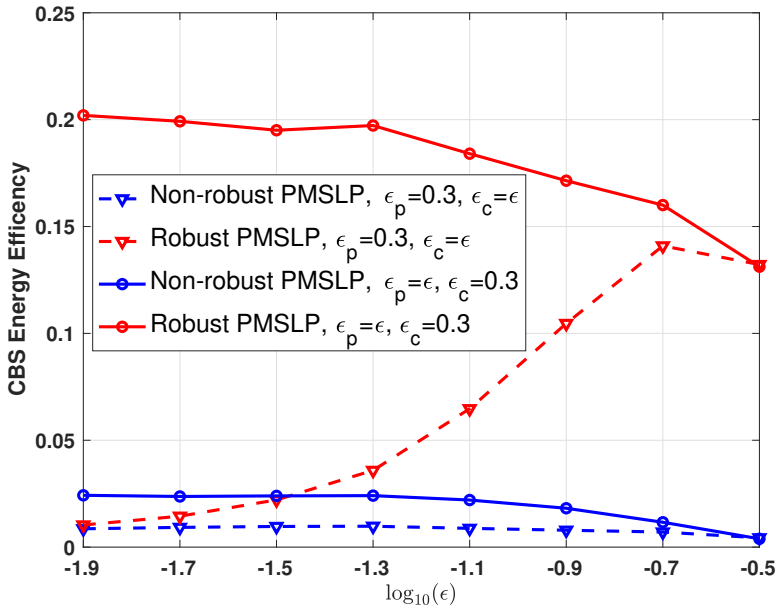

Figure 4.6: Energy efficiency vs. error norm bound where $P_p = 10$, $\delta_p^0 = \delta_c^0 = 1.5$, QPSK.

CBS to operate with significantly more power, especially as the error bound increases. It is clear from these results that the worst-case approach based on the norm-bounded CSI error leads to a conservative design.

In order to quantify the power-performance trade-off between the robust and non-robust designs, in Fig. 4.6 we plot the energy efficiency (EE) of the approaches, defined as the ratio between the throughput calculated from Eq. (4.65) and the transmit power per channel:

$$\text{EE} = \frac{\tau}{T \times \|\check{\mathbf{x}}_c\|^2}. \tag{4.67}$$

We see that despite the increase in transmit power, the proposed robust SLP algorithm achieves a significantly higher energy efficiency. When the uncertainty ϵ_c in $\mathbf{H}_{pc}$ is fixed, the energy efficiency at the CBS decreases with greater uncertainty in $\mathbf{H}_{pp}$ since the CBS needs to consume more power to meet the SM constraint at the PUs.

The remaining examples use the probabilistic SM constraints discussed in Section 4.4 based on the AQNM approximation, although the actual quantized CSI is generated using a non-

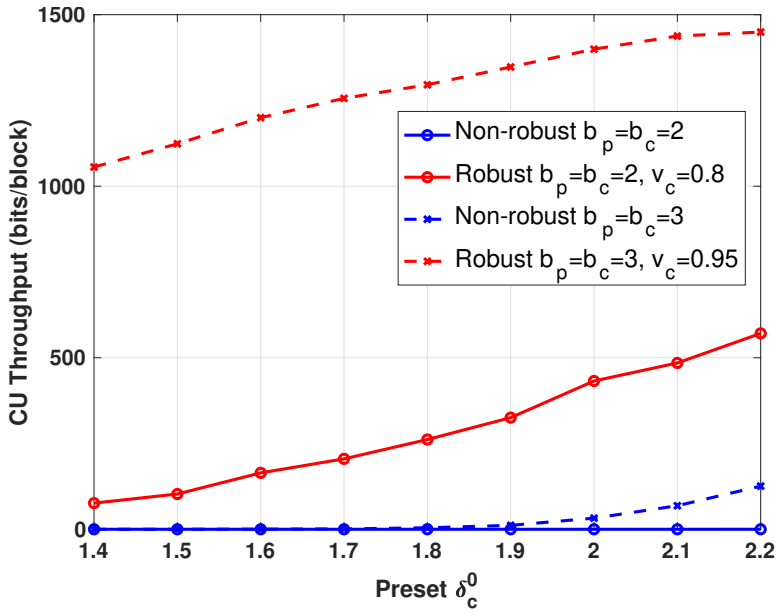

Figure 4.7: Throughput of CUs vs. preset SM at the CUs where $P_p = 10$, $\delta_p^0 = 1.5$, $Q = 1$, QPSK.

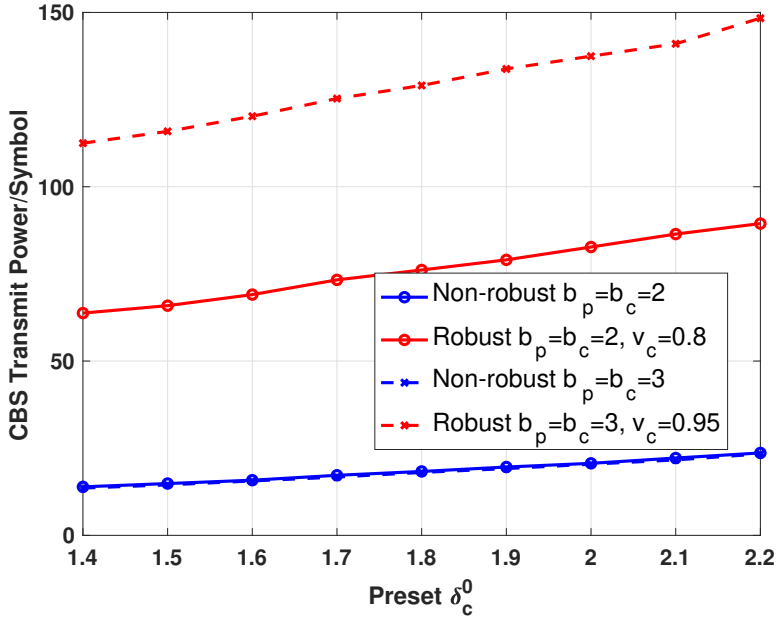

Figure 4.8: Transmit power at CBS vs. preset SM at the CUs where $P_p = 10$, $\delta_p^0 = 1.5$, $Q = 1$, QPSK.

uniform Lloyd Max quantizer [54, 55]. In this case, the PBS and CBS are assumed to have $M_p = M_c = 16$ antennas and the number of PUs and CUs are both set at $N_p = N_c = 8$. The receiver is capable of correcting $Q = 1$ bit error in each block [94]. The probability v was set

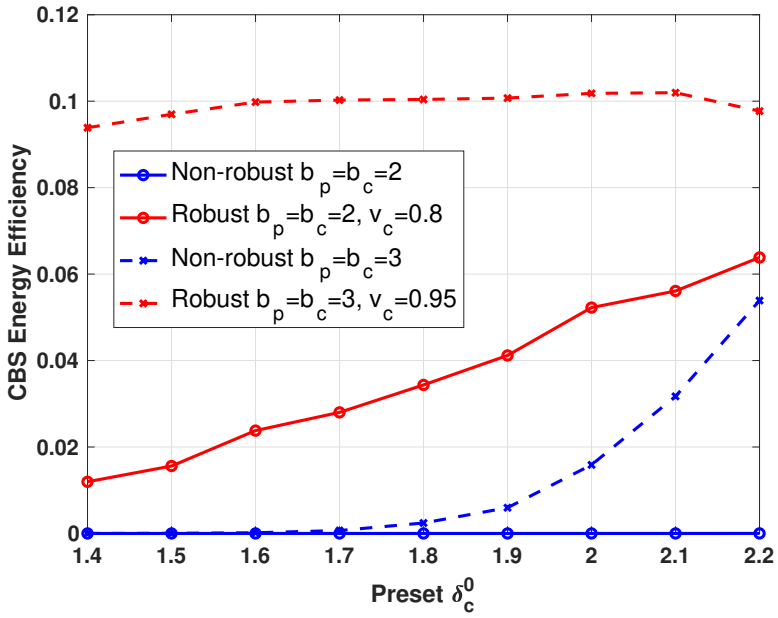

Figure 4.9: Energy efficiency at CBS vs. preset SM at the CUs where $P_p = 10$, $\delta_p^0 = 1.5$, $Q = 1$, QPSK.

with the value used in [45]. Fig. 4.7 shows the throughput of the CUs as a function of the preset SM threshold at the CUs, assuming either $b = 2$ or $b = 3$ quantization bits per channel coefficient and different probability constraints. We see that the CUs reap benefits from the robust SLP design, achieving significantly higher throughput. Again illustrating the trade-off of robustness with increased power, we see in Fig. 4.8 that as the preset δ_c^0 increases, the CBS in the robust SLP approach requires more power to meet the SM constraint than the non-robust SLP. In order to fairly compare different SLP methods, we plot the EE at the CBS in Fig. 4.9. It is clear that the greater the preset SM, or the higher the quantization resolution, the higher the EE. For the case of $b = 2$, the EE of the non-robust SLP is nearly 0, but the robust SLP approach performs particularly well even with very low-resolution CSI.

In the final example, we study the allocation of the quantization bits on the system performance [56]. In particular, in Fig. 4.10 we plot the energy efficiency at the CBS when the direct $\mathbf{h}_{pp,k}$ and interference channels $\mathbf{h}_{pc,j}$ are quantized with different resolutions. For the non-robust SLP schemes (blue curves), the CBS achieves higher EE in cases where $b_p > b_c$,

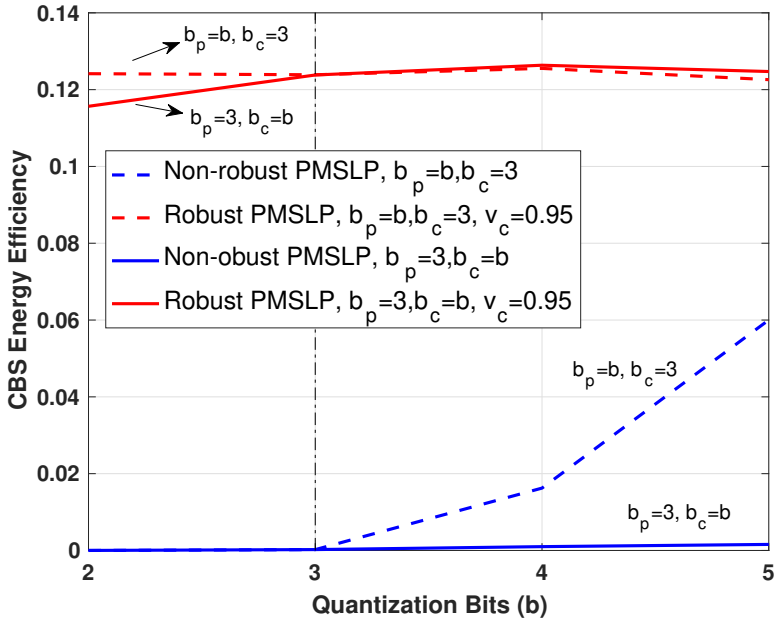

Figure 4.10: Energy efficiency at the CBS vs. quantization resolution where $P_p = 10$, $\delta_p^0 = \delta_c^0 = 1.5$, $Q = 1$, QPSK.

indicating that for a fixed number of quantization bits, it is more energy efficient for the cognitive system to receive a more accurate representation of the direct channel than the interference channel. However, the robust-SLP schemes are less sensitive to the allocation of the quantization bits, and show roughly the same performance regardless of which channel is more accurately represented.

4.6 Conclusion

In this chapter, we have designed non-robust and robust SLP schemes for overlay CR systems with the goal of minimizing the transmission power and simultaneously ensuring the QoS of all users. Unlike traditional CR precoding techniques, we set the SM threshold in the interference constraints instead of using SINR or BER metrics in order to fully exploit constructive interference as much as possible. First, under the assumption of perfect CSI, we propose an SLP algorithm that performs significantly better than a prior CR-based SLP

approach modified to address our overlay problem. In the proposed algorithm, not only the CUs but also the PUs benefit from the constructive interference. Then, using two different CSI error models, we derive two robust SLP methods, one based on a max-min optimization of the worst-case CSI error and the other on a probability-constrained problem using AQNM to approximate the impact of the CSI quantization. All of the proposed optimization problems result in a quadratic objective function with linear inequality constraints that can be efficiently solved. Our numerical results demonstrate that our robust SLP schemes can deal with various types of CSI error and still maintain a high energy efficiency. A key observation from our results is that, by enabling the PUs to exploit constructive interference as well as the CUs, the presence of the cognitive network can actually *improve* the PU network performance rather than degrade it.

Chapter 5

SLP designs for Systems with IGI

To the best of our knowledge, there is no work on designing SLP approaches in additive improper noise systems, which requires comprehensive investigation. In this chapter, we firstly studied the effect of improper noise on the MSM approach. The original MSM approach in [84] ignored the correlation structure of noise, which can lead to biased estimates of the jammer's effect. To deal with non-circular noise, we use a whitening transformation to decorrelate the noise, which is a common method to map the correlated noise to uncorrelated one [98]. We then propose a novel SLP approach with knowing covariance matrix of the jammer's signals, which is designed to minimize the transmit power and meanwhile satisfy our defined upper and lower SM separately. We firstly employed confidence ellipse to describe the disturbance and then utilize bounding box to calculate the upper/lower SM [76, 77]. Secondly, in scenarios where covariance of the non-circular noise is not achievable at the BS, we introduced a robust SLP design and simplified the search strategy for the optimum solution. In order to comprehensively evaluate our proposed methods in comparison with traditional BLP approaches, we apply the MMSE criterion to obtain different BLP designs both with and without the availability of the non-circularity in noise. The numerical results reveal the superior performance of our proposed SLP in terms of SER and energy efficiency

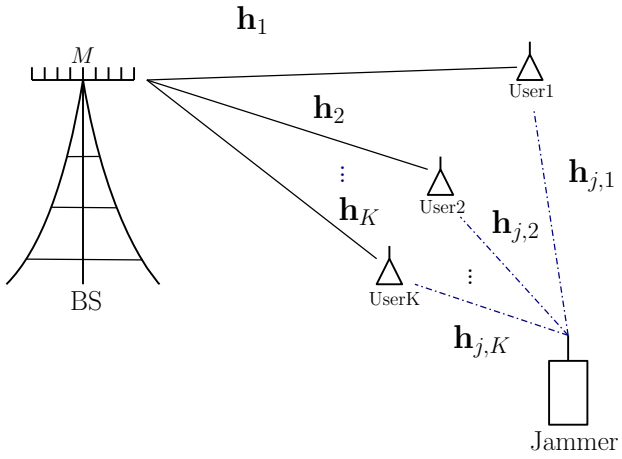

Figure 5.1: System Model

(EE), especially in the robust design where SLP exhibits significant advantages over BLP designs.

5.1 System Model

We consider the MIMO downlink system depicted in Fig. 5.1, with an M-antenna BS, K single-antenna users, and a single-antenna jammer. the received signal at user k can be expressed as

$$y_k = \mathbf{h}_k \mathbf{x} + h_{j,k} z + n_k \triangleq \mathbf{h}_k \mathbf{x} + c_k \ , \tag{5.1}$$

where $\mathbf{h}_k$ and $h_{j,k}$ respectively denote the channel from the BS and the jammer to the kth user, $\mathbf{x}$ represents the precoded signal transmitted by the BS, z is a Gaussian interference signal transmitted by the jammer, and n_k is circular zero-mean Gaussian background noise. We combine together the noise and jamming interence as $c_k = h_{j,k} z + n_k$, and refer to this as

the *effective* noise in the sequel. For a given row vector $\mathbf{a} \in \mathbb{C}^{1\times q}$, we introduce the operators

$$\bar{\mathbf{a}} = \begin{bmatrix} \mathcal{R}\{\mathbf{a}\} \\ \mathcal{I}\{\mathbf{a}\} \end{bmatrix} \in \mathbb{R}^{2\times q} \, , \bar{\mathbf{A}} = \begin{bmatrix} \mathcal{R}\{\mathbf{a}\} & -\mathcal{I}\{\mathbf{a}\} \\ \mathcal{I}\{\mathbf{a}\} & \mathcal{R}\{\mathbf{a}\} \end{bmatrix} \in \mathbb{R}^{2\times 2q} \, ,$$

and rewrite Eq. (5.1) with real-valued quantities

$$\begin{aligned} \begin{bmatrix} \mathcal{R}\{y_k\} \\ \mathcal{I}\{y_k\} \end{bmatrix} = & \begin{bmatrix} \mathcal{R}\{\mathbf{h}_k\} & -\mathcal{I}\{\mathbf{h}_k\} \\ \mathcal{I}\{\mathbf{h}_k\} & \mathcal{R}\{\mathbf{h}_k\} \end{bmatrix} \begin{bmatrix} \mathcal{R}\{\mathbf{x}\} \\ \mathcal{I}\{\mathbf{x}\} \end{bmatrix} \\ & + \begin{bmatrix} \mathcal{R}\{h_{j,k}\} & -I\{h_{j,k}\} \\ \mathcal{I}\{h_{j,k}\} & \mathcal{R}\{h_{j,k}\} \end{bmatrix} \begin{bmatrix} \mathcal{R}\{z\} \\ \mathcal{I}\{z\} \end{bmatrix} \\ & + \begin{bmatrix} \mathcal{R}\{n_k\} \\ \mathcal{I}\{n_k\} \end{bmatrix} \, , \end{aligned}$$

which we equivalently denote by

$$\bar{\mathbf{y}}_k = \bar{\mathbf{H}}_k \bar{\mathbf{x}} + \bar{\mathbf{H}}_{j,k} \bar{\mathbf{z}} + \bar{\mathbf{n}}_k \, . \tag{5.2}$$

We assume that in general the real and imaginary parts of the jammer signal z are correlated; i.e., the jammer signal is noncircular or improper [60], and we describe it as follows:

$$\bar{\mathbf{z}} = \rho \mathbf{T} \begin{bmatrix} v_R \\ v_I \end{bmatrix} = \rho \mathbf{T} \bar{\mathbf{v}} \, , \tag{5.3}$$

where ρ^2 is the jammer transmit power, $\bar{\mathbf{v}} \sim \mathcal{N}(\mathbf{0}, \mathbf{I}_{2N})$, and the matrix $\mathbf{T}$ is normalized such that $\mathbf{Q} = \mathbf{T}\mathbf{T}^T$ satisfies $\mathrm{Tr}\{\mathbf{Q}\} = 1$. The additive noise n_k is distributed as $\bar{\mathbf{n}}_k \sim \mathcal{N}(\mathbf{0}, \frac{1}{2}\sigma_k^2 \mathbf{I}_2)$. The matrix $\mathbf{Q} = \mathbf{Q}^T \succeq 0$ defines the degree to which the jammer signal $\bar{\mathbf{z}}$ is non-circular. If $\mathbf{Q} = \frac{1}{2}\mathbf{I}_2$, the jammer signal is circular, while unequal diagonal terms or non-zero off-diagonal

entries indicate an improper signal. With $\bar{\mathbf{c}}_k = \bar{\mathbf{H}}_{j,k}\bar{\mathbf{z}} + \bar{\mathbf{n}}_k$, we can write the covariance of $\bar{\mathbf{c}}_k$ as

$$\mathbb{E}(\bar{\mathbf{c}}_k\bar{\mathbf{c}}_k^T) = \bar{\mathbf{H}}_{j,k}\mathbb{E}(\bar{\mathbf{z}}\bar{\mathbf{z}}^T)\bar{\mathbf{H}}_{j,k}^T + \mathbb{E}(\bar{\mathbf{n}}_k\bar{\mathbf{n}}_k^T) \tag{5.4}$$

$$= \rho^2\bar{\mathbf{H}}_{j,k}\mathbf{Q}\bar{\mathbf{H}}_{j,k}^T + \frac{1}{2}\sigma_k^2\mathbf{I}_2 \tag{5.5}$$

$$\triangleq \mathbf{G}_k\ . \tag{5.6}$$

Due to the non-circularity of $\bar{z}$, $\mathbf{G}_k$ will in general not be diagonal, and hence conventional precoding techniques that assume circular noise should be reconsidered.

In this downlink scenario, the BS desires to send a symbol s_k to user k for $k = 1, \cdots, K$. In BLP with circular noise, the transmitted signal would be expressed as a linear function of the complex symbols: $\mathbf{x} = \mathbf{P}_c\mathbf{s}$, where $\mathbf{s} = [s_1\ \cdots\ s_K]^T$ and $\mathbf{P}_c$ is the $M \times K$ precoder. In the non-circular case, we separate the real and imaginary parts and write the linear BLP transmit signal as $\bar{\mathbf{x}} = \mathbf{P}\bar{\mathbf{s}}$. In general, $\mathbf{P} \neq \bar{\mathbf{P}}_c$, hence the need to modify the precoder for non-circular noise. For the case of SLP, the transmit signal $\mathbf{x}$ or more generally $\bar{\mathbf{x}}$ is a non-linear function of $\mathbf{s}$ or $\bar{\mathbf{s}}$, respectively. For simplicity, we will assume that the elements of $\mathbf{s}$ are PSK symbols, although the methods can be generalized to other (e.g., QAM) constellations.

5.2 Pre-Whitening Methods

If each user k has knowledge of its own interference-plus-noise covariance $\mathbf{G}_k$, then a straightforward way of dealing with improper interference is through a pre-whitening step that decorrelates and normalizes the real and imaginary parts of the interference. This prewhitening also impacts the BS-user channels, so the BS will also need to know $\mathbf{G}_k$ for each user, presumably through a feedback channel from the users. In this section we describe how to

implement BLP and SLP with non-circular interference pre-whitening at each user. The results derived here will be useful in later sections of the chapter.

5.2.1 Block Level Precoding

There is limited research on precoding methods that address improper noise. In this section, we use the MMSE criterion to develop a benchmark BLP approach. According to Eqs. (5.2)-(5.6), the non-circular disturbance $\bar{\mathbf{c}}_k$ can be pre-whitened as follows:

$$\mathbf{G}_k^{-\frac{1}{2}}\bar{\mathbf{y}}_k = \mathbf{G}_k^{-\frac{1}{2}}\bar{\mathbf{H}}_k\bar{\mathbf{x}} + \mathbf{G}_k^{-\frac{1}{2}}\bar{\mathbf{c}}_k \ . \tag{5.7}$$

Using the following definitions for all users:

$$\begin{bmatrix} y_{E,k}^1 \\ y_{E,k}^2 \end{bmatrix} = \mathbf{G}_k^{-\frac{1}{2}}\bar{\mathbf{y}}_k \ , \ \begin{bmatrix} \mathbf{h}_{E,k}^1 \\ \mathbf{h}_{E,k}^2 \end{bmatrix} = \mathbf{G}_k^{-\frac{1}{2}}\bar{\mathbf{H}}_k \ , \ \begin{bmatrix} c_{E,k}^1 \\ c_{E,k}^2 \end{bmatrix} = \mathbf{G}_k^{-\frac{1}{2}}\bar{\mathbf{c}}_k \ ,$$

the received symbols can be expressed as

$$\mathbf{y}_E = \mathbf{H}_E\mathbf{P}\bar{\mathbf{s}} + \mathbf{c}_E \ , \tag{5.8}$$

where

$$\mathbf{y}_E = \begin{bmatrix} y_{E,1}^1 & \cdots & y_{E,K}^1 & y_{E,1}^2 & \cdots & y_{E,K}^2 \end{bmatrix}^T \ , \tag{5.9}$$

$$\mathbf{H}_E = \begin{bmatrix} {\mathbf{h}_{E,1}^1}^T & \cdots & {\mathbf{h}_{E,K}^1}^T & {\mathbf{h}_{E,1}^2}^T & \cdots & {\mathbf{h}_{E,K}^2}^T \end{bmatrix}^T \ , \tag{5.10}$$

$$\mathbf{c}_E = \begin{bmatrix} c_{E,1}^1 & \cdots & c_{E,K}^1 & c_{E,1}^2 & \cdots & c_{E,K}^2 \end{bmatrix}^T \ .$$

For a given $\mathbf{H}_E$, we consider minimizing mean square error (MMSE) as the criterion to design the BLP [72–74], which is formulated as

$$\min_{\mathbf{P},\beta} \quad \mathbb{E}\{\|\beta^{-1}\mathbf{y}_E - \bar{\mathbf{s}}\|^2\} \tag{5.11}$$

$$\text{subject to} \quad \mathbb{E}\{\|\mathbf{P}\bar{\mathbf{s}}\|^2\} \leq P_t \ , \tag{5.12}$$

where β is a scaling factor, and P_t is the transmit power budget. The corresponding Lagrangian function is

$$\begin{aligned}\mathcal{L}(\mathbf{P},\beta,\lambda) &= \mathbb{E}\{\|\beta^{-1}\mathbf{y}_E - \bar{\mathbf{s}}\|^2\} + \lambda(\mathbb{E}\{\|\mathbf{P}\bar{\mathbf{s}}\|^2\} - P_t) \\ &= K - \frac{1}{2}\beta^{-1}\operatorname{Tr}\{\mathbf{H}_E\mathbf{P} + \mathbf{P}^T\mathbf{H}_E^T\} \\ &\quad + \frac{1}{2}\beta^{-2}\operatorname{Tr}\{\mathbf{H}_E\mathbf{P}\mathbf{P}^T\mathbf{H}_E^T\} + 2K\beta^{-2} \\ &\quad + \frac{1}{2}\lambda\operatorname{Tr}\{\mathbf{P}\mathbf{P}^T\} - \lambda P_t \ ,\end{aligned}$$

where $\lambda \geq 0$ denotes the Lagrange multiplier, and $\mathbb{E}\{\bar{\mathbf{s}}\bar{\mathbf{s}}^T\} = \frac{1}{2}\mathbf{I}_{2K}$, $\mathbb{E}\{\mathbf{c}_E\mathbf{c}_E^T\} = \mathbf{I}_{2K}$.

The solution to (5.11) should satisfy the matrix equations

$$\frac{d\mathcal{L}(\mathbf{P},\beta,\lambda)}{d\mathbf{P}} = -\beta^{-1}\mathbf{H}_E^T + \beta^{-2}\mathbf{H}_E^T\mathbf{H}_E\mathbf{P} + \lambda\mathbf{P} = \mathbf{0}_{2M\times 2K} \tag{5.13}$$

$$\frac{d\mathcal{L}(\mathbf{P},\beta,\lambda)}{d\beta} = \beta^{-2}\operatorname{Tr}\{\mathbf{H}_E\mathbf{P}\} - \beta^{-3}\operatorname{Tr}\{\mathbf{H}_E\mathbf{P}\mathbf{P}^T\mathbf{H}_E^T\} - 4K\beta^{-3} = 0 \ , \tag{5.14}$$

which ultimately yields

$$\mathbf{P} = \beta\boldsymbol{\Delta}\mathbf{H}_E^T \tag{5.15}$$

$$\beta = \sqrt{\frac{2P_t}{\operatorname{Tr}\{\boldsymbol{\Delta}\mathbf{H}_E^T\mathbf{H}_E\boldsymbol{\Delta}\}}} \ , \tag{5.16}$$

where $\mathbf{\Delta} = (\mathbf{H}_E^T \mathbf{H}_E + a\mathbf{I}_{2M})^{-1}$ and $a = \frac{2K}{P_t}$. Since this BLP method takes into account the non-circularity of the interference, we refer to it as "pre-whitened BLP" or PW-BLP.

5.2.2 Symbol Level Precoding

As discussed in [84], the MSM SLP approach is designed such that the noise-free received signal for user k will be located within the CIR of the transmitted symbol with a safety margin of δ_k. For the case of circular noise, the choice of δ_k is made based on a certain desired level of reliability given the variance of the noise seen at the receiver, which we denote as σ_k^2. The value of δ_k can, for example, be chosen to minimize an upper bound on the symbol error probability (SEP) [84]. To maintain consistency with the definition of δ_k in the case of non-circular interference, we pre-whiten user k's signal as follows:

$$\gamma_k \mathbf{G}_k^{-\frac{1}{2}} \bar{\mathbf{y}}_k = \gamma_k \mathbf{G}_k^{-\frac{1}{2}} \bar{\mathbf{H}}_k \bar{\mathbf{x}} + \gamma_k \mathbf{G}_k^{-\frac{1}{2}} (\bar{\mathbf{H}}_{j,k} \bar{\mathbf{z}} + \bar{\mathbf{n}}_k) \,, \tag{5.17}$$

where γ_k is a scaling factor chosen to ensure that the total power of the jammer plus noise remains the same as in the noise-only case, i.e.,

$$\mathbb{E}\left\{ \mathrm{Tr}\left\{ \gamma_k^2 \mathbf{G}_k^{-\frac{1}{2}} \bar{\mathbf{c}}_k \bar{\mathbf{c}}_k^T (\mathbf{G}_k^{-\frac{1}{2}})^T \right\} \right\} = \sigma_k^2 \,. \tag{5.18}$$

Thus, the scaling should be chosen as $\gamma_k = \frac{\sigma_k}{\sqrt{2}}$.

If we define

$$\gamma_k \mathbf{G}_k^{-\frac{1}{2}} \bar{\mathbf{H}}_k \triangleq \begin{bmatrix} \mathbf{h}_{e1,k} \\ \mathbf{h}_{e2,k} \end{bmatrix} \,, \tag{5.19}$$

and the effective *complex* channel after whitening is denoted as $\mathbf{h}_{e,k}$, then the received noiseless symbol in Eq. (5.17) can be rewritten in real-valued form as

$$\gamma_k \mathbf{G}_k^{-\frac{1}{2}} \bar{\mathbf{H}}_k \bar{\mathbf{x}} = \begin{bmatrix} \mathbf{h}_{e1,k}\bar{\mathbf{x}} \\ \mathbf{h}_{e2,k}\bar{\mathbf{x}} \end{bmatrix} = \begin{bmatrix} \mathcal{R}\{\mathbf{h}_{e,k}\mathbf{x}\} \\ \mathcal{I}\{\mathbf{h}_{e,k}\mathbf{x}\} \end{bmatrix} . \tag{5.20}$$

As an example, for unit-magnitude D-PSK signals $s_k \in \{s | s = \exp(j\pi(2d+1)/D),\ d \in \{0, \cdots, D-1\}\}$, the safety margin can be calculated as [84]

$$\delta_k = \mathcal{R}\{s_k^* \mathbf{h}_{e,k}\mathbf{x}\} \sin\theta - |\mathcal{I}\{s_k^* \mathbf{h}_{e,k}\mathbf{x}\}| \cos\theta . \tag{5.21}$$

Furthermore, to express the SM more clearly, we derive

$$\begin{aligned} \mathcal{R}\{s_k^* \mathbf{h}_{e,k}\mathbf{x}\} &= \mathcal{R}\{s_k^*\}\mathcal{R}\{\mathbf{h}_{e,k}\mathbf{x}\} - \mathcal{I}\{s_k^*\}\mathcal{I}\{\mathbf{h}_{e,k}\mathbf{x}\} \\ &= \mathcal{R}\{s_k^*\}\mathbf{h}_{e1,k}\bar{\mathbf{x}} - \mathcal{I}\{s_k^*\}\mathbf{h}_{e2,k}\bar{\mathbf{x}} , \\ &= \tilde{\mathbf{h}}_{e,k}^{-}\bar{\mathbf{x}} , \end{aligned}$$

$$\begin{aligned} \mathcal{I}\{s_k^* \mathbf{h}_{e,k}\mathbf{x}\} &= \mathcal{I}\{s_k^*\}\mathcal{R}\{\mathbf{h}_{e,k}\mathbf{x}\} + \mathcal{R}\{s_k^*\}\mathcal{I}\{\mathbf{h}_{e,k}\mathbf{x}\} \\ &= \mathcal{I}\{s_k^*\}\mathbf{h}_{e1,k}\bar{\mathbf{x}} + \mathcal{R}\{s_k^*\}\mathbf{h}_{e2,k}\bar{\mathbf{x}} , \\ &= \tilde{\mathbf{h}}_{e,k}^{+}\bar{\mathbf{x}} , \end{aligned}$$

where $\tilde{\mathbf{h}}_{e,k}^{-}\bar{\mathbf{x}} = \mathcal{R}\{s_k^*\}\mathbf{h}_{e1,k} - \mathcal{I}\{s_k^*\}\mathbf{h}_{e2,k}$, and $\tilde{\mathbf{h}}_{e,k}^{+}\bar{\mathbf{x}} = \mathcal{I}\{s_k^*\}\mathbf{h}_{e1,k} + \mathcal{R}\{s_k^*\}\mathbf{h}_{e2,k}$. Then, one possible SLP optimization problem is to maximize the smallest safety margin over all K

users for a given transmit power budget, as follows:

$$\begin{aligned} \max_{\bar{\mathbf{x}}} \quad & \delta \\ \text{subject to} \quad & (\tilde{\mathbf{h}}_{e,k}^{-} \sin\theta - \tilde{\mathbf{h}}_{e,k}^{+} \cos\theta)\bar{\mathbf{x}} \geq \delta, \ \forall k \\ & (\tilde{\mathbf{h}}_{e,k}^{-} \sin\theta + \tilde{\mathbf{h}}_{e,k}^{+} \cos\theta)\bar{\mathbf{x}} \geq \delta, \ \forall k \\ & \|\bar{\mathbf{x}}\|^2 \leq P_t \ . \end{aligned}$$

This approach is essentially equivalent to the conventional MSM method in [84], with the only difference being the pre-whitening transformation of the channel to account for the non-circularity of the effective noise. An alternative formulation is to minimize the transmit power subject to given safety margin constraints $\delta_1^0, \cdots, \delta_K^0$ for each user:

$$\begin{aligned} \min_{\bar{\mathbf{x}}} \quad & \|\bar{\mathbf{x}}\|^2 \\ \text{subject to} \quad & (\tilde{\mathbf{h}}_{e,k}^{-} \sin\theta - \tilde{\mathbf{h}}_{e,k}^{+} \cos\theta)\bar{\mathbf{x}} \geq \delta^0, \ \forall k \\ & (\tilde{\mathbf{h}}_{e,k}^{-} \sin\theta + \tilde{\mathbf{h}}_{e,k}^{+} \cos\theta)\bar{\mathbf{x}} \geq \delta^0, \ \forall k \ . \end{aligned}$$

We will refer to the above algorithms as pre-whitened SLP, or simply PW-SLP, and our numerical results will illustrate the performance gain achieved by adjusting the conventional SLP approach in scenarios with IGI.

5.3 SLP with Transmit-Only Processing

The SLP design of the previous section requires not only the precoding but also receiver processing for pre-whitening the received signal, which prompts the question of whether we can implement an IGI-aware SLP design solely at the transmitter by directly optimizing the SM and CIR. In this section we show that if the covariance matrix $\mathbf{G}_k$ of the jammer

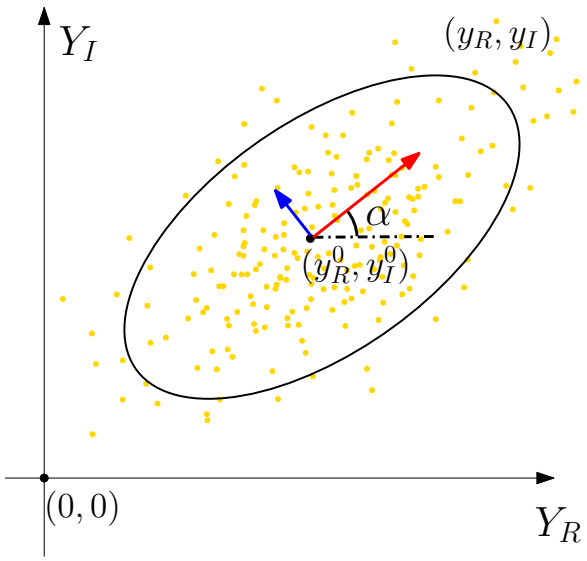

Figure 5.2: Confidence ellipse with correlated 2D data samples.

signal at each user is known, the definition of SM in [84,85] can be adjusted to appropriately account for the IGI. Intuitively, IGI will produce an elliptical rather than a circular cloud around the noiseless received signal, and for the case of PSK this will require the definition of two safety margins in order to guarantee the user QoS, defined as the likelihood that the received signal lies in the CIR. We will employ confidence ellipses [76, 77] to formulate the SM and CIR.

5.3.1 Confidence Ellipse

Given normally distributed two-dimensional (2D) data $\{Y_R, Y_I\}$, when the two variables are correlated with covariance matrix $\mathbf{G}$, we can draw a confidence ellipse to define a region that contains data samples (y_R, y_I) with a preset confidence value. For example, in Fig. 5.2, the center of the ellipse is (y_R^0, y_I^0), where $y_R^0 = \mathbb{E}\{Y_R\}$ and $y_I^0 = \mathbb{E}\{Y_I\}$ are the mean values of the two variables. The orientation of the ellipse is denoted by the angle α $(0 \leq \alpha < 180°)$ between the major axis of the ellipse and the Y_R-axis. When $\mathbf{G}$ is diagonal, we have $\alpha = 0$. The eigenvectors of $\mathbf{G}$ correspond to the directions of the major and minor axes of the ellipse

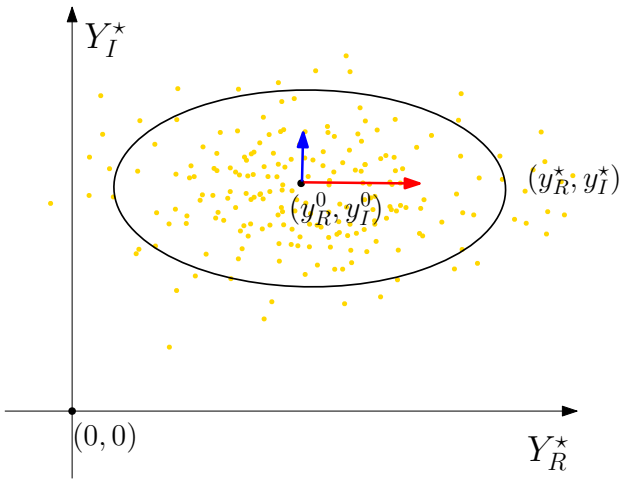

Figure 5.3: Confidence ellipse after rotation to decorrelate the 2D data samples.

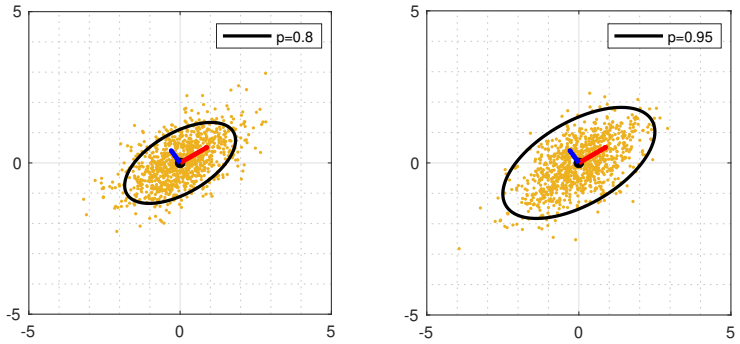

Figure 5.4: The preset p decides the size of confidence ellipses.

as depicted by the red and blue arrows in Fig. 5.2, while the square root of the eigenvalues $\lambda_1,\ \lambda_2$ of $\mathbf{G}$ correspond to the spread of data in the two directions. It is easy to show that

$$\alpha = \arctan \frac{v_2}{v_1} \tag{5.22}$$

where $\mathbf{v} = [v_1\ v_2]^T$ is the principle eigenvector of $\mathbf{G}$ corresponding to the largest eigenvalue [76, 77].

The size of the ellipse depends on the chosen confidence level $0 \leq p \leq 1$, which represents the asymptotic fraction of the data samples located inside the ellipse, as illustrated in Fig. (5.4). To mathematically express the relationship governing p, we first decorrelate Y_R and Y_I by

rotating the data samples with respect to the ellipse center by the angle $-\alpha$:

$$\mathbf{R} = \begin{bmatrix} \cos\alpha & \sin\alpha \\ -\sin\alpha & \cos\alpha \end{bmatrix} . \tag{5.23}$$

The rotated data samples in Fig. 5.3 are defined by

$$\begin{bmatrix} y_R^\star \\ y_I^\star \end{bmatrix} = \mathbf{R} \begin{bmatrix} y_R \\ y_I \end{bmatrix} , \tag{5.24}$$

and the covariance matrix for $\{Y_R^\star, Y_I^\star\}$,

$$\mathbf{G}^\star = \mathbf{R}\mathbf{G}\mathbf{R}^H , \tag{5.25}$$

is diagonal, with eigenvalues equal to $\lambda_1,\ \lambda_2$ due to the orthogonality of $\mathbf{R}$. Since $Y_R^\star$ and $Y_I^\star$ are independent normally distributed random variables, according to the χ^2 distribution we can express the confidence ellipse as

$$\mathbb{P}\left\{ \frac{(y_R^\star - y_R^0)^2}{\lambda_1} + \frac{(y_I^\star - y_I^0)^2}{\lambda_2} \leq \omega \right\} = p , \tag{5.26}$$

where $\omega = -2\ln(1-p)$.

5.3.2 Constructive Interference Region for IGI

To describe the CIR in a unified way, we rotate the original coordinate system for PSK symbols by the negative phase of the desired constellation symbol, i.e., $\measuredangle s_k^*$, to obtain the modified coordinate system in Fig. 5.5. We can see that with IGI, the safety margin must be determined separately for the two symbol decision boundaries; in particular, we define the minimum distance from the confidence ellipses to the two decision boundaries as the upper

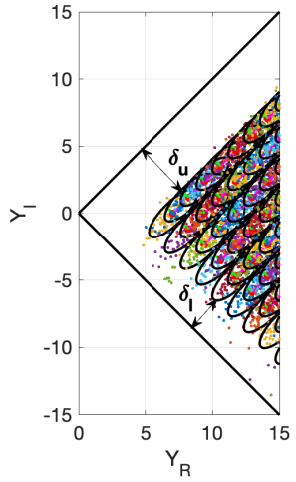

Figure 5.5: CIR with IGI added to noise-free received signals.

safety margin (δ_u^0) and lower safety margin (δ_l^0), where $\delta_u^0 \neq \delta_l^0$. In Fig. 5.6, we plot one of the ellipses, with the center at the kth user's noiseless received signal $(\bar{\mathbf{H}}_k^1\bar{\mathbf{x}}, \bar{\mathbf{H}}_k^2\bar{\mathbf{x}})$ in the modified coordinate system, where

$$\bar{\mathbf{H}}_k^1 = \begin{bmatrix} \mathcal{R}\{s_k^*\mathbf{h}_k\} & -\mathcal{I}\{s_k^*\mathbf{h}_k\} \end{bmatrix} \tag{5.27}$$

$$\bar{\mathbf{H}}_k^2 = \begin{bmatrix} \mathcal{I}\{s_k^*\mathbf{h}_k\} & \mathcal{R}\{s_k^*\mathbf{h}_k\} \end{bmatrix} . \tag{5.28}$$

The closest point on the ellipse to each decision boundary, $y_\mathcal{I} = \pm(\tan\theta)y_\mathcal{R}$, is where the tangent line of the ellipse is parallel to the corresponding boundary, as illustrated in Fig. 5.6, where $\theta = \frac{\pi}{D}$ for D-PSK. In the discussion below, we show how to obtain expressions for the SMs $\delta_{u,k}^0$ and $\delta_{l,k}^0$ in the presence of IGI, so that the SLP approach can be implemented.

5.3.3 SLP for Non-Circular Interference

We will develop the SLP precoding problem to minimize the BS transmit power while achieving the users' various SM constraints. In the modified coordinate system, we obtain the real

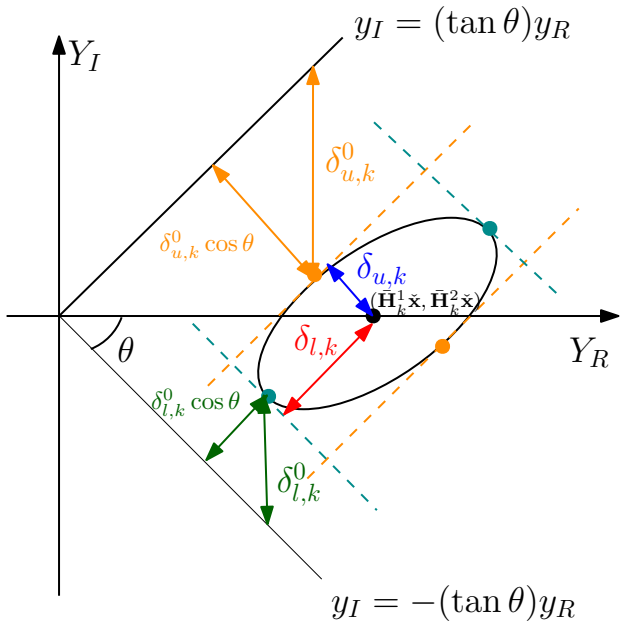

Figure 5.6: Distance from confidence ellipse to decision boundaries.

and imaginary parts of the interference signal as

$$\begin{bmatrix} \mathcal{R}\{s_k^* c_k\} \\ \mathcal{I}\{s_k^* c_k\} \end{bmatrix} = \bar{\mathbf{S}}_k^T \bar{\mathbf{c}}_k \ , \tag{5.29}$$

where $\bar{\mathbf{S}}_k = \begin{bmatrix} \mathcal{R}\{s_k\} & -\mathcal{I}\{s_k\} \\ \mathcal{I}\{s_k\} & \mathcal{R}\{s_k\} \end{bmatrix}$, and its covariance matrix is given by

$$\mathbb{E}\left(\bar{\mathbf{S}}_k^T \bar{\mathbf{c}}_k \left(\bar{\mathbf{S}}_k^T \bar{\mathbf{c}}_k\right)^T\right) = \bar{\mathbf{S}}_k^T \mathbf{G}_k \bar{\mathbf{S}}_k \triangleq \check{\mathbf{G}}_k \ . \tag{5.30}$$

We obtain the orientation angle of the confidence ellipse using Eq. (5.22):

$$\check{\alpha}_k = \arctan \frac{\check{v}_{k,2}}{\check{v}_{k,1}} \ , \tag{5.31}$$

where $\check{\mathbf{v}}_k = [\check{v}_{k,1} \ \check{v}_{k,1}]^T$ is the eigenvector of $\check{\mathbf{G}}_k$ corresponding to the largest eigenvalue. To decorrelate the real and imaginary parts of the received signals, we rotate them by $-\check{\alpha}_k$ so

the IGI can be written in a real-valued form as

$$\check{\mathbf{R}}_k \bar{\mathbf{S}}_k^T \bar{\mathbf{c}}_k = \check{\mathbf{R}}_k \begin{bmatrix} y_k^R - \bar{\mathbf{H}}_k^1 \bar{\mathbf{x}} \\ y_k^I - \bar{\mathbf{H}}_k^2 \bar{\mathbf{x}} \end{bmatrix} = \begin{bmatrix} (y_k^R - \bar{\mathbf{H}}_k^1 \bar{\mathbf{x}}) \cos\check{\alpha}_k + (y_k^I - \bar{\mathbf{H}}_k^2 \bar{\mathbf{x}}) \sin\check{\alpha}_k \\ -(y_k^R - \bar{\mathbf{H}}_k^1 \bar{\mathbf{x}}) \sin\check{\alpha}_k + (y_k^I - \bar{\mathbf{H}}_k^2 \bar{\mathbf{x}}) \cos\check{\alpha}_k \end{bmatrix} ,$$

where $\check{\mathbf{R}}_k$ is the rotation matrix in Eq. (5.23) with angle $\check{\alpha}_k$, and y_k^R (y_k^I) is the real (imaginary) part of user k's received signal. As in Eq. (5.25), after rotation the covariance of the effective noise for user k is

$$\check{\mathbf{G}}_k^\star = \check{\mathbf{R}}_k \check{\mathbf{G}}_k \check{\mathbf{R}}_k^H , \tag{5.32}$$

which is diagonal.

The eigenvalues of $\check{\mathbf{G}}_k^\star$ are equal to those of $\mathbf{G}_k$ and are denoted by $\lambda_{1,k},\ \lambda_{2,k}$, due to the orthogonality of $\bar{\mathbf{S}}_k$ and $\check{\mathbf{R}}_k$. The confidence ellipse corresponding to the effective IGI can be expressed as

$$\begin{aligned} &\frac{\left((y_k^R - \bar{\mathbf{H}}_k^1 \bar{\mathbf{x}}) \cos\check{\alpha}_k + (y_k^I - \bar{\mathbf{H}}_k^2 \bar{\mathbf{x}}) \sin\check{\alpha}_k\right)^2}{\lambda_{1,k}} \\ &\quad + \frac{\left(-(y_k^R - \bar{\mathbf{H}}_k^1 \bar{\mathbf{x}}) \sin\check{\alpha}_k + (y_k^I - \bar{\mathbf{H}}_k^2 \bar{\mathbf{x}}) \cos\check{\alpha}_k\right)^2}{\lambda_{2,k}} = \omega_k , \end{aligned} \tag{5.33}$$

which can be rewritten as

$$\begin{aligned} f(y_k^R, y_k^I) &= \lambda_{2,k}(y_k^R \cos\check{\alpha}_k + y_k^I \sin\check{\alpha}_k + a_k)^2 + \lambda_{1,k}(-y_k^R \sin\check{\alpha}_k + y_k^I \cos\check{\alpha}_k + b_k)^2 \\ &= \omega_k \lambda_{1,k} \lambda_{2,k} , \end{aligned} \tag{5.34}$$

where $a_k = \bar{\mathbf{H}}_k^1 \bar{\mathbf{x}} \cos\check{\alpha}_k + \bar{\mathbf{H}}_k^2 \bar{\mathbf{x}} \sin\check{\alpha}_k$ and $b_k = \bar{\mathbf{H}}_k^1 \bar{\mathbf{x}} \sin\check{\alpha}_k - \bar{\mathbf{H}}_k^2 \bar{\mathbf{x}} \cos\check{\alpha}_k$. Considering y_k^I as a function of y_k^R, we set the following derivative to zero,

$$\frac{df(y_k^R, y_k^I)}{dy_k^R} = 2A_k \left(\cos\check{\alpha}_k + \sin\check{\alpha}_k \frac{dy_k^I}{dy_k^R}\right) + 2B_k \left(-\sin\check{\alpha}_k + \cos\check{\alpha}_k \frac{dy_k^I}{dy_k^R}\right) = 0 , \tag{5.35}$$

where $A_k = \lambda_{2,k}(y_k^R \cos\check{\alpha}_k + y_k^I \sin\check{\alpha}_k + a_k)$ and $B_k = \lambda_{1,k}(-y_k^R \sin\check{\alpha}_k + y_k^I \cos\check{\alpha}_k + b_k)$. It is easy to show that

$$\frac{dy_k^I}{dy_k^R} = -\frac{A_k \cos\check{\alpha}_k - B_k \sin\check{\alpha}_k}{A_k \sin\check{\alpha}_k + B_k \cos\check{\alpha}_k} , \tag{5.36}$$

which is equal to the slope of the tangent line to the ellipse at the point (y_k^R, y_k^I).

To ensure the confidence ellipse is inside the decision region, we use two lines to constrain its location to satisfy

$$y_k^R \sin\theta - y_k^I \cos\theta \geq 0 , \tag{5.37}$$

$$y_k^R \sin\theta + y_k^I \cos\theta \geq 0 , \tag{5.38}$$

and we set constraints for the four points on the ellipse where the slope of the tangent line is either $\tan\theta$ or $-\tan\theta$. These points include the two closest points to the decision boundaries, as illustrated in Fig. 5.6. The four lines defined by these points form a bounding box that contains the ellipse. The two points on the ellipse where the slope of the tangent line is $\tan\theta$ can be obtained by simultaneously solving

$$\begin{cases} \tan\theta = -\dfrac{A_k \cos\check{\alpha}_k - B_k \sin\check{\alpha}_k}{A_k \sin\check{\alpha}_k + B_k \cos\check{\alpha}_k} , & (5.39) \\ \dfrac{B_k^2}{\lambda_{1,k}} + \dfrac{A_k^2}{\lambda_{2,k}} = \omega_k . & (5.40) \end{cases}$$

From Eq. (5.39) we can get $A_k = \kappa_k B_k$ where

$$\kappa_k = \frac{\sin\check{\alpha}_k - \cos\check{\alpha}_k \tan\theta}{\cos\check{\alpha}_k + \sin\check{\alpha}_k \tan\theta} = \tan(\check{\alpha}_k - \theta) . \tag{5.41}$$

Substituting this into Eq. (5.40) yields $B_k = \pm\sqrt{\frac{\omega_k}{d_k}}$ where

$$d_k = \frac{1}{\lambda_{1,k}} + \frac{\kappa_k^2}{\lambda_{2,k}} \ . \tag{5.42}$$

Then y_k^R, y_k^I can be found by solving the following equations

$$\begin{cases} -y_k^R \sin\check{\alpha}_k + y_k^I \cos\check{\alpha}_k = \pm e_k - b_k & (5.43) \\ f_k y_k^R + g_k y_k^I = a_k\lambda_{2,k} + b_k c_k \lambda_{1,k} \ , & (5.44) \end{cases}$$

where $e_k = \sqrt{\frac{\lambda_{2,k}\omega_k}{\lambda_{1,k}d_k}}$, $f_k = \lambda_{2,k}\cos\check{\alpha}_k + \lambda_{1,k}\kappa_k \sin\check{\alpha}_k$, and $g_k = \lambda_{2,k}\sin\check{\alpha}_k - \lambda_{1,k}\kappa_k\cos\check{\alpha}_k$. It is easy to show that

$$\begin{cases} f_k\cos\check{\alpha}_k + g_k\sin\check{\alpha}_k = \lambda_{2,k} & (5.45) \\ f_k\sin\check{\alpha}_k - g_k\cos\check{\alpha}_k = \kappa_k\lambda_{1,k} \ . & (5.46) \end{cases}$$

The two orange points in Fig. 5.6 are then given by

$$y_k^R = \bar{\mathbf{H}}_k^1\bar{\mathbf{x}} - u_k \ , y_k^I = \bar{\mathbf{H}}_k^2\bar{\mathbf{x}} + v_k \tag{5.47}$$

$$y_k^R = \bar{\mathbf{H}}_k^1\bar{\mathbf{x}} + u_k \ , y_k^I = \bar{\mathbf{H}}_k^2\bar{\mathbf{x}} - v_k \ , \tag{5.48}$$

where $u_k = \frac{g_k e_k}{\lambda_{2,k}}$ and $v_k = \frac{f_k e_k}{\lambda_{2,k}}$.

Defining the *upper SM* as $\delta_{u,k}^0$, the SM constraint corresponding to each of these points is given by

$$y_k^R\sin\theta - y_k^I\cos\theta \geq \delta_{u,k}^0\cos\theta \ . \tag{5.49}$$

Substituting Eqs. (5.47) and (5.48) into Eq. (5.49) leads to

$$(\bar{\mathbf{H}}_k^1 \sin\theta - \bar{\mathbf{H}}_k^2 \cos\theta)\bar{\mathbf{x}} \geq \delta_{u,k} + \delta_{u,k}^0 \cos\theta \tag{5.50}$$

$$(\bar{\mathbf{H}}_k^1 \sin\theta - \bar{\mathbf{H}}_k^2 \cos\theta)\bar{\mathbf{x}} \geq -\delta_{u,k} + \delta_{u,k}^0 \cos\theta \ , \tag{5.51}$$

where

$$\delta_{u,k} = u_k \sin\theta + v_k \cos\theta \tag{5.52}$$

$$= \sqrt{\omega_k}\sqrt{\lambda_{1,k}\sin^2(\check{\alpha}_k - \theta) + \lambda_{2,k}\cos^2(\check{\alpha}_k - \theta)} \tag{5.53}$$

represents the distance from the noise-free received signal to the tangent line of the bounding box that intersects the orange points in Fig. 5.6. This is a critical dimension, since it represents how much the interference can perturb the received signal and still remain in the confidence ellipse defined by p. In general, the larger this distance, the more power that will be required to satisfy the given safety margin.

Similarly, for the green points on the ellipse in Fig. 5.6 where the slope of the tangent line is $-\tan\theta$, we obtain

$$(\bar{\mathbf{H}}_k^1 \sin\theta + \bar{\mathbf{H}}_k^2 \cos\theta)\bar{\mathbf{x}} \geq \delta_{l,k} + \delta_{l,k}^0 \cos\theta \tag{5.54}$$

$$(\bar{\mathbf{H}}_k^1 \sin\theta + \bar{\mathbf{H}}_k^2 \cos\theta)\bar{\mathbf{x}} \geq -\delta_{l,k} + \delta_{l,k}^0 \cos\theta \tag{5.55}$$

where $\delta_{l,k}^0$ denotes the preset *lower SM*,

$$\delta_{l,k} = u_k' \sin\theta - v_k' \cos\theta \tag{5.56}$$

$$= \sqrt{\omega_k}\sqrt{\lambda_{1,k}\sin^2(\check{\alpha}_k + \theta) + \lambda_{2,k}\cos^2(\check{\alpha}_k + \theta)} \ , \tag{5.57}$$

Algorithm 1 Non-Circular Symbol Level Precoding

Input: $\mathbf{h}_k$, $h_{j,k}$, s_k, $\delta^0_{u,k}$, $\delta^0_{l,k}$, σ_k, ω_k, $\forall k$, ρ, $\mathbf{Q}$, and θ.
Output: $\bar{\mathbf{x}}^{\text{nc}}$.
for $k \in \{1, \cdots, K\}$ **do**
    Calculate $\mathbf{A}_k^-$ in (5.58) , and $\mathbf{A}_k^+$ in (5.61).
    Calculate $\mathbf{G}_k$ using (5.6), and its eigenvalues $\lambda_{1,k},\ \lambda_{2,k}$.
    Calculate $\check{\mathbf{G}}_k$ using (5.30, and $\check{\alpha}_k$ using (5.31).
    Calculate $\delta_{u,k}$ using (5.53) and $\delta_{l,k}$ using (5.57).
end for
Solve the optimization problem (5.62) to obtain the optimal precoded vector $\bar{\mathbf{x}}^{\text{nc}}$.

and u'_k, v'_k can be found using $\kappa'_k = \tan(\check{\alpha}_k + \theta)$ and steps similar to those above. The value of $\delta_{l,k}$ represents the distance from the noise-free received signal to the tangent lines intersecting the green points, and like $\delta_{u,k}$, a larger $\delta_{l,k}$ generally means a higher required transmit power.

If we denote

$$\mathbf{A}_k^- = \bar{\mathbf{H}}_k^1 \sin\theta - \bar{\mathbf{H}}_k^2 \cos\theta \ , \tag{5.58}$$

Eq. (5.50) and (5.51) can be combined as

$$\mathbf{A}_k^- \bar{\mathbf{x}} - \delta^0_{u,k} \cos\theta \geq |\delta_{u,k}| \ . \tag{5.59}$$

Similarly, Eq. (5.54) and (5.55) can be combined to yield

$$\mathbf{A}_k^+ \bar{\mathbf{x}} - \delta^0_{l,k} \cos\theta \geq |\delta_{l,k}| \ , \tag{5.60}$$

where

$$\mathbf{A}_k^+ = \bar{\mathbf{H}}_k^1 \sin\theta + \bar{\mathbf{H}}_k^2 \cos\theta \ . \tag{5.61}$$

One possible SLP optimization problem that results from the derivations above is to design the signal $\bar{\mathbf{x}}$ that minimizes the transmit power at the BS and satisfies preset upper/lower safety margins at each user:

$$\min_{\bar{\mathbf{x}}} \quad \bar{\mathbf{x}}^H \bar{\mathbf{x}} \tag{5.62}$$

$$\text{subject to} \quad \mathbf{A}_k^- \bar{\mathbf{x}} - \delta_{u,k}^0 \cos\theta \geq |\delta_{u,k}| \ , \forall k \ , \tag{5.63}$$

$$\mathbf{A}_k^+ \bar{\mathbf{x}} - \delta_{l,k}^0 \cos\theta \geq |\delta_{l,k}| \ , \forall k \ . \tag{5.64}$$

This is a quadratic programming problem with linear inequality constraints that can be efficiently solved using standard numerical methods. An alternative formulation of the problem is possible in which the upper and lower SMs are maximized for a given maximum transmit power. In either case, we refer to this approach as "non-circular SLP," or simply NC-SLP. The steps required to implement the algorithm are listed in Algorithm. 1.

In contrast, when the BS ignores the non-circularity of the interference and implements the conventional SLP approach assuming circular interference, we will refer to this approach as "naive SLP." For a fair comparison, in implementing the naive SLP approach we will assume that the safety margin is set assuming the same total power as in the case of IGI, i.e., $\sigma_k^2 = \text{Tr}\{\mathbf{G}_k\}$.

5.4 Robust Non-Circular Precoding

The methods discussed above assume that the covariance matrix $\mathbf{G}_k$ of the effective noise at user k is known, at both the users and the BS. In this section, we relax this assumption, and only assume that the jammer CSI $\bar{\mathbf{H}}_k$ for all k is available, while the "shape" of the non-circularity $\mathbf{Q}$ is not. For example, the jammer may choose to change $\mathbf{Q}$ from time to time to confuse the legitimate receivers. Our goal is to design precoders that are robust to knowledge

of the jammer non-circularity. In Section 5.4.1 we address robustness to knowledge of $\mathbf{Q}$ for the case of BLP, and in Section 5.4.2 we do the same for SLP.

5.4.1 Robust BLP

To make the MMSE BLP approach described in Section 5.2.1 robust to knowledge of the jammer circularity $\mathbf{Q}$, we minimize the worst-case MSE over all possible choices of $\mathbf{Q}$. The optimization problem can be formulated as

$$\begin{aligned} &\min_{\mathbf{P},\beta} \left\{ \max_{\mathbf{Q}\in\mathcal{S}} \mathbb{E}\{\|\beta^{-1}\mathbf{y}_E - \bar{\mathbf{s}}\|^2\} \right\} \\ &\text{subject to} \quad \mathbb{E}\{\|\mathbf{P}\bar{\mathbf{s}}\|^2\} \leq P_t \ , \end{aligned} \tag{5.65}$$

where $\mathcal{S} = \{\mathbf{Q} | \operatorname{Tr}\{\mathbf{Q}\} = 1,\ \mathbf{Q} \succeq 0\}$. As a first step, in the lemma below we prove that for MMSE BLP, the worst-case $\mathbf{Q}$ actually corresponds to circular jamming.

Lemma 5.1. *The maximum MSE*

$$\max_{\mathbf{Q}\in\mathcal{S}} \mathbb{E}\{\|\beta^{-1}\mathbf{y}_E - \bar{\mathbf{s}}\|^2\} \tag{5.66}$$

is achieved with $\mathbf{Q} = \frac{1}{2}\mathbf{I}_2$.

Proof. See Appendix. □

Interestingly, the robust BLP design assumes that the effective noise is uncorrelated in the real and imaginary part. Then we will have $\mathbf{G}_k = \frac{1}{2}(\rho^2|h_{j,k}|^2 + \sigma_k^2)\mathbf{I}_2$. After plugging $\mathbf{G}_k$ into Eq. (5.15) and (5.16), we will have the solution of "robust BLP".

5.4.2 Robust SLP

Here we study the robustness of SLP to the jammer's choice of $\mathbf{Q}$. Due to the higher complexity of finding the SLP solution, this is a challenging problem. Fortunately, we will show below that only the extreme cases where the degree of non-circularity is maximum need be considered to find the worst-case scenario. Thus, only rank-deficient $\mathbf{Q}$ need be considered, and we show how the worst-case $\mathbf{Q}$ can be found via a one-dimensional search.

As with the robust MMSE BLP approach, we will design the SLP algorithm to minimize the worst-case transmit power with respect to all possible $\mathbf{Q}$. This can be achieved by reformulating the non-circular SLP problem in (5.62) as follows:

$$\begin{aligned} &\min_{\bar{\mathbf{x}}} \ \bar{\mathbf{x}}^T \bar{\mathbf{x}} \\ \text{subject to} \quad &\mathbf{A}_k^- \bar{\mathbf{x}} - \delta_{u,k}^0 \cos\theta \geq \max_{\mathbf{Q}\in\mathcal{S}} |\delta_{u,k}| \ , \forall k \ , \\ &\mathbf{A}_k^+ \bar{\mathbf{x}} - \delta_{l,k}^0 \cos\theta \geq \max_{\mathbf{Q}\in\mathcal{S}} |\delta_{l,k}| \ , \forall k \ . \end{aligned} \tag{5.67}$$

In other words, for each k, we find the the worst-case $\mathbf{Q}$ that maximizes the size of the confidence ellipse and pushes it closer to the decision boundaries. The closer any of these points is to the decision boundary, the larger the transmit power required to satisfy the desired safety margin. Unlike (5.62), this is a challenging problem; as it stands, 5.67 requires solving a convex SLP problem for every possible $\mathbf{Q}$ to find the one that requires the most transmit power.

Fortunately, the complexity of the problem can be significantly reduced based on the following lemma.

Lemma 5.2. *The* $\mathbf{Q}$ *corresponding to the worst-case (maximum) transmit power in (5.67) will be rank-deficient.*

Proof. As mentioned above, the transmit power $\bar{\mathbf{x}}^H\bar{\mathbf{x}}$ required to satisfy the constraints in (5.67) will increase when the worst case SM thresholds $|\delta_{u,k}|$ and $|\delta_{l,k}|$ increase. Hence, to find the maximum transmit power, we first find the $\mathbf{Q}$ that maximizes the SM thresholds. Based on $\mathbf{G}_k$ in Eq. (5.5), if λ_1^Q and λ_1^Q are eigenvalues of $\mathbf{Q}$, we will obtain

$$\lambda_{1,k} = \rho^2|h_{j,k}|^2\lambda_1^Q + \frac{1}{2}\sigma_k^2 \,, \tag{5.68}$$

$$\lambda_{2,k} = \rho^2|h_{j,k}|^2\lambda_2^Q + \frac{1}{2}\sigma_k^2 \,, \tag{5.69}$$

where $\lambda_1^Q + \lambda_2^Q = 1$. Then the term under the square root of Eq. (5.53) can be written as

$$\begin{aligned} p_k \triangleq & \lambda_{1,k}\sin^2(\check{\alpha}_k - \theta) + \lambda_{2,k}\cos^2(\check{\alpha}_k - \theta) \\ = & \rho^2|h_{j,k}|^2\left(\lambda_1^Q\sin^2(\check{\alpha}_k - \theta) + \lambda_2^Q\cos^2(\check{\alpha}_k - \theta)\right) + \frac{1}{2}\sigma_k^2 \\ = & \rho^2|h_{j,k}|^2\lambda_1^Q\left(\sin^2(\check{\alpha}_k - \theta) - \cos^2(\check{\alpha}_k - \theta)\right) + \rho^2|h_{j,k}|^2\cos^2(\check{\alpha}_k - \theta) + \frac{1}{2}\sigma_k^2 \,. \end{aligned} \tag{5.70}$$

When $\check{\alpha}_k$ is fixed, p_k is a linear function of λ_1^Q. Since $0 \le \lambda_1^Q \le 1$, we can find the maximum value of p_k as follows:

- When $\sin^2(\check{\alpha}_k - \theta) \ge \cos^2(\check{\alpha}_k - \theta)$, we have

$$p_k^{u1} \triangleq \max\ p_k = \rho^2|h_{j,k}|^2\sin^2(\check{\alpha}_k - \theta) + \frac{1}{2}\sigma_k^2 \,, \tag{5.71}$$

  with $\lambda_1^Q = 1,\ \lambda_2^Q = 0$;

- When $\sin^2(\check{\alpha}_k - \theta) \le \cos^2(\check{\alpha}_k - \theta)$, we have

$$p_k^{u2} \triangleq \max\ p_k = \rho^2|h_{j,k}|^2\cos^2(\check{\alpha}_k - \theta) + \frac{1}{2}\sigma_k^2 \,, \tag{5.72}$$

  with $\lambda_1^Q = 0,\ \lambda_2^Q = 1$.

Algorithm 2 Robust Symbol Level Precoding

Input: $\mathbf{h}_k$, $h_{j,k}$, s_k, $\delta_{u,k}^0$, $\delta_{l,k}^0$, σ_k, ω_k, $\forall k$, ρ, θ, and N_{div}.
Output: $\bar{\mathbf{x}}^{\text{robust}}$.
for $n \in \{1, \cdots, N_{div}\}$ **do**
    Calculate ϕ^n using (5.78).
    Calculate $\mathbf{v}^n$, the principle eigenvector of $\mathbf{Q}$ by (5.75).
    for $k \in \{1, \cdots, K\}$ **do**
        Calculate $\mathbf{A}_k^-$ in (5.58) , and $\mathbf{A}_k^+$ in (5.61).
        Calculate $\check{\mathbf{v}}_k^n$ using (5.76).
        Calculate $\check{\alpha}_k^n$ using (5.77).
        Calculate $p_k^{u1}(n)$, $p_k^{u2}(n)$, $p_k^{l1}(n)$, $p_k^{l2}(n)$ using (5.71)-(5.74).
    end for
    Solve the optimization problem (5.79) to obtain the optimal precoded vector $\bar{\mathbf{x}}^{n\star}$, as well as the transmit power $|\bar{\mathbf{x}}^{n\star}|^2$.
end for
Return $\bar{\mathbf{x}}^{\text{robust}} = \bar{\mathbf{x}}^n$, where $n = \arg\max_{n\star} |\bar{\mathbf{x}}^{n\star}|^2$.

Similarly, for the lower SM constraints in Eq. (5.57), if $q_k \triangleq \lambda_{1,k} \sin^2(\check{\alpha}_k+\theta)+\lambda_{2,k} \cos^2(\check{\alpha}_k+\theta)$, we can obtain the maxima

$$p_k^{l1} \triangleq \max \; q_k = \rho^2 |h_{j,k}|^2 \sin^2(\check{\alpha}_k + \theta) + \frac{1}{2}\sigma_k^2 \tag{5.73}$$

or

$$p_k^{l2} \triangleq \max \; q_k = \rho^2 |h_{j,k}|^2 \cos^2(\check{\alpha}_k + \theta) + \frac{1}{2}\sigma_k^2 \; . \tag{5.74}$$

Thus, to achieve the maximum value of $|\delta_{u,k}|$ in (5.53) or the maximum value of $|\delta_{l,k}|$ in (5.57), either λ_1^Q or λ_2^Q should be zero, which means the matrix $\mathbf{Q}$ will be rank deficient. □

Lemma 5.2 stands in contrast to Lemma 5.1; while a circular interference signal generates the worst-case MMSE for BLP, for SLP it is a maximally non-circular jammer signal with a rank deficient $\mathbf{Q}$ that leads to the worst performance. To solve 5.67, we must evaluate the worst case $|\delta_{u,k}|$ and $\delta_{l,k}$ for the orientations $\check{\alpha}$ that result from rank-deficient $\mathbf{Q}$. To do this,

we express the principle eigenvector of $\mathbf{Q}$ with direction ϕ as

$$\mathbf{v} = \begin{bmatrix} \cos\phi \\ \sin\phi \end{bmatrix} , \tag{5.75}$$

from which we can use Eq. (5.6),(5.25), and (5.30), to get the principle eigenvector of $\check{\mathbf{G}}_k$ as

$$\check{\mathbf{v}}_k = \begin{bmatrix} \cos\check{\alpha}_k \\ \sin\check{\alpha}_k \end{bmatrix} \propto \frac{\bar{\mathbf{S}}_k^T \bar{\mathbf{H}}_{j,k}}{|h_{j,k}|} \mathbf{v} , \tag{5.76}$$

and hence

$$\check{\alpha}_k = \arctan \frac{\check{\mathbf{v}}_k(2)}{\check{\mathbf{v}}_k(1)} = \phi + \measuredangle h_{j,k} - \measuredangle s_k . \tag{5.77}$$

We see that the orientation of the ellipse at user k depends on the channel from the jammer to user k, user k's symbol from the BS, and the rotation angle due to $\mathbf{Q}$ which is shared by all users. For the results presented in the next section, we discretize ϕ in $(0, \pi]$:

$$\phi^n = \frac{n\pi}{N_{div}}, \ n \in \{1, \cdots, N_{div}\} . \tag{5.78}$$

For each direction ϕ^n, we find $\check{\alpha}_k^n$ for each user and substitute this value into (5.71)-(5.74) to find the worst case bounds for the SLP optimization:

$$\begin{aligned} \bar{\mathbf{x}}^{n\star} = \arg\min_{\bar{\mathbf{x}}^n} \ & (\bar{\mathbf{x}}^n)^T \bar{\mathbf{x}}^n \\ \text{subject to} \quad & \mathbf{A}_k^- \bar{\mathbf{x}}^n - \delta_{u,k}^0 \cos\theta \geq \sqrt{\omega_k}\sqrt{p_k^{u1}(n)} , \forall k , \\ & \mathbf{A}_k^- \bar{\mathbf{x}}^n - \delta_{u,k}^0 \cos\theta \geq \sqrt{\omega_k}\sqrt{p_k^{u2}(n)} , \forall k , \\ & \mathbf{A}_k^+ \bar{\mathbf{x}}^n - \delta_{l,k}^0 \cos\theta \geq \sqrt{\omega_k}\sqrt{p_k^{l1}(n)} , \forall k , \\ & \mathbf{A}_k^+ \bar{\mathbf{x}}^n - \delta_{l,k}^0 \cos\theta \geq \sqrt{\omega_k}\sqrt{p_k^{l2}(n)} , \forall k . \end{aligned} \tag{5.79}$$

The solution is then the $\bar{\mathbf{x}}^{n\star}$ for $n = 1, \cdots, N_{div}$ with largest norm. Algorithm 2 above outlines the detailed steps to implement this "robust SLP" approach.

5.5 Numerical Results

In this section we use Monte Carlo simulations over 1000 independent channel realizations to assess the performance of the proposed BLP and SLP approaches. For each channel realization, a block of 200 symbols is transmitted. The channels $\mathbf{h}_k$ and $h_{j,k}$ are composed of i.i.d. Gaussian random variables with zero mean and unit variance. The power of the additive white Gaussian noise (AWGN) n_k is assumed to be same ($\sigma = 1$ if not specified) for all users, and the probability $p_k = p$ defining the confidence ellipses is identical for all users. We also employ the same safety margin (δ) for all users with respect to a given SNR threshold (ψ), where the relation between δ and ψ can be expressed as [80]

$$\psi = \frac{\delta^2}{(\sin\theta)^2(\rho^2 + \sigma^2)} \, .$$

In some cases we will use the energy efficiency (EE) to quantify the power-performance trade-off of different designs, which is defined as the ratio between the throughput τ and the transmit power per channel:

$$\text{EE} = \frac{\tau}{T \times \|\bar{\mathbf{x}}_c\|^2},$$

where τ is defined in [85, 94] as:

$$\tau = (1 - P_B) \times c \times T \times K,$$

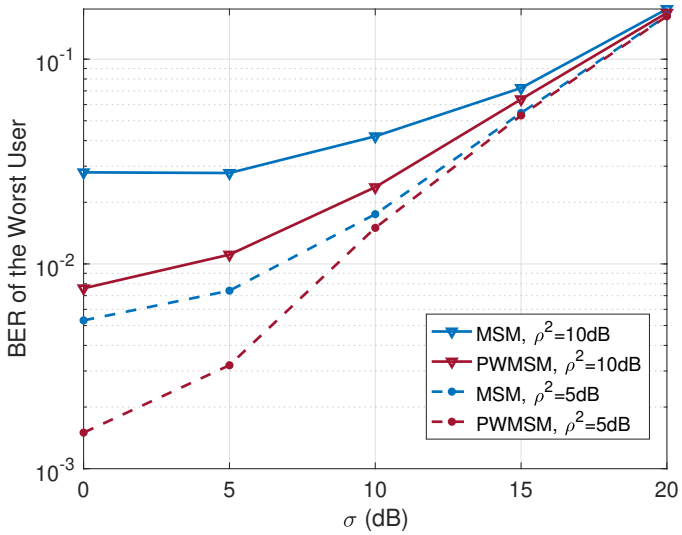

Figure 5.7: BER of the worst user v.s. power of AWGN, with $M = K = 8$, $P_t = 30$dB, QPSK.

where P_B is the block error rate (BLER), $c = \log_2 D$ is the number of bits per modulation symbol, T is the block length and K is the number of receivers.

Table 5.1: Summary of Precoding Approaches

Name	**Q**	Criterion
PW-MSM	Available	MSM
PW-SLP	Available	Minimum Power
Naive BLP	Overlook	MMSE
Naive SLP	Overlook	Minimum Power
PW-BLP	Available	MMSE
NC-SLP	Available	Minimum Power
Robust BLP	$\frac{1}{2}\mathbf{I}_2$	MMSE
Robust SLP	Rank-deficient	Minimum Power

5.5.1 The impact of improper noise

First, we explore the impact of improper noise on the MSM algorithm [82, 84]. We compare it with the PW-MSM approach in Section. 5.2.2, which considers the IGI and employs a pre-whitening transformation to decorrelate the interference. Fig. 5.7 shows that PW-MSM achieves a lower BER, especially at lower SNR where the impact of the interference is greater.

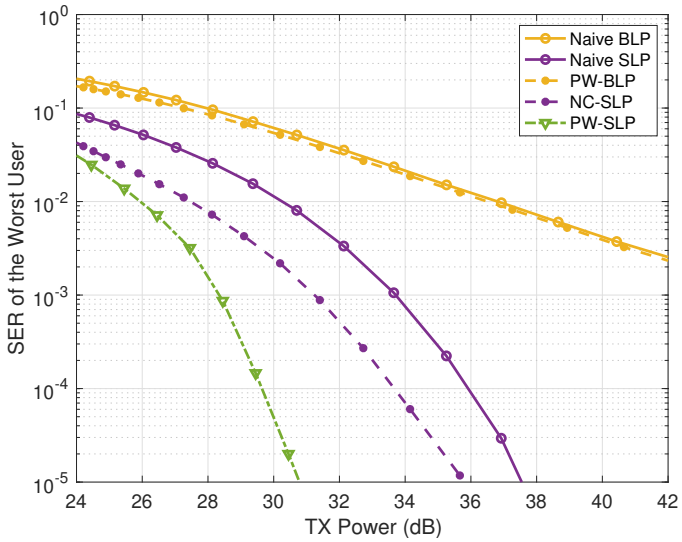

Figure 5.8: SER of the worst user v.s. different SNR (ψ) threshold, with $\rho^2 = 10$dB, $M = K = 8$, $p = 80\%$, QPSK.

Moreover, as power of the jammer gets stronger from 5dB to 10 dB, the gap between the two approaches becomes wider. As the AWGN power σ increases, the circular AWGN noise becomes more dominant in distorting the desired signals, while the impact of the non-circular jammer's signal diminishes. Consequently, the effective noise (resulting from the combination of jammer and AWGN) exhibits circular characteristics. Therefore, with high AWGN power, the PW-MSM approach convergences towards the traditional MSM approach, which aligns with our expectation.

Fig .(5.8) illustrates the SER of the worst user when the BLP/SLP approaches are designed with or without taking the IGI into account. Generally, SLP techniques achieve significantly lower SER for the worst user compared to BLP designs. Its advantage is particularly pronounced in the high SNR region, where the propsed SLP design can provide more than 10dB improvement compared to BLP designs. Our proposed PW-SLP which requires the pre-whitened process at the receiver performs superior, can achieve up to 6dB better than the naive SLP, and hence it is significant to redesign the SLP approaches for systems with IGI. If it is not possible to design the receiver, we can employ the proposed transmission-only SLP designs: NC-SLP, which also exhibits great capability to deal with IGI. In Fig. 5.9, we

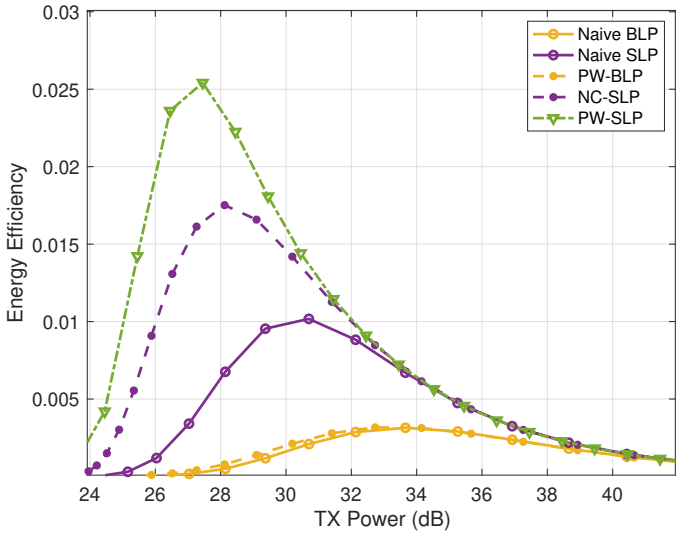

Figure 5.9: Energy efficiency v.s. different transmit power, with $\rho^2 = 10$dB, $M = K = 8$, $p = 80\%$, QPSK.

plot the energy efficiency versus the transmit power for each designs. The SLP designs are more energy efficient compared to BLP designs, and their EE can be further improved if the IGI is taken into account.

5.5.2 The impact of probability constraints p

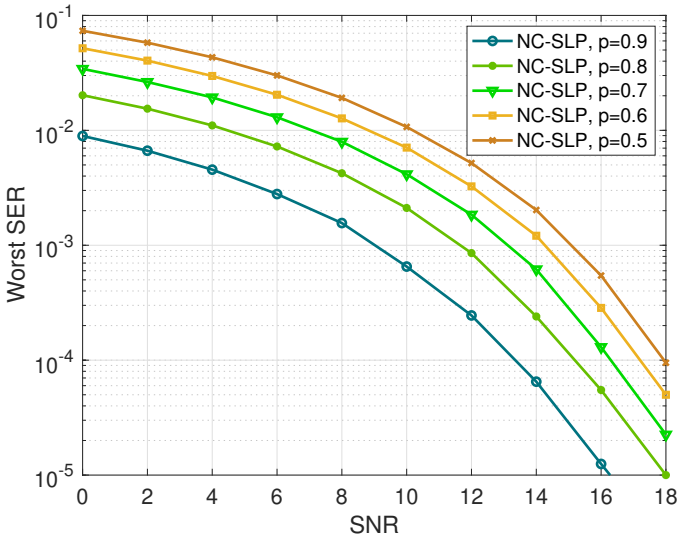

Figure 5.10: The effect of probability constraints on SER pf the worst user when using NC-SLP, with $\rho^2 = 10$dB, $M = K = 8$, QPSK.

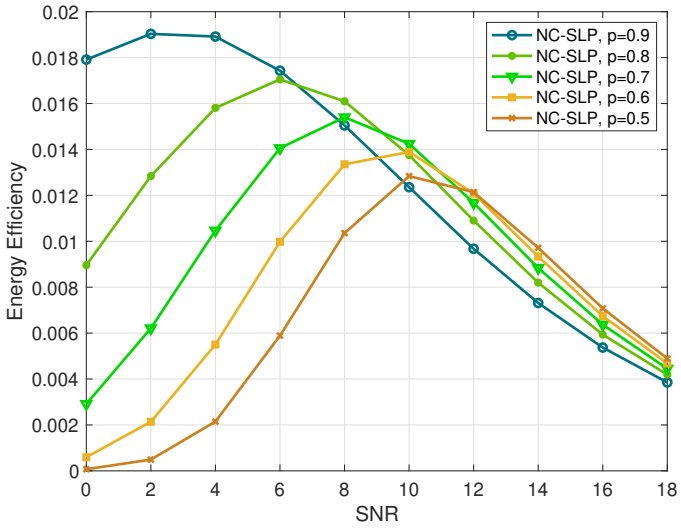

Figure 5.11: The effect of probability constraints on energy efficiency when using NC-SLP, with $\rho^2 = 10$dB, $M = K = 8$, QPSK.

From Section. 5.3, it is evident that the probability constraint also plays an important role in SLP design. Fig. 5.10 illustrates that the higher probability constraint leads to a lower SER. Fig. 5.11 shows the EE of the NC-SLP approach under different probability settings. In the low SNR region, the larger probability constraint improves EE of NC-SLP, however, in the high SNR region, it is better to preset a lower probability. Interestingly, as p increases from 0.5 to 0.9, the transition point where EE starts to deteriorate shifts towards a lower SNR region. This insight is valuable for power budgeting. For instance, when $p = 0.8$, the optimal SNR constraint to achieve the best EE would be around 6dB, beyond which additional power does not yield EE growth.

5.5.3 A deep dive into robust designs

One of the main contribution of this work is the proposal of robust BLP/SLP designs for systems affected by improper interference. In the following, we will discuss them comprehensively.

5.5.3.1 Robust BLP

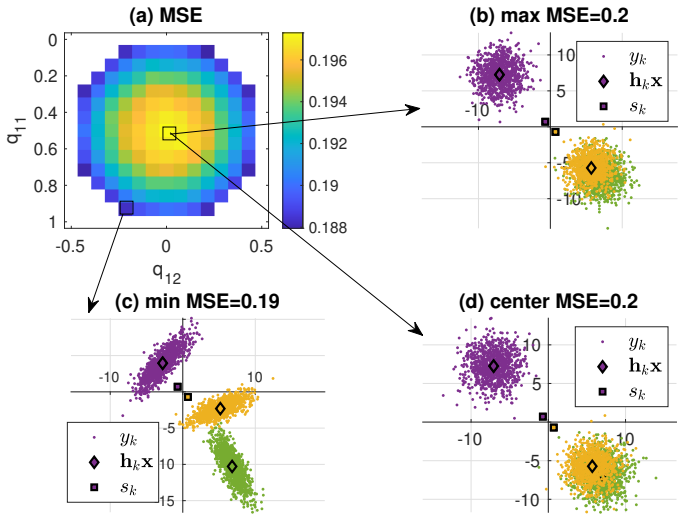

Figure 5.12: PW-BLP designs based on MMSE, with $P_t = 20$dB, $\rho^2 = 10$dB, $M = K = 3$, QPSK. (a) Color map of MSE with various q_{11} and q_{12}; (b) constellations of the desired symbol (s_k), received noiseless symbols ($\mathbf{h}_k\mathbf{x}$), received symbols plus improper noise (y_k) when MSE is the maximum; (c) when MSE is the minimum; (d) when MSE is calculated with $\mathbf{Q} = \frac{1}{2}\mathbf{I}_2$.

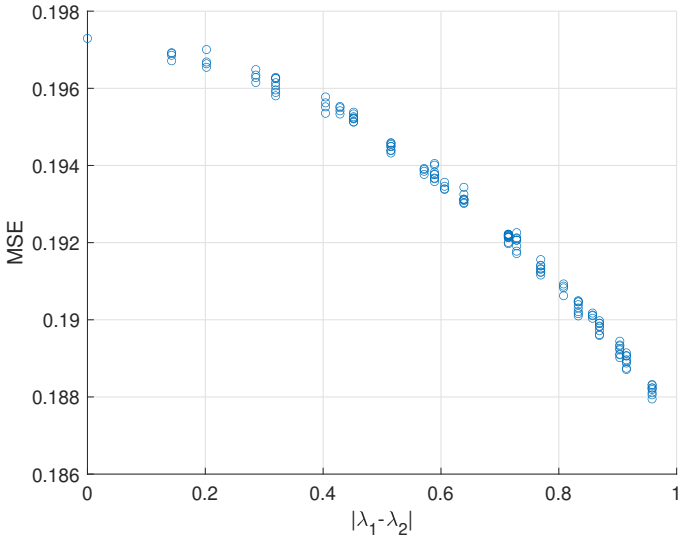

Figure 5.13: MSE v.s. difference of the two eigenvalues of $\mathbf{Q}$.

Fig. 5.12 depicts the result of an exhaustive search for $\mathbf{Q}$ matrices in the set $\mathcal{S} = \{\mathbf{Q} | \text{Tr}\{\mathbf{Q}\} = 1,\ \mathbf{Q} \succeq 0\}$, using 15 steps for each element q_{11} and q_{12}, where $q_{11}(1 - q_{11}) - q_{12}^2 \leq 0$, for $0 \leq q_{11} \leq 1$ and $-0.5 \leq q_{12} \leq 0.5$. In Fig. 5.12(a) color map, the coordinates of each grid are determined by $\mathbf{Q}$, and the color represents the MSE averaged over 10^6 symbols

using Eq. (B.1) for the corresponding $\mathbf{Q}$. Notably, the largest MSE consistently appears at the center, where $\mathbf{Q}$ is $\frac{1}{2}\mathbf{I}_2$. Fig. 5.13 illustrates the MSE in the color map plotted against the difference of these two eigenvalues. A smaller difference between the two eigenvalues corresponds to a larger MSE. When $\lambda_1^Q = \lambda_1^Q = \frac{1}{2}$, we will get the maximum MSE, which should be minimized in (5.65) to design a robust BLP approach. This result is consistent with our proof in Section. 5.4.1.

5.5.3.2 Robust SLP

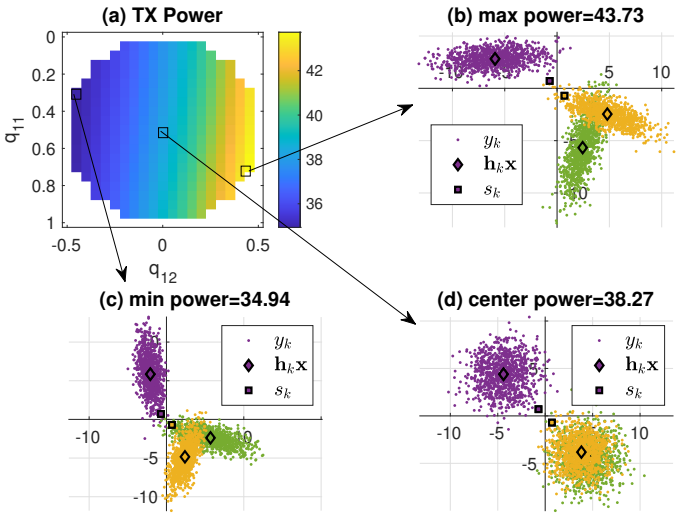

Figure 5.14: NC-SLP designs to minimize power, with $p = 0.95$, $\rho^2 = 10$dB, $M = K = 3$, QPSK. (a) Color map of the transmit power with various q_{11} and q_{12}; (b) constellations of the desired symbol (s_k), received noiseless symbols ($\mathbf{h}_k\mathbf{x}$), received symbols plus improper noise (y_k) when TX power is the maximum; (c) when TX power is the minimum; (d) when TX power is calculated with $q_{11} = 0.5$, $q_{12} = 0$.

Similarly, for given constellation symbols of 3 users, Fig. 5.14(a) shows a color map of the transmit power obtained by solving (5.62) with various $\mathbf{Q}$ in the SLP designs, where q_{11} and q_{12} are each explored in 21 steps. The maximum transmit power (in the brightest color) consistently appears on the boundary of the feasible region $\mathcal{S}$, where $\mathbf{Q}$ is rank deficient with a determinant equal to 0. This implies that the disturbance on the noiseless symbol will degenerate from an ellipse shape to a straight line, pushing the desired symbol in only

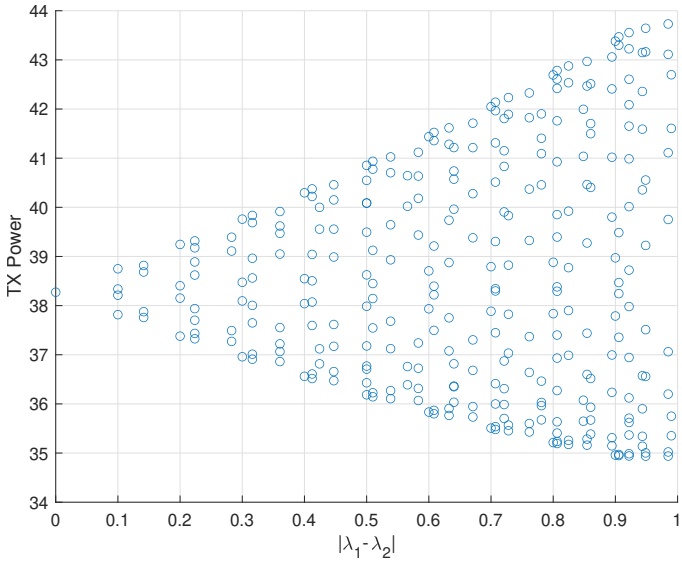

Figure 5.15: Transmit power v.s. difference of the two eigenvalues of $\mathbf{Q}$.

one direction instead of two dimensions. In Fig. (5.15), we plot the transmit power versus $\lambda_1^Q - \lambda_1^Q$, revealing a different pattern compared to the BLP case. The maximum and minimum transmit power are both achieved when $\lambda_1^Q - \lambda_1^Q = 1$. Given that $\lambda_1^Q + \lambda_1^Q = 1$, $\mathbf{Q}$ has to be rank deficient. This insight aligns with our proof of Lemma. 5.2 in Section. 5.4.2.

5.5.3.3 The robustness with different ranks of Q

From the above discussion, we find that the BLP and SLP designs favor different ranks of $\mathbf{Q}$. To investigate how the robust designs perform when $\mathbf{Q}$ is with various ranks, we plotted SER of the worst user in Fig. 5.16 and EE in Fig. 5.17 for rank-1 $\mathbf{Q}$, $\mathbf{Q} = 0.5\mathbf{I}_2$ and random $\mathbf{Q}$ cases. Notably, the robust SLP design is more sensitive to the rank of $\mathbf{Q}$ compared to the BLP designs. This observation supports our lemmas that the robust designs for the SLP and BLP should differ due to the non-circularity in the systems with IGI.

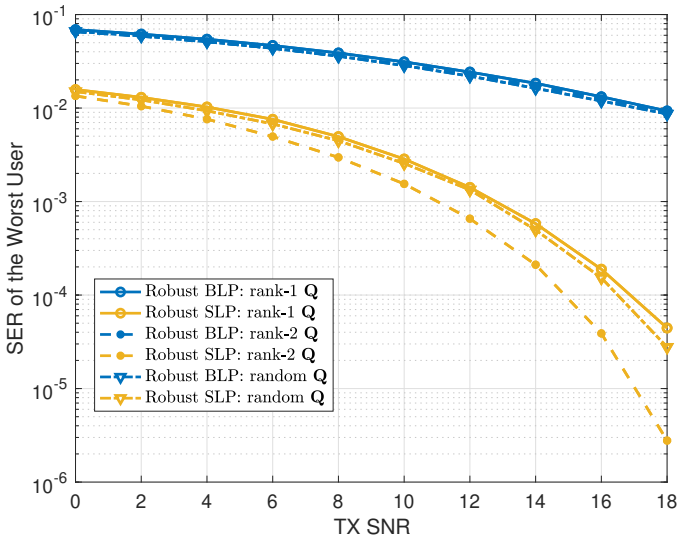

Figure 5.16: SER of the worst user when $\mathbf{Q}$ is generated with different ranks, with $\rho^2 = 10$dB, $M = K = 8$, $p = 95\%$, QPSK.

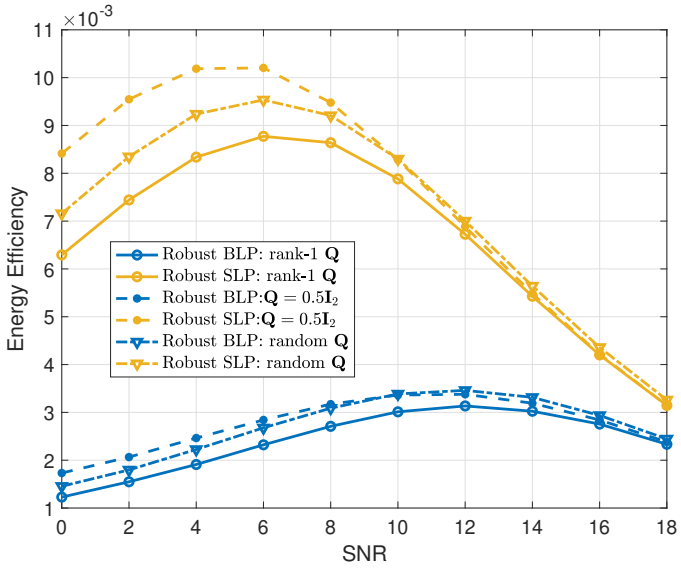

Figure 5.17: EE when $\mathbf{Q}$ is generated with different ranks, with $\rho^2 = 10$dB, $M = K = 8$, $p = 95\%$, QPSK..

5.5.3.4 Convergence of the fast search method for the robust SLP

To investigate the convergence speed of the fast search method described by Algorithm. 2, we tested different numbers of angle sections N_{div}. In Fig. 5.18, we plotted the cumulative distribution function (CDF) of the transmit power $\bar{\mathbf{x}}^H\bar{\mathbf{x}}$. The results shows that with more than two angle sections, the algorithm will converge effectively. It is intuitive from Fig. 5.14(a)

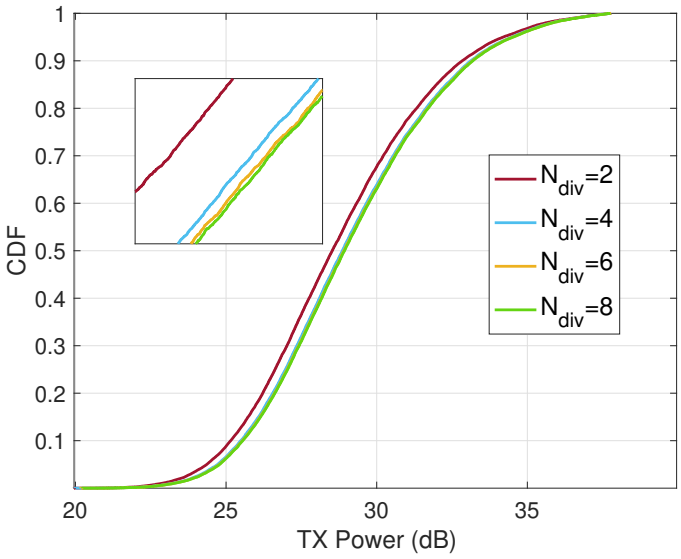

Figure 5.18: Convergence of Algorithm. 2 designed with different numbers of searching angle sections N_{div}, with $\rho^2 = 10$dB, SNR=10dB, $M = K = 8$, $p = 80\%$, QPSK.

that the power is symmetrically distributed on the edge and the maximum/minimum power concentrates within almost a quarter of the perimeter.

5.6 conclusion

Our work focuses on enhancing BLP and SLP designs in wireless communication systems, particularly in the context of the jammer creating improper/non-circular interference to the desired signals. We firstly investigate the impact of improper noise on the MSM approach, which is essential for SLP strategies but often overlooks the correlation structure of noise, leading to biased estimates of the jammer's effect. To mitigate the effects of non-circular noise, we employ a pre-whitening transformation firstly to map correlated noise to uncorrelated forms. However, these pre-whitening methods require receiver processing. When only the transmission processing is feasible, we introduce a novel SLP approach that leverages knowledge of the jammer's signal covariance matrix. Unlike traditional SLP designs that assume circular noise, we employ confidence ellipse to model the distribution of improper

noise. Moreover, we address scenarios in which the non-circularity is not known at the BS. In response, we introduce robust BLP and SLP designs, where they select totally different covariance matrices as the worst case in the optimization to achieve robustness. The numerical results show the superiority of our proposed approaches.

Chapter 6

User Selection and Closed-form SLP

In this chapter, we explore the user selection approaches with SLP designs. There are limited study about this topic.

6.1 System Model and Power Constraint

In a downlink MU-MISO system, the BS is equipped with N antennas serving K single-antenna users. The channels are assumed to be i.i.d Rayleigh fading channels. $\mathbf{H} \in \mathbb{C}^{K \times N}$ is the channel matrix and $\mathbf{h}_k$ is the k-th user's channel. $\mathbf{W}$ is the precoding matrix. $\mathbf{s} = [s_1, s_2, \cdots, s_K]$ is the PSK-modulated signal vector for K users. $\mathbf{n}$ is the noise vector and the noise at k-th user is the AWGN where $n_k \sim \mathcal{CN}(0, \sigma_k^2)$. The received signal can be written as,

$$\mathbf{y} = f\mathbf{HWs} + \mathbf{n} \tag{6.1}$$

where f is the transmit power scaling factor. The transmitted symbol at the BS antennas can be expressed as

$$\mathbf{x} = f \cdot \mathbf{W} \cdot \mathbf{s} = f \cdot \sum_{k=1}^{K} \mathbf{w}_k s_k \ . \tag{6.2}$$

When the average power at the transmitter is $\mathbb{E}\left\{\|\mathbf{x}\|^2\right\} = P$, we will have

$$\mathbb{E}\left\{\mathrm{Tr}\{f^2 \cdot \mathbf{W} \cdot \mathbf{s} \cdot \mathbf{s}^H \cdot \mathbf{W}^H\}\right\} = P \ , \tag{6.3}$$

$$\Rightarrow f^2 \cdot \mathrm{Tr}\{\mathbf{W} \cdot \mathbb{E}\left\{\mathbf{s} \cdot \mathbf{s}^H\right\} \cdot \mathbf{W}^H\} = P \ , \tag{6.4}$$

$$\Rightarrow f = \sqrt{\frac{P}{\mathrm{Tr}\{\mathbf{W}\mathbf{W}^H\}}} \ . \tag{6.5}$$

Take the traditional block-level ZF as an example. We have $\mathbf{x}_{ZF} = f_{ZF} \cdot \mathbf{H}^H \cdot (\mathbf{H}\mathbf{H}^H)^{-1} \cdot \mathbf{s}$, where $f_{ZF} = \frac{P}{\sqrt{\mathrm{Tr}\{(\mathbf{H}\mathbf{H}^H)^{-1}\}}}$.

If the transmitter has an instantaneous power constraint as $\|\mathbf{x}\|^2 = P$, we will get

$$\mathrm{Tr}\{f^2 \cdot \mathbf{W} \cdot \mathbf{s} \cdot \mathbf{s}^H \cdot \mathbf{W}^H\} = P \ , \tag{6.6}$$

$$\Rightarrow f^2 \cdot \mathrm{Tr}\{\mathbf{W} \cdot \mathbf{s} \cdot \mathbf{s}^H \cdot \mathbf{W}^H\} = P \ , \tag{6.7}$$

$$\Rightarrow f = \sqrt{\frac{P}{\mathrm{Tr}\{\mathbf{W} \cdot \mathbf{s} \cdot \mathbf{s}^H \cdot \mathbf{W}^H\}}} \ , \tag{6.8}$$

which takes the instantaneous symbol information into consideration.

For instance, CIZF Precoding takes instantaneous power into account in [14]:

$$\mathbf{W}_{\mathrm{CR}} = \cdot \mathbf{H}^H \cdot (\mathbf{H}\mathbf{H}^H)^{-1} \cdot \mathbf{R}_\phi \tag{6.9}$$

where f_{CR} is the scaling factor which ensures the power normalization. $\mathbf{R}_\phi$ is the correlation rotation matrix which aims at making the transmitted signals be constructively received at

each user without destructive interference. The instantaneous power at antennas is

$$
\begin{aligned}
f_{\mathrm{CR}}^2(\mathbf{W}_{\mathrm{CR}}\mathbf{s})^H\mathbf{W}_{\mathrm{CR}}\mathbf{s} &= f_{\mathrm{CR}}^2 \cdot \mathbf{s}^H \cdot {\mathbf{R}_\phi}^H \cdot (\mathbf{H}\mathbf{H}^H)^{-1} \cdot \mathbf{H} \cdot \mathbf{H}^H \cdot (\mathbf{H}\mathbf{H}^H)^{-1} \cdot \mathbf{R}_\phi \cdot \mathbf{s} && (6.10)\\
&= f_{\mathrm{CR}}^2 \cdot \mathbf{s}^H \cdot {\mathbf{R}_\phi}^H \cdot (\mathbf{H}\mathbf{H}^H)^{-1} \cdot \mathbf{R}_\phi \cdot \mathbf{s} && (6.11)\\
&= P\ , && (6.12)\\
\Rightarrow f_{\mathrm{CR}} &= \frac{P}{\sqrt{\mathbf{s}^H\mathbf{R}_\phi^H\left(\mathbf{H}\mathbf{H}^H\right)^{-1}\mathbf{R}_\phi\mathbf{s}}} && (6.13)
\end{aligned}
$$

where the correlation rotation matrix is $\mathbf{R}_\phi = \mathbf{R} \circ \mathbf{\Phi}$. and

$$
\begin{aligned}
\mathbf{\Phi}_{m,n} &= exp\{j(\measuredangle s_m - \measuredangle(s_n \cdot \rho_{mn}))\}\\
&= exp\{j\measuredangle s_m\} \cdot exp\{-j(\measuredangle s_n + \measuredangle\rho_{mn})\}\\
&= s_m \cdot exp\{-j\measuredangle s_n\} \cdot exp\{-j\measuredangle\rho_{mn}\}\\
&= s_m \cdot s_n^* \cdot \frac{\rho_{mn}^*}{|\rho_{mn}|}\ .
\end{aligned}
\qquad (6.14)
$$

Furthermore, we can derive the elements in the correlation rotation matrix as

$$
(\mathbf{R}_\phi)_{m,n} = \mathbf{R}_{m,n}\mathbf{\Phi}_{m,n} = \rho_{mn} \cdot s_m \cdot s_n^* \cdot \frac{\rho_{mn}^*}{|\rho_{mn}|} = s_m \cdot s_n^* \cdot |\rho_{mn}|\ . \qquad (6.15)
$$

If we denote $\mathbf{\Upsilon}_{m,n} = |\rho_{mn}|$, then the correlation rotation matrix can be rewritten as

$$
\mathbf{R}_\phi = \mathrm{diag}(\mathbf{s}) \cdot \mathbf{\Upsilon} \cdot \mathrm{diag}(\mathbf{s}^H) = \mathbf{S}\mathbf{\Upsilon}\mathbf{S}^H \qquad (6.16)
$$

where $\mathbf{S} = \mathrm{diag}(\mathbf{s})$.

Substituting the $\mathbf{R}_\phi$ in (6.16) into (6.13), we can find

$$\begin{aligned} f_{\text{CR}} &= \frac{1}{\sqrt{\mathbf{s}^H \text{diag}(\mathbf{s}) \boldsymbol{\Upsilon}^H \text{diag}(\mathbf{s}^H)(\mathbf{H}\mathbf{H}^H)^{-1} \text{diag}(\mathbf{s}) \boldsymbol{\Upsilon} \text{diag}(\mathbf{s}^H)\mathbf{s}}} \\ &= \frac{1}{\sqrt{\mathbf{1}_{K\times 1}^H \cdot \boldsymbol{\Upsilon}^H \cdot \mathbf{V} \cdot \boldsymbol{\Upsilon} \cdot \mathbf{1}_{K\times 1}}} \end{aligned} \tag{6.17}$$

where $\mathbf{V} = \text{diag}(\mathbf{s}^H)(\mathbf{H}\mathbf{H}^H)^{-1}\text{diag}(\mathbf{s})$. And $\mathbf{1}_{K\times 1} = \text{diag}(\mathbf{s}^H)\mathbf{s}$ is a vector of all ones with length of K.

As by constructive interferece precoding the resulting interferece contributes to the useful signal power, the received instantaneous SNR at user k using CI precoding technique can be written as

$$\gamma_k = \frac{|\mathbf{h}_k \mathbf{W}\mathbf{b}|^2}{\sigma_k^2} \tag{6.18}$$

By substituting (6.9) and (6.16) into (6.18), the SNR_k can be expressed as

$$\begin{aligned} \gamma_k &= \frac{\left| f_{\text{CR}} \cdot \mathbf{h}_k \cdot \mathbf{H}^H \cdot (\mathbf{H}\mathbf{H}^H)^{-1} \cdot \text{diag}(\mathbf{s}) \cdot \boldsymbol{\Upsilon} \cdot \text{diag}(\mathbf{s}^H) \cdot \mathbf{s} \right|^2}{\sigma_k^2} \\ &= \frac{\left| f_{\text{CR}} \cdot \mathbf{e}_k \cdot \mathbf{H} \cdot \mathbf{H}^H \cdot (\mathbf{H}\mathbf{H}^H)^{-1} \cdot \text{diag}(\mathbf{s}) \cdot \boldsymbol{\Upsilon} \cdot \mathbf{1} \right|^2}{\sigma_k^2} \\ &= \frac{|f_{\text{CR}} \cdot \mathbf{e}_k \cdot \text{diag}(\mathbf{s}) \cdot \boldsymbol{\Upsilon} \cdot \mathbf{1}|^2}{\sigma_k^2} \\ &= \frac{|f_{\text{CR}} \cdot \mathbf{e}_k \cdot \boldsymbol{\Upsilon} \cdot \mathbf{1} \cdot b_k|^2}{\sigma_k^2} \\ &= \frac{1}{\mathbf{1} \cdot \boldsymbol{\Upsilon}^H \cdot \mathbf{V} \cdot \boldsymbol{\Upsilon} \cdot \mathbf{1}} \cdot \frac{|\mathbf{e}_k \cdot \boldsymbol{\Upsilon} \cdot \mathbf{1}|^2}{\sigma_k^2} \end{aligned} \tag{6.19}$$

where $\mathbf{e}_k$ is a $K \times 1$ vector all the elements of this vector are zeros except the k-th element is one.

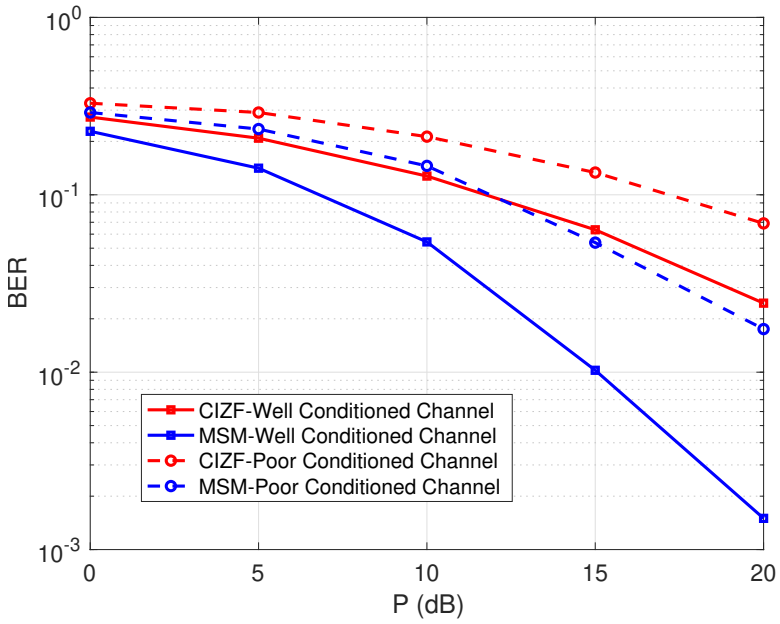

Figure 6.1: Impact of different channels on SLP designs.

6.2 The Impact of User Selection on SLP

According to [14], the received symbol at each user k can be written as

$$r_k = f_{CR} \cdot (\sum_{j=1}^{K} |\rho_{ij}|) \cdot s_k + n_k = \lambda_k \cdot s_k + n_k \ , \tag{6.20}$$

where

$$\begin{aligned} \lambda_k = f_{CR} \cdot (\sum_{j=1}^{K} |\rho_{ij}|) &= \frac{\sum_{j=1}^{K} |\rho_{ij}|}{\sqrt{\mathrm{Tr}\{\boldsymbol{\Upsilon}\mathbf{S}^H(\mathbf{H}\mathbf{H}^H)^{-1}\mathbf{S}\boldsymbol{\Upsilon}\}}} \\ &= \frac{\mathbf{e}_k^T \cdot \boldsymbol{\Upsilon} \cdot \mathbf{1}_{K\times 1}}{\sqrt{\mathrm{Tr}\{\boldsymbol{\Upsilon}\mathbf{S}^H(\mathbf{H}\mathbf{H}^H)^{-1}\mathbf{S}\boldsymbol{\Upsilon}\}}} \end{aligned} \tag{6.21}$$

and $\rho_{ij} = \sum_{k=1}^{K} h_{i,k} h_{k,j}^*$ is the element (i, j) of the channel correlation matrix $\mathbf{H}\mathbf{H}^H$. From Eq. (6.20), it is easy to find that the power of the received symbol r_k highly depends on λ_k which is decided by channels. In order to verify this, we test the performance of different SLP designs when the channel is well conditioned and poor conditioned in Fig. (6.1). The

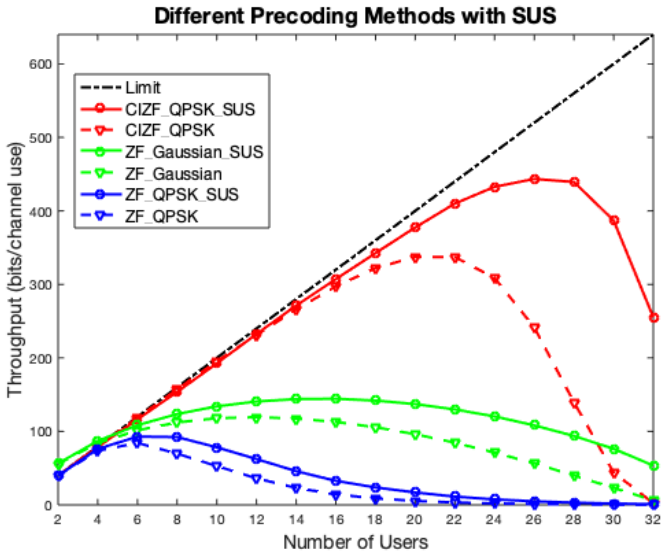

Figure 6.2: Compare different precoding approaches with and without user selection strategy.

number of BS antennas is $N = 10$, the number of users is $K = 10$, and the modulation is QPSK. Well conditioned channels are independent with Gaussian complex distribution, whereas the poor conditioned channels are high correlated among users whose correlation matrix can be generated using the Toeplitz matrix. It is illustrated that the SLP designs highly depends on the condition of the channel. When the channel is well structured, SLP approaches will show more advantage than the ones with poor conditioned channels.

To guarantee QoS of the system, we take the user selection problem into account. Fig. (6.2) illustrate the impact of user selection on different precoding techniques. We employ the well-known user selection method "SUS" in [99] to select different number of users from the total 100 users. The number of antennas at the transmitter will change with the number of selected users, and $N = K$. In Fig. (6.2), "Gaussian" means that Gaussian complex symbols are transmitted without modulation, "US" means with user selection, and "limit" is the upper bound of the throughput calculated by BLER discussed in former chapters. We can conclude that the user selection will improve the performance of precoding approaches, especially for the CIZF which gains more benefit from the user selection.

Algorithm 3 CIZF-based User Selection-Greedy Algorithm

Step (1) Initialization:
$\mathcal{T}_0 = \{1, \ldots, N\}$.
$\mathcal{S}_0 = \varnothing$ (empty set).
$\pi(1) = \arg\max_k \|\mathbf{h}_k\|$, given that $k \in \mathcal{T}_0$.
$\mathcal{S} = \mathcal{S}_0 + \{\pi(1)\}$, set of selected users.
$\mathcal{T} = \mathcal{T}_0 - \{\pi(1)\}$, set of unselected users.
Step (2) Selection:
for $i = 2, \cdots, K$ **do**
    $Q = |\mathcal{T}|$.
    for $m = 1, \cdots, Q$ **do**
        $\mathcal{S}_{temp} = \mathcal{S} + \mathcal{T}(m)$.
        for $t = 1, \cdots, N$ **do**
            Calculate $\alpha(m,t) = \sum_s \lambda(s,t)$ using (6.21), given that $s \in \mathcal{S}_{temp}$, $\mathbf{b}(\mathcal{S}_{temp})$, and $\mathbf{H}(\mathcal{S}_{temp})$.
        end for
        $\sigma(m) = \sum_t \alpha(m,t)$.
    end for
    $\pi(i) = \arg\max \sigma(m)$, given that $m \in \mathcal{T}$.
    $\mathcal{S} = \mathcal{S} + \{\pi(i)\}$, which is set of selected users.
    $\mathcal{T} = \mathcal{T} - \{\pi(i)\}$, which is the set of other users.
end for

After taking the SLP technique into consideration, we try to better design the user selection which is different from SUS. The method depends on both CSI and symbol information. Based on Eq. (6.20), our user selection algorithm tries to find the optimal group of users who generates the largest sum of λ_k in order to get the maximum SINR. The steps of selecting K out of N users are outlined in Algorithm. 3.

Fig. 6.3 shows the comparison between our proposed greedy algorithm (with CIZF precoding) with the SUS (with ZF precoding). The number of BS antennas is $N = 32$ and the number of total users is $M = 32$ as well. We need to select K users out of $M = 32$. QPSK is employed. From Fig. 6.3, we find that our proposed greedy algorithm performs better than the block-level user selection and precoding approach, especially when the number of served users is close to the number of BS antennas, the performance gap between the two approached increases.

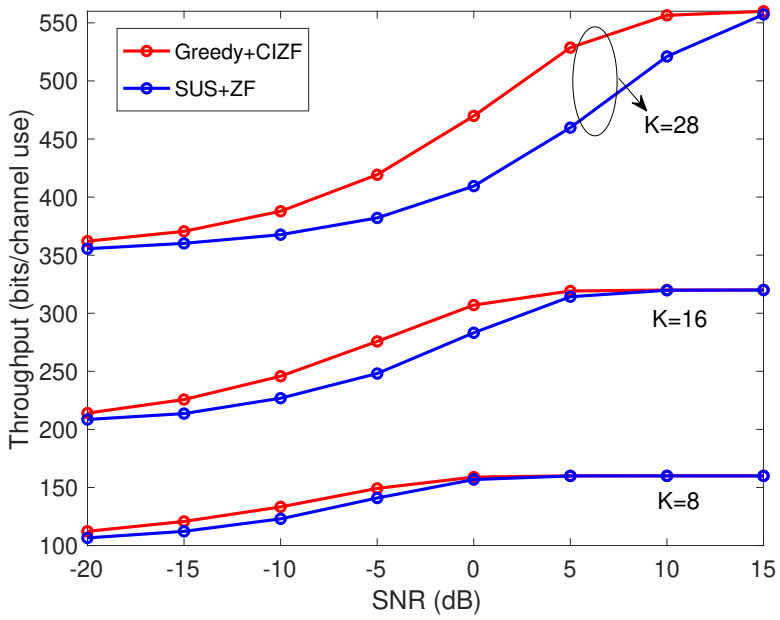

Figure 6.3: Comparison of user selection between our proposed greedy algorithm with SUS.

6.3 Closed-form SLP

Traditional SLP approaches require symbol-level broadcasting of the rescaling factor to users for accurate demodulation, which complicates practical implementation. In order to decrease the complexity of SLP and make it practical, some researchers have started to work on the closed-form SLP [80] or propose a block-level rescaling [100] recently. In this sections, we will show our work on the closed-form SLP and hope it will be helpful for future work.

For the jth user, the noiseless received symbol in the modified coordinate system is $z_j = s_j^* r_j = s_j^* \mathbf{h}_j \mathbf{x}$, which in vector form for all users becomes $\mathbf{z} = \mathbf{S}^{\mathrm{H}}\mathbf{H}\mathbf{x} = \widetilde{\mathbf{H}}\mathbf{x}$, where $\widetilde{\mathbf{H}} \triangleq \mathbf{S}^{\mathrm{H}}\mathbf{H}$. The safety margin for each CU is

$$\delta_j = \mathcal{R}\{z_j\} \sin\theta - |\mathcal{I}\{z_j\}| \cos\theta. \tag{6.22}$$

If the preset SM of all users is δ^0, the constraint ensuring the QoS can be expressed as

$$\mathcal{R}\{z_j\} \sin\theta - |\mathcal{I}\{z_j\}| \cos\theta \geq \delta_c^0 \quad \forall j \in \mathcal{J} \tag{6.23}$$

The BS designs the transmit signal vector $\mathbf{x}$ to maximize δ., where the constraint can be formulated in matrix form as follows, for BPSK:

$$\mathcal{R}\{\mathbf{z}\} \geq \delta^0 \mathbf{1}_N \tag{6.24}$$

and for DPSK ($D > 2$):

$$-\mathcal{R}\{\mathbf{z}\}\tan\theta + \frac{\delta^0}{\cos\theta}\mathbf{1}_N \leq \mathcal{I}\{\mathbf{z}\} \leq \mathcal{R}\{\mathbf{z}\}\tan\theta - \frac{\delta^0}{\cos\theta}\mathbf{1}_N \tag{6.25}$$

Using the real-valued matrix representation,

$$\mathcal{R}\{\mathbf{z}\} = \mathcal{R}\{\widetilde{\mathbf{H}}\mathbf{x}\} \tag{6.26}$$

$$= \begin{bmatrix} \mathcal{R}\{\widetilde{\mathbf{H}}\} & -\mathcal{I}\{\widetilde{\mathbf{H}}\} \end{bmatrix} \begin{bmatrix} \mathcal{R}\{\mathbf{x}\} \\ \mathcal{I}\{\mathbf{x}\} \end{bmatrix} \tag{6.27}$$

$$\triangleq \mathbf{G}\check{\mathbf{x}} \tag{6.28}$$

$$\mathcal{I}\{\mathbf{z}\} = \mathcal{I}\{\widetilde{\mathbf{H}}\mathbf{x}\} \tag{6.29}$$

$$= \begin{bmatrix} \mathcal{I}\{\widetilde{\mathbf{H}}\} & \mathcal{R}\{\widetilde{\mathbf{H}}\} \end{bmatrix} \begin{bmatrix} \mathcal{R}\{\mathbf{x}\} \\ \mathcal{I}\{\mathbf{x}\} \end{bmatrix} \tag{6.30}$$

$$\triangleq \mathbf{Q}\check{\mathbf{x}}\,, \tag{6.31}$$

the constraints in (6.24) and (6.25) can be rewritten as

$$-\mathbf{G}\check{\mathbf{x}} + \delta^0 \mathbf{1}_N \leq \mathbf{0}_N \quad \text{(BPSK)} \tag{6.32}$$

$$\begin{bmatrix} -\mathbf{G}\tan\theta + \mathbf{Q} \\ -\mathbf{G}\tan\theta - \mathbf{Q} \end{bmatrix} \check{\mathbf{x}} + \frac{\delta^0}{\cos\theta}\mathbf{1}_{2N} \leq \mathbf{0}_{2N} \ (D\text{PSK},\ D > 2). \tag{6.33}$$

If we define

$$\mathbf{B} = \begin{bmatrix} -\mathbf{G}\tan\theta + \mathbf{Q} \\ -\mathbf{G}\tan\theta - \mathbf{Q} \end{bmatrix} \tag{6.34}$$

$$\mathbf{d} = \frac{1}{\cos\theta}\mathbf{1}_{2N}\ , \tag{6.35}$$

the problem with modulation order higher than 2 can be reformulated as

$$\underset{\check{\mathbf{x}}}{\text{minimize}} \quad \|\check{\mathbf{x}}\|^2 \tag{6.36}$$

$$\text{subject to} \quad \mathbf{B}\check{\mathbf{x}} + \mathbf{d}\delta^0 \leq \mathbf{0}_{2N}\ , \tag{6.37}$$

We analyze this problem with Lagrangian and KKT conditions. The Lagrangian is expressed as [101]:

$$\mathcal{L}(\check{\mathbf{x}}, \boldsymbol{\mu}) = \check{\mathbf{x}}^T\check{\mathbf{x}} + \boldsymbol{\mu}^T(\mathbf{B}\check{\mathbf{x}} + \delta^0\mathbf{d}), \tag{6.38}$$

where $\boldsymbol{\mu} = \begin{bmatrix} \mu_1 & \cdots & \mu_{2N} \end{bmatrix}^T$ contains the dual variables and $\mu_i \geq 0, \forall\ 1 \leq i \leq 2N$. It is obvious that the primal problem is convex and the optimal solution satisfies the following KKT conditions such as

$$\frac{\partial\mathcal{L}}{\partial\check{\mathbf{x}}} = 2\check{\mathbf{x}} + \mathbf{B}^T\boldsymbol{\mu} = 0 \tag{6.39}$$

$$\mathbf{B}\check{\mathbf{x}} + \delta^0\mathbf{d} \leq \mathbf{0}_{2N} \tag{6.40}$$

$$\mu_i \geq 0,\ \forall 1 \leq i \leq 2N \tag{6.41}$$

$$\mu_i(\mathbf{B}_i\check{\mathbf{x}} + \delta^0\mathbf{d}_i) = 0,\ \forall 1 \leq i \leq 2N \tag{6.42}$$

From Eq. (6.39), we can get the optimal transmit symbol should satisfy

$$\check{\mathbf{x}} = -\frac{1}{2}\mathbf{B}^T\boldsymbol{\mu}. \tag{6.43}$$

Therefore, the dual function is

$$g(\boldsymbol{\mu}) = -\frac{1}{4}\boldsymbol{\mu}^T\mathbf{B}\mathbf{B}^T\boldsymbol{\mu} + (\delta^0\mathbf{d})^T\boldsymbol{\mu}. \tag{6.44}$$

The primal problem is convex, and the Slater's condition qualifies here, therefore the strong duality holds here which means we can get the primal optimal solution by maximizing the dual function. The Lagrange dual problem is

$$\underset{\boldsymbol{\mu}}{\text{maximize}} \quad -\frac{1}{4}\boldsymbol{\mu}^T\mathbf{B}\mathbf{B}^T\boldsymbol{\mu} + (\delta^0\mathbf{d})^T\boldsymbol{\mu} \tag{6.45}$$

$$\text{subject to} \quad \boldsymbol{\mu} \geq 0, \tag{6.46}$$

which is a non-negative least square (NNLS) problem with many sophisticated algorithms to solve it such as an active-set method published by Lawson and Hanson [102]. Here we can see that the size of the dual variable $\boldsymbol{\mu}$ is $1 \times 2N$ whereas the size of the primal variable $\check{\mathbf{x}}$ is $1 \times 2M$. In practical MIMO system, since $M \gg N$, we would efficiently and tremendously decrease the complexity of designing the SLP. This optimization problem is referred to as Minimizing Power SLP (MinPowerSLP).

Lemma 6.1. *If $M \gg N$, the NNLS problem is equivalent to the LS problem which means the optimal solution $\boldsymbol{\mu}_{opt}$ of*

$$\underset{\boldsymbol{\mu}}{\text{maximize}} \quad -\frac{1}{4}\boldsymbol{\mu}^T\mathbf{B}\mathbf{B}^T\boldsymbol{\mu} + (\delta^0\mathbf{d})^T\boldsymbol{\mu}, \tag{6.47}$$

is element-wise positive, i.e., $\boldsymbol{\mu} \geq \mathbf{0}$.

Proof. The optimal solution $\boldsymbol{\mu}_{opt}$ of $g(\boldsymbol{\mu})$ can be derived by

$$\frac{\partial g(\boldsymbol{\mu})}{\partial \boldsymbol{\mu}} = -\frac{1}{2}\mathbf{B}\mathbf{B}^T\boldsymbol{\mu} + \mathbf{d}\delta^0 = \mathbf{0}, \tag{6.48}$$

therefore

$$\mathbf{B}\mathbf{B}^T\boldsymbol{\mu} = 2\delta^0\mathbf{d}\ . \tag{6.49}$$

where

$$\mathbb{E}\{\mathbf{B}\mathbf{B}^T\} \triangleq \mathbf{M} = \frac{M}{\cos\theta^2}\begin{bmatrix} \mathbf{I}_N & -\cos 2\theta\mathbf{I}_N \\ -\cos 2\theta\mathbf{I}_N & \mathbf{I}_N \end{bmatrix}\ . \tag{6.50}$$

It is easy to see that the non-diagonal elements of $\mathbf{M}$ is non-positive, therefore it is a real Z-matrix. If we express $\mathbf{M}$ as

$$\mathbf{M} = \frac{M}{\cos\theta^2}\mathbf{I}_{2N} - \mathbf{T}\ , \tag{6.51}$$

where

$$\mathbf{T} = \frac{M}{\cos\theta^2}\begin{bmatrix} \mathbf{0}_N & \cos 2\theta\mathbf{I}_N \\ \cos 2\theta\mathbf{I}_N & \mathbf{0}_N \end{bmatrix} \tag{6.52}$$

is a matrix with all elements non-negative and with all the eigenvalues

$$\lambda = \frac{M}{\cos\theta^2}\cos 2\theta \leq \frac{M_c}{\cos\theta^2}\ , \tag{6.53}$$

$\mathbf{M}$ is obviously a M-matrix. According to the "monotone" property of M-matrix, $\mathbf{M}\mathbf{x} \geq \mathbf{0}$ implies $\mathbf{x} \geq \mathbf{0}$, then look back Eq. (6.49), we can easily get $\boldsymbol{\mu} \geq \mathbf{0}$ due to $\delta^0\mathbf{d} \geq \mathbf{0}_{2N}$ and $\mathbf{B}\mathbf{B}^T$ is a M-matrix when $M \gg N$. □

Based on the lemma, we can get that if the number of transmit antennas is much greater than the number of users, the original NNLS problem for SLP will change to a standard LS problem, which is easy to find the optimal closed-form solution. In future, we can find more applications and probability with this result.

Chapter 7

Conclusion and Future Work

In this dissertation, we mainly work on the robust SLP designs in CR systems and systems with IGI. We firstly proposed several SLP algorithms for underlay and overlay CR networks that exploit constructive interference. The result shows that the PUs can achieve benefits from the CR transmission with SLP designs. We reformulated the SINR balancing problem to optimize CUs performance while meeting interference constraints for PUs. We generalized previous zero-forcing and interference balancing approaches, extending SINR balancing and maximum safety margin algorithms to use shared channel and data information from the PBS. Our algorithms outperform prior solutions by naturally exploiting constructive interference without relaying PU symbols.

Secondly, using two CSI error models, we derived two robust SLP methods: one based on max-min optimization of the worst-case CSI error, and the other on a probability-constrained problem using AQNM to approximate CSI quantization impact. These optimization problems result in a quadratic objective function with linear inequality constraints that are efficiently solvable. Our numerical results show that our robust SLP schemes handle various CSI errors while maintaining high energy efficiency, and can improve PU network performance.

Thirdly, we enhance SLP design in wireless communication systems, focusing on non-circular interference resulted from the jammer's signal. We first investigate the impact of improper noise on the MSM approach, essential for SLP strategies but often overlooking noise correlation, leading to biased jammer effect estimates. To mitigate non-circular noise effects, we employ a whitening transformation to map correlated noise to uncorrelated forms. Numerical results demonstrate that considering noise non-circularity significantly enhances MSM precoder performance, highlighting the importance of accurate safety margin formulation and CIR with respect to noise characteristics. Additionally, we introduce a novel SLP approach leveraging the jammer's signal covariance matrix knowledge to minimize transmit power while satisfying upper and lower safety margin constraints. In response, we propose robust BLP and SLP designs, selecting different covariance matrices for optimization to achieve robustness. Numerical results show the superiority of our proposed SLP approaches.

Future work will explore the relationship between SER and probability constraints in the robust SLP designs. For example, when considering quantized CSI with AQNM in the Chapter. 4, the preset probability affects the constraint for SM and hence makes difference in robustness as well as SER. Moreover, in the systems with IGI, when using confidence ellipse to facilitate the robust SLP designs, we show the numerical result that with different preset confidence of the ellipse, the energy efficiency will change, which motivates us to think about the relationship between them in order to efficiently find the optimal solution. Based on the work in Chapter. 5, we can further study the robust designs in systems with IGI, when both the CSI from the jammer to user and the non-circularity are unknown. Additionally, the user selection and closed-form problems in SLP are challenging. We only explore some basic ideas in Chapter. 6, and there are more potential work on these topics.

Bibliography

[1] B. Zong, C. Fan, X. Wang, X. Duan, B. Wang, and J. Wang, "6G technologies: Key drivers, core requirements, system architectures, and enabling technologies," *IEEE Veh. Technol. Mag.*, vol. 14, no. 3, pp. 18–27, 2019.

[2] W. Saad, M. Bennis, and M. Chen, "A vision of 6G wireless systems: Applications, trends, technologies, and open research problems," *IEEE network*, vol. 34, no. 3, pp. 134–142, 2019.

[3] D. Gesbert, S. Hanly, H. Huang, S. Shamai S., O. Simeone, and W. Yu, "Multi-cell MIMO cooperative networks: A new look at interference," *IEEE J. Sel. Areas Commun.*, vol. 28, no. 9, pp. 1380–1408, 2010.

[4] R. Zhang and Y.-C. Liang, "Exploiting multi-antennas for opportunistic spectrum sharing in cognitive radio networks," *IEEE J. Sel. Topics Signal Process.*, vol. 2, no. 1, pp. 88–102, 2008.

[5] T. K. Y. Lo, "Maximum ratio transmission," *IEEE Trans. Commun.*, vol. 47, pp. 1458–1461, Oct. 1999.

[6] Q. H. Spencer, A. Swindlehurst, and M. Haardt, "Zero-forcing methods for downlink spatial multiplexing in multiuser MIMO channels," *IEEE Trans. Signal Process.*, vol. 52, pp. 461–471, Jan. 2004.

[7] C. Peel, B. Hochwald, and A. Swindlehurst, "A vector-perturbation technique for near-capacity multiantenna multiuser communication-part I: Channel inversion and regularization," *IEEE Trans. Commun.*, vol. 53, pp. 195–202, Feb. 2005.

[8] E. Björnson, M. Bengtsson, and B. Ottersten, "Optimal multiuser transmit beamforming: A difficult problem with a simple solution structure," *IEEE Signal Process. Mag.*, vol. 31, pp. 142–148, June 2014.

[9] O. Tervo, L.-N. Tran, and M. Juntti, "Optimal energy-efficient transmit beamforming for multi-user MISO downlink," *IEEE Trans. Signal Process.*, vol. 63, pp. 5574–5588, July 2015.

[10] M. Schubert and H. Boche, "Iterative multiuser uplink and downlink beamforming under SINR constraints," *IEEE Trans. Signal Process.*, vol. 53, pp. 2324–2334, June 2005.

[11] M. Alodeh, D. Spano, A. Kalantari, C. G. Tsinos, D. Christopoulos, S. Chatzinotas, and B. Ottersten, "Symbol-level and multicast precoding for multiuser multiantenna downlink: A state-of-the-art, classification, and challenges," *IEEE Commun. Surveys Tuts.*, vol. 20, no. 3, pp. 1733–1757, 2018.

[12] A. Li, D. Spano, J. Krivochiza, S. Domouchtsidis, C. G. Tsinos, C. Masouros, S. Chatzinotas, Y. Li, B. Vucetic, and B. Ottersten, "A tutorial on interference exploitation via symbol-level precoding: Overview, state-of-the-art and future directions," *IEEE Commun. Surveys Tuts.*, vol. 22, pp. 796–839, Mar. 2020.

[13] C. Masouros and E. Alsusa, "Dynamic linear precoding for the exploitation of known interference in MIMO broadcast systems," *IEEE Trans. Wireless Commun.*, vol. 8, pp. 1396–1404, Mar. 2009.

[14] C. Masouros, "Correlation rotation linear precoding for MIMO broadcast communications," *IEEE Trans. Signal Process.*, vol. 59, pp. 252–262, Oct. 2010.

[15] C. Masouros, T. Ratnarajah, M. Sellathurai, C. B. Papadias, and A. K. Shukla, "Known interference in the cellular downlink: A performance limiting factor or a source of green signal power?," *IEEE Commun. Mag.*, vol. 51, pp. 162–171, Oct. 2013.

[16] C. Masouros and E. Alsusa, "A novel transmitter-based selective-precoding technique for DS/CDMA systems," *IEEE Signal Process. Lett.*, vol. 14, no. 9, pp. 637–640, 2007.

[17] M. Alodeh, S. Chatzinotas, and B. Ottersten, "Energy-efficient symbol-level precoding in multiuser MISO based on relaxed detection region," *IEEE Trans. Wireless Commun.*, vol. 15, pp. 3755–3767, Feb. 2016.

[18] J. Mitola and G. Maguire, "Cognitive radio: Making software radios more personal," *IEEE Personal Commun. Mag.*, vol. 6, pp. 13–18, Aug. 1999.

[19] S. Haykin, "Cognitive radio: Brain-empowered wireless communications," *IEEE J. Sel. Areas Commun.*, vol. 23, pp. 201–220, Feb. 2005.

[20] A. Goldsmith, S. A. Jafar, I. Maric, and S. Srinivasa, "Breaking spectrum gridlock with cognitive radios: An information theoretic perspective," *Proc. IEEE*, vol. 97, pp. 894–914, Apr. 2009.

[21] I. F. Akyildiz, W. Y. Lee, M. C. Vuran, and S. Mohanty, "NeXt generation/dynamic spectrum access/cognitive radio wireless networks: A survey," *Comput. Netw.*, vol. 50, pp. 2127–2159, Sept. 2006.

[22] Y.-C. Liang, K.-C. Chen, G. Y. Li, and P. Mahonen, "Cognitive radio networking and communications: An overview," *IEEE Trans. Veh. Technol.*, vol. 60, pp. 3386–3407, June 2011.

[23] Y. Xing, C. N. Mathur, M. Haleem, R. Chandramouli, and K. Subbalakshmi, "Dynamic spectrum access with QoS and interference temperature constraints," *IEEE Trans. Mobile Comput.*, vol. 6, no. 4, pp. 423–433, 2007.

[24] B. Wang and K. R. Liu, "Advances in cognitive radio networks: A survey," *IEEE J. Sel. Topics Signal Process.*, vol. 5, no. 1, pp. 5–23, 2010.

[25] N. Devroye, P. Mitran, and V. Tarokh, "Achievable rates in cognitive radio channels," *IEEE Trans. Inf. Theory*, vol. 52, no. 5, pp. 1813–1827, 2006.

[26] A. Jovicic and P. Viswanath, "Cognitive radio: An information-theoretic perspective," *IEEE Trans. Inf. Theory*, vol. 55, no. 9, pp. 3945–3958, 2009.

[27] K. L. Law, C. Masouros, and M. Pesavento, "Transmit precoding for interference exploitation in the underlay cognitive radio Z-channel," *IEEE Trans. Signal Process.*, vol. 65, no. 14, pp. 3617–3631, 2017.

[28] C. Masouros and T. R., "Interference as a source of green signal power in cognitive relay assisted co-existing MIMO wireless transmissions," *IEEE Trans. Commun.*, vol. 60, no. 2, pp. 525–536, 2012.

[29] F. A. Khan, C. Masouros, and T. Ratnarajah, "Interference-driven linear precoding in multiuser MISO downlink cognitive radio network," *IEEE Trans. Veh. Technol.*, vol. 61, pp. 2531–2543, May 2012.

[30] M. Alodeh, S. Chatzinotas, and B. Ottersten, "Symbol based precoding in the downlink of cognitive MISO channel," in *Proc. Int. Conf. on Cog. Rad. Oriented Wireless Netw. (CrownCom)*, EAI, 2015.

[31] M. Alodeh, D. Spano, S. Chatzinotas, and B. Ottersten, "Peak power minimization in symbol-level precoding for cognitive MISO downlink channels," in *Proc. IEEE Int. Conf. on Digit. Signal Process. (DSP)*, IEEE, 2016.

[32] N. Jindal, "MIMO broadcast channels with finite-rate feedback," *IEEE Trans. Inf. Theory*, vol. 52, pp. 5045–5060, Oct. 2006.

[33] N. Vucic and H. Boche, "Robust QoS-constrained optimization of downlink multiuser MISO systems," *IEEE Trans. Signal Process.*, vol. 57, pp. 714–725, Oct. 2008.

[34] X. Liang, Y. Li, W. Cao, S. Zhao, S. Liu, and X. Zhao, "Power allocation and performance analysis in overlay cognitive cooperative V2V communication system with outdated CSI," *IEEE Trans. Intell. Transp. Syst.*, vol. 23, no. 11, pp. 21440–21449, 2022.

[35] A. Pascual-Iserte, D. P. Palomar, A. I. Pérez-Neira, and M. A. Lagunas, "A robust maximin approach for MIMO communications with imperfect channel state information based on convex optimization," *IEEE Trans. Signal Process.*, vol. 54, pp. 346–360, Dec. 2005.

[36] G. Zheng, K. K. Wong, and B. Ottersten, "Robust cognitive beamforming with bounded channel uncertainties," *IEEE Trans. Signal Process.*, vol. 57, pp. 4871–4881, July 2009.

[37] X. Zhang, D. P. Palomar, and B. Ottersten, "Statistically robust design of linear MIMO transceivers," *IEEE Trans. Signal Process.*, vol. 56, pp. 3678–3689, July 2008.

[38] M. B. Shenouda and T. N. Davidson, "Probabilistically-constrained approaches to the design of the multiple antenna downlink," in *Proc. Asilomar Conf. on Signals, Syst., and Comput.*, pp. 1120–1124, Oct. 2008.

[39] D. Bertsimas and M. Sim, "Tractable approximations to robust conic optimization problems," *Math. Prgram.*, vol. 107, pp. 5–36, June 2006.

[40] A. Ben-Tal and A. Nemirovski, "On safe tractable approximations of chance-constrained linear matrix inequalities," *Math. of Operations Research*, vol. 34, pp. 1–25, Feb. 2009.

[41] G. Zheng, S. Ma, K. K. Wong, and T. S. Ng, "Robust beamforming in cognitive radio," *IEEE Trans. Wireless Commun.*, vol. 9, pp. 570–576, Feb. 2010.

[42] S. Ma and D. Sun, "Chance constrained robust beamforming in cognitive radio networks," *IEEE Commun. Lett.*, vol. 17, pp. 67–70, Nov. 2012.

[43] I. Wajid, M. Pesavento, Y. C. Eldar, and D. Ciochina, "Robust downlink beamforming with partial channel state information for conventional and cognitive radio networks," *IEEE Trans. Signal Process.*, vol. 61, pp. 3656–3670, May 2013.

[44] C. Masouros and G. Zheng, "Exploiting known interference as green signal power for downlink beamforming optimization," *IEEE Trans. Signal Process.*, vol. 63, no. 14, pp. 3628–3640, 2015.

[45] A. Haqiqatnejad, F. Kayhan, and B. Ottersten, "Robust SINR-constrained symbol-level multiuser precoding with imperfect channel knowledge," *IEEE Trans. Signal Process.*, vol. 68, pp. 1837–1852, Mar. 2020.

[46] W. Liang, S. X. Ng, and L. Hanzo, "Cooperative overlay spectrum access in cognitive radio networks," *IEEE Commun. Surveys Tuts.*, vol. 19, no. 3, pp. 1924–1944, 2017.

[47] K. Huang and R. Zhang, "Cooperative feedback for multiantenna cognitive radio networks," *IEEE Trans. Signal Process.*, vol. 59, pp. 747–758, Oct. 2010.

[48] H. A. Suraweera, P. J. Smith, and M. Shafi, "Capacity limits and performance analysis of cognitive radio with imperfect channel knowledge," *IEEE Trans. Veh. Technol.*, vol. 59, pp. 1811–1822, Feb. 2010.

[49] Q. Bai, A. Mezghani, and J. A. Nossek, "On the optimization of ADC resolution in multi-antenna systems," in *Proc. Int. Symp. on Wireless Commun. Syst. (ISWCS)*, pp. 1–5, Aug. 2013.

[50] Q. Bai and J. A. Nossek, "Energy efficiency maximization for 5G multi-antenna receivers," *Trans. Emerg. Telecommun. Technol.*, vol. 26, pp. 3–14, Jan. 2015.

[51] A. K. Fletcher, S. Rangan, V. K. Goyal, and K. Ramchandran, "Robust predictive quantization: Analysis and design via convex optimization," *IEEE J. Sel. Topics Signal Process.*, vol. 1, pp. 618–632, Dec. 2007.

[52] L. Fan, S. Jin, C.-K. Wen, and H. Zhang, "Uplink achievable rate for massive MIMO systems with low-resolution ADC," *IEEE Commun. Lett.*, vol. 19, pp. 2186–2189, Oct. 2015.

[53] J. Zhang, L. Dai, Z. He, S. Jin, and X. Li, "Performance analysis of mixed-ADC massive MIMO systems over Rician fading channels," *IEEE J. Sel. Areas Commun.*, vol. 35, pp. 1327–1338, Mar. 2017.

[54] J. Max, "Quantizing for minimum distortion," *IEEE Trans. Inf. Theory*, vol. 6, pp. 7–12, Mar. 1960.

[55] S. Lloyd, "Least squares quantization in PCM," *IEEE Trans. Inf. Theory*, vol. 28, pp. 129–137, Mar. 1982.

[56] X. Yang and A. Swindlehurst, "Limited rate feedback for two-user MISO Gaussian interference channel with and without secrecy," *IEEE Trans. Signal Process.*, vol. 66, pp. 4884–4897, Sept. 2018.

[57] L. Liu and A. Swindlehurst, "Overlay cognitive radio using symbol level precoding with quantized CSI," in *Proc. IEEE Int. Conf. Acoust. Speech Signal Process. (ICASSP)*, pp. 1–5, IEEE, 2023.

[58] S. M. Kay, *Fundamentals of Statistical Signal Processing: Estimation Theory*. Prentice-Hall, Inc., 1993.

[59] T. Adali, P. J. Schreier, and L. L. Scharf, "Complex-valued signal processing: The proper way to deal with impropriety," *IEEE Trans. Signal Process.*, vol. 59, no. 11, pp. 5101–5125, 2011.

[60] P. J. Schreier and L. L. Scharf, *Statistical Signal Processing of Complex-valued Data: The Theory of Improper and Noncircular Signals*. Cambridge University Press, 2010.

[61] A. E. Canbilen, M. M. Alsmadi, E. Basar, S. S. Ikki, S. S. Gultekin, and I. Develi, "Spatial modulation in the presence of I/Q imbalance: Optimal detector & performance analysis," *IEEE Commun. Lett.*, vol. 22, no. 8, pp. 1572–1575, 2018.

[62] T. Dao and G. Hueber, "I/Q imbalance calibration method for 5G ultra-wideband transceivers," *IEEE Trans. Circuits Syst. II*, vol. 67, no. 12, pp. 3048–3052, 2020.

[63] M. Kim, J. H. Cho, and J. S. Lehnert, "Asymptotically optimal low-complexity SC-FDE with noise prediction in data-like improper-complex interference," *IEEE Trans. Wireless Commun.*, vol. 15, no. 3, pp. 2090–2103, 2016.

[64] C. Lameiro, I. Santamaría, W. Utschiclk, and P. J. Schreier, "Maximally improper interference in underlay cognitive radio networks," in *Proc. IEEE Int. Conf. Acoust. Speech Signal Process. (ICASSP)*, pp. 3666–3670, IEEE, 2016.

[65] M. M. Alsmadi, N. A. Ali, and S. S. Ikki, "SSK in the presenzce of improper Gaussian noise: Optimal receiver design and error analysis," in *Proc. IEEE Wireless Commun. Netw. Conf. (WCNC)*, pp. 1–6, IEEE, 2018.

[66] S. Sallem, J.-P. Delmas, and P. Chevalier, "Optimal SIMO MLSE receivers for the detection of linear modulation corrupted by noncircular interference," in *IEEE Statist. Signal Process. Workshop (SSP)*, pp. 840–843, 2012.

[67] M. M. Alsmadi, A. E. Canbilen, N. A. Ali, and S. S. Ikki, "Effect of generalized improper Gaussian noise and in-phase/quadrature-phase imbalance on quadrature spatial modulation," *IEEE Open J. of Signal Process.*, vol. 2, pp. 295–308, 2021.

[68] Y. Zeng, R. Zhang, E. Gunawan, and Y. L. Guan, "Optimized transmission with improper Gaussian signaling in the K-user MISO interference channel," *IEEE Trans. Wireless Commun.*, vol. 12, no. 12, pp. 6303–6313, 2013.

[69] O. De C., H. Jedda, A. Mezghani, A. L. Swindlehurst, and J. A. Nossek, "Reconsidering linear transmit signal processing in 1-bit quantized multi-user MISO systems," *IEEE Trans. Wireless Commun.*, vol. 18, no. 1, pp. 254–267, 2018.

[70] M. Soleymani, I. Santamaria, and P. J. Schreier, "Improper Gaussian signaling for the K-user MIMO interference channels with hardware impairments," *IEEE Trans. Veh. Technol.*, vol. 69, no. 10, pp. 11632–11645, 2020.

[71] H. D. Nasir, A. A.and Tuan, T. Q. Duong, and H. V. Poor, "Improper Gaussian signaling for broadcast interference networks," *IEEE Signal Process. Lett.*, vol. 26, no. 6, pp. 808–812, 2019.

[72] F. Sterle, "Widely linear MMSE transceivers for MIMO channels," *IEEE Trans. Signal Process.*, vol. 55, no. 8, pp. 4258–4270, 2007.

[73] D. Darsena, G. Gelli, and F. Verde, "Widely-linear precoders and decoders for MIMO channels," in *Proc. Int. Symp. on Wireless Commun. Syst. (ISWCS)*, pp. 1–5, VDE, 2013.

[74] W. Zhang, R. C. de Lamare, C. Pan, M. Chen, J. Dai, B. Wu, and X. Bao, "Widely linear precoding for large-scale MIMO with IQI: Algorithms and performance analysis," *IEEE Trans. Wireless Commun.*, vol. 16, no. 5, pp. 3298–3312, 2017.

[75] S. Javed, O. Amin, B. Shihada, and M.-S. Alouini, "A journey from improper Gaussian signaling to asymmetric signaling," *IEEE Commun. Surveys Tuts.*, vol. 22, no. 3, pp. 1539–1591, 2020.

[76] G. Strang, *Introduction to Linear Algebra*. Society for Ind. and Appl. Math. (SIAM), 2022.

[77] C. D. Meyer and I. Stewart, *Matrix Analysis and Applied Linear Algebra*. Society for Ind. and Appl. Math. (SIAM), 2023.

[78] A. Li, C. Masouros, X. Liao, Y. Li, and B. V., "Multiplexing more data streams in the MU-MISO downlink by interference exploitation precoding," in *Proc. IEEE Wireless Commun. Netw. Conf. (WCNC)*, IEEE, 2020.

[79] A. Haqiqatnejad, F. Kayhan, and B. Ottersten, "Symbol-level precoding design based on distance preserving constructive interference regions," *IEEE Trans. Signal Process.*, vol. 66, pp. 5817–5832, Oct. 2018.

[80] A. Li and C. Masouros, "Interference exploitation precoding made practical: Optimal closed-form solutions for PSK modulations," *IEEE Trans. Wireless Commun.*, vol. 17, pp. 7661–7676, Sept. 2018.

[81] R. Liu, Z. Bo, M. Li, and Q. Liu, "End-to-end learning for symbol-level precoding and detection with adaptive modulation," *IEEE Wireless Commun. Lett.*, vol. 12, no. 1, pp. 50–54, 2022.

[82] H. Jedda, A. Mezghani, J. A. Nossek, and A. Swindlehurst, "Massive MIMO downlink 1-bit precoding with linear programming for PSK signaling," in *Proc. IEEE Int. Workshop on Signal Process. Adv. in Wireless Commun. (SPAWC)*, July 2017.

[83] A. Li, C. Masouros, B. Vucetic, Y. Li, and A. Swindlehurst, "Interference exploitation precoding for multi-level modulations: Closed-form solutions," *IEEE Trans. Commun.*, vol. 69, pp. 291–308, Oct. 2021.

[84] H. Jedda, A. Mezghani, A. Swindlehurst, and J. A. Nossek, "Quantized constant envelope precoding with PSK and QAM signaling," *IEEE Trans. Wireless Commun.*, vol. 17, pp. 8022–8034, Oct. 2018.

[85] L. Liu, C. Masouros, and A. Swindlehurst, "Robust symbol level precoding for overlay cognitive radio networks," *IEEE Trans. Wireless Commun.*, vol. 23, no. 2, pp. 1403–1415, 2024.

[86] A. Kalantari, M. Soltanalian, S. Maleki, S. Chatzinotas, and B. Ottersten, "Directional modulation via symbol-level precoding: A way to enhance security," *IEEE J. Sel. Topics Signal Process.*, vol. 10, pp. 1478–1493, Aug. 2016.

[87] A. Swindlehurst, A. Saxena, A. Mezghani, and I. Fijalkow, "Minimum probability-of-error perturbation precoding for the one-bit massive MIMO downlink," in *Proc. IEEE Int. Conf. Acoust. Speech Signal Process. (ICASSP)*, pp. 6483–6487, June 2017.

[88] A. Swindlehurst, H. Jedda, and I. Fijalkow, "Reduced dimension minimum BER PSK precoding for constrained transmit signals in massive MIMO," in *Proc. IEEE Int. Conf. Acoust. Speech Signal Process. (ICASSP)*, pp. 3584–3588, Apr. 2018.

[89] A. Haqiqatnejad, F. Kayhan, and B. Ottersten, "Constructive interference for generic constellations," *IEEE Signal Process. Lett.*, vol. 25, pp. 586–590, Feb. 2018.

[90] W. S. H. M. W. Ahmad, N. A. M. Radzi, F. S. Samidi, A. Ismail, F. Abdullah, M. Z. Jamaludin, and M. N. Zakaria, "5G technology: Towards dynamic spectrum sharing using cognitive radio networks," *IEEE Access*, vol. 8, pp. 14460–14488, 2020.

[91] K.-J. Lee, H. Sung, and I. Lee, "Linear precoder designs for cognitive radio multiuser MIMO downlink systems," in *Proc. IEEE Int. Conf. Commun. (ICC)*, IEEE, 2011.

[92] K. Hamdi, M. O. Hasna, A. Ghrayeb, and K. B. Letaief, "Priority-based zero-forcing in spectrum sharing cognitive systems," *IEEE Commun. Lett.*, vol. 17, no. 2, pp. 313–316, 2013.

[93] M. Schubert and H. Boche, "Solution of the multiuser downlink beamforming problem with individual SINR constraints," *IEEE Trans. Veh. Technol.*, vol. 53, no. 1, pp. 18–28, 2004.

[94] A. Salem and C. Masouros, "Error probability analysis and power allocation for interference exploitation over Rayleigh fading channels," *IEEE Trans. Wireless Commun.*, Apr. 2021.

[95] R. Eaves and A. Levesque, "Probability of block error for very slow Rayleigh fading in Gaussian noise," *IEEE Trans. Commun.*, vol. 25, pp. 368–374, Mar. 1977.

[96] S. Catreux, V. Erceg, D. Gesbert, and R. W. Heath, "Adaptive modulation and MIMO coding for broadband wireless data networks," *IEEE Commun. Mag.*, vol. 40, no. 6, pp. 108–115, 2002.

[97] A. Mayouche, W. A. Martins, S. Chatzinotas, and B. Ottersten, "Data-driven precoded MIMO detection robust to channel estimation errors," *IEEE Open J. Commun. Soc.*, vol. 2, pp. 1144–1157, 2021.

[98] H. L. Van T., *Detection, Estimation, and Modulation Theory, Part I: Detection, Estimation, and Linear Modulation Theory*. John Wiley and Sons, 2004.

[99] T. Yoo and A. Goldsmith, "On the optimality of multiantenna broadcast scheduling using zero-forcing beamforming," *IEEE J. Sel. Areas Commun.*, vol. 24, no. 3, pp. 528–541, 2006.

[100] A. Li, F. Liu, X. Liao, Y. Shen, and C. Masouros, "Symbol-level precoding made practical for multi-level modulations via block-level rescaling," in *Proc. IEEE Int. Workshop on Signal Process. Adv. in Wireless Commun. (SPAWC)*, pp. 71–75, IEEE, 2021.

[101] S. P. Boyd and L. Vandenberghe, *Convex Optimization*. Cambridge University Press, 2004.

[102] C. L. Lawson and R. J. Hanson, *Solving Least Squares Problems*. Society for Ind. and Appl. Math. (SIAM), 1995.

[103] A. Kessy, A. Lewin, and K. Strimmer, "Optimal whitening and decorrelation," *The American Statist.*, vol. 72, pp. 309–314, Oct. 2018.

Appendix A

Proof of Lemma 4.1

From [45] we note that eliminating the (possible) correlation between the entries of $\mathbf{q}_{c,j}$ by applying a whitening transform can ease the difficulty of finding the desired approximation. In particular, we will apply the whitening matrix from [103] which is optimal in terms of mean-squared error, i.e.,

$$\mathbb{R}_{\mathbf{q}_{c,j}}^{-\frac{1}{2}} = \frac{\sqrt{2}}{\sqrt{P_p \beta_c \alpha_c (2-\alpha_c)}} \begin{bmatrix} 1 & -\cos 2\theta \\ -\cos 2\theta & 1 \end{bmatrix}^{-\frac{1}{2}} . \tag{A.1}$$

The determinant of $\begin{bmatrix} 1 & -\cos 2\theta \\ -\cos 2\theta & 1 \end{bmatrix}$ is $1 - \cos^2 2\theta = \sin^2 2\theta$, and thus is always non-negative, and non-zero for $\theta \neq 90°$. Thus $\mathbb{R}_{\mathbf{q}_{c,j}}$ is non-singular, positive definite and invertible.

As a result, the probability expression in (4.60) can be equivalently written as

$$\begin{aligned}\mathbb{P}\{\mathbf{w}_{c,j}(\check{\mathbf{x}}_c) \geq \mathbf{q}_{c,j}\} &= \mathbb{P}\{\mathbf{w}_{c,j}(\check{\mathbf{x}}_c) \geq \mathbb{R}_{\mathbf{q}_{c,j}}^{\frac{1}{2}} \mathbb{R}_{\mathbf{q}_{c,j}}^{-\frac{1}{2}} \mathbf{q}_{c,j}\} \\ &= \mathbb{P}\{\mathbb{R}_{\mathbf{q}_{c,j}}^{-\frac{1}{2}} \mathbf{w}_{c,j}(\check{\mathbf{x}}_c) \geq \mathbb{R}_{\mathbf{q}_{c,j}}^{-\frac{1}{2}} \mathbf{q}_{c,j}\} \\ &= \mathbb{P}\{\bar{\mathbf{w}}_{c,j}(\check{\mathbf{x}}_c) \geq \bar{\mathbf{q}}_{c,j}\} \end{aligned} \tag{A.2}$$

where $\bar{\mathbf{w}}_{c,j}(\check{\mathbf{x}}_c) \triangleq \mathbb{R}_{\mathbf{q}_{c,j}}^{-\frac{1}{2}} \mathbf{w}_{c,j}(\check{\mathbf{x}}_c)$ and $\bar{\mathbf{q}}_{c,j} \triangleq \mathbb{R}_{\mathbf{q}_{c,j}}^{-\frac{1}{2}} \mathbf{q}_{c,j}$. Consequently, the chance constraint (4.60) is equivalent to

$$\mathbb{P}\{\bar{\mathbf{w}}_{c,j}(\check{\mathbf{x}}_c) \geq \bar{\mathbf{q}}_{c,j}\} \geq v_c \tag{A.3}$$

with $\bar{\mathbf{q}}_{c,j} \sim \mathcal{N}(\mathbf{0},\ \mathbf{I})$.

To obtain an efficiently computable constraint, we apply the *Safe Approximation I* method in [45]. The two entries of $\bar{\mathbf{q}}_{c,j}$ are uncorrelated and independent. Defining

$$\bar{\mathbf{q}}_{c,j} \triangleq \begin{bmatrix} \bar{q}_{c,j}^1 \\ \bar{q}_{c,j}^2 \end{bmatrix},\ \bar{\mathbf{w}}_{c,j}(\check{\mathbf{x}}_c) \triangleq \begin{bmatrix} \bar{w}_{c,j}^1 \\ \bar{w}_{c,j}^2 \end{bmatrix}\ , \tag{A.4}$$

the Gaussian cumulative distribution function can be used to calculate the joint probability in (A.2) as follows:

$$\mathbb{P}\{\bar{\mathbf{w}}_{c,j}(\check{\mathbf{x}}_c) \geq \bar{\mathbf{q}}_{c,j}\} = \mathbb{P}\{\bar{w}_{c,j}^1 \geq \bar{q}_{c,j}^1\}\mathbb{P}\{\bar{w}_{c,j}^2 \geq \bar{q}_{c,j}^2\} = \frac{1+\mathrm{erf}(\frac{\bar{w}_{c,j}^1}{\sqrt{2}})}{2} \times \frac{1+\mathrm{erf}(\frac{\bar{w}_{c,j}^2}{\sqrt{2}})}{2}\ ,$$

where the error function is given by

$$\mathrm{erf}(x) = \frac{2}{\sqrt{\pi}} \int_0^x \exp(-t^2)\, dt\,.$$

Due to the monotonicity of $\mathrm{erf}(x)$, the desired probability is bounded below by

$$\mathbb{P}\{\bar{\mathbf{w}}_{c,j}(\check{\mathbf{x}}_c) \geq \bar{\mathbf{q}}_{c,j}\} \geq \left[\frac{1+\mathrm{erf}(\frac{\min\{\bar{w}^1_{c,j},\bar{w}^2_{c,j}\}}{\sqrt{2}})}{2}\right]^2 . \tag{A.5}$$

In order to satisfy the chance constraint (A.3), it is sufficient to consider the deterministic constraint

$$\left[\frac{1+\mathrm{erf}\left(\frac{\min\{\bar{w}^1_{c,j},\bar{w}^2_{c,j}\}}{\sqrt{2}}\right)}{2}\right]^2 \geq v_c \, . \tag{A.6}$$

Since $\bar{\mathbf{w}}_{c,j}(\check{\mathbf{x}}_c) \triangleq \mathbb{R}^{-\frac{1}{2}}_{\mathbf{q}_{c,j}} \mathbf{w}_{c,j}(\check{\mathbf{x}}_c)$, the constraint can be rewritten as

$$\mathbb{R}^{-\frac{1}{2}}_{\mathbf{q}_{c,j}} \mathbf{w}_{c,j}(\check{\mathbf{x}}_c) \geq \sqrt{2}\,\mathrm{erf}^{-1}\left(2\sqrt{v_c}-1\right)\mathbf{1}_2 \, , \tag{A.7}$$

where $\mathrm{erf}^{-1}(\cdot)$ denotes the inverse error function. We thus finally arrive at the following linear inequality constraint:

$$\widetilde{\mathbf{H}}^{\upsilon}_{cc,j}\check{\mathbf{x}}_c \geq \bar{\alpha_c}\eta_c \mathbb{R}^{\frac{1}{2}}_{\mathbf{q}_{c,j}}\mathbf{1}_2 + \delta^0_{c,j}\mathbf{1}_2 \, , \tag{A.8}$$

where $\eta_c \triangleq \sqrt{2}\,\mathrm{erf}^{-1}\left(2\sqrt{v_c}-1\right)$.

Appendix B

Proof of Lemma 5.1

According to (5.14), the optimal precoding $\mathbf{P}_{opt}$ should satisfy

$$\mathrm{Tr}\{\mathbf{H}_E\mathbf{P}\} - \beta^{-1}\,\mathrm{Tr}\{\mathbf{H}_E\mathbf{P}\mathbf{P}^T\mathbf{H}_E^T\} = -4K\beta^{-1}\ .$$

Then the mean square error (MSE) in (5.66) can be rewritten as

$$\mathbb{E}\{\|\beta^{-1}\mathbf{y}_E - \bar{\mathbf{s}}\|^2\} = K - M + \frac{1}{2}\,\mathrm{Tr}\left\{\left(\mathbf{I} + \frac{1}{a}\sum_k \bar{\mathbf{H}}_k^T\mathbf{G}_k^{-1}\bar{\mathbf{H}}_k\right)^{-1}\right\}\ . \tag{B.1}$$

Define

$$\mathbf{D} = \mathbf{I}_{2M} + \frac{1}{a}\sum_k \bar{\mathbf{H}}_k^T\mathbf{G}_k^{-1}\bar{\mathbf{H}}_k \tag{B.2}$$

$$= \mathbf{I}_{2M} + \frac{1}{a}\mathbf{F}^T\mathbf{G}^{-1}\mathbf{F}\ , \tag{B.3}$$

where

$$\mathbf{F}^T = \left[\bar{\mathbf{H}}_1^T \ \cdots \ \bar{\mathbf{H}}_K^T\right] \tag{B.4}$$

$$\mathbf{G} = \text{blockdiag}\left\{\mathbf{G}_1, \cdots, \mathbf{G}_K\right\}, \tag{B.5}$$

so that maximizing the MSE is equivalent to maximizing $\text{Tr}\{\mathbf{D}^{-1}\}$.

Next, note that

$$\mathbf{G}_k = \rho^2 \bar{\mathbf{H}}_{jk} \mathbf{Q} \bar{\mathbf{H}}_{jk}^T + \frac{\sigma_k^2}{2}\mathbf{I}_2 \tag{B.6}$$

$$= \bar{\mathbf{H}}_{jk}\left(\rho^2 \mathbf{Q} + \frac{\sigma_k^2}{2\|\mathbf{h}_{jk}\|^2}\mathbf{I}_2\right)\bar{\mathbf{H}}_{jk}^T \tag{B.7}$$

$$= \rho^2 \bar{\mathbf{H}}_{jk}\left(\mathbf{Q} + \frac{\sigma_k^2}{2\rho^2\|\mathbf{h}_{jk}\|^2}\mathbf{I}_2\right)\bar{\mathbf{H}}_{jk}^T \tag{B.8}$$

$$= \rho^2 \bar{\mathbf{H}}_{jk}\left(\mathbf{Q} + b_k \mathbf{I}_2\right)\bar{\mathbf{H}}_{jk}^T, \tag{B.9}$$

where $b_k = \sigma_k^2/(2\rho^2\|\mathbf{h}_{jk}\|^2)$ and we have used the fact that

$$\mathbf{H}_{jk}\mathbf{H}_{jk}^T = \|\mathbf{h}_{jk}\|^2 \mathbf{I}_2 . \tag{B.10}$$

Thus, we can write

$$\mathbf{G} = \rho^2 \tilde{\mathbf{H}}_j \left(\mathbf{I}_K \otimes \mathbf{Q} + \mathbf{B} \otimes \mathbf{I}_2\right)\tilde{\mathbf{H}}_j^T \tag{B.11}$$

$$\mathbf{G}^{-1} = \frac{1}{\rho^2}\left(\tilde{\mathbf{H}}_j^T\right)^{-1}\left(\mathbf{I}_K \otimes \mathbf{Q} + \mathbf{B} \otimes \mathbf{I}_2\right)^{-1}\left(\tilde{\mathbf{H}}_j\right)^{-1}, \tag{B.12}$$

where $\tilde{\mathbf{H}}_j = \text{blockdiag}\left\{\bar{\mathbf{H}}_{j1}, \cdots, \bar{\mathbf{H}}_{jK}\right\}$ and $\mathbf{B} = \text{diag}\left\{b_1, \cdots, b_K\right\}$. Thus,

$$\mathbf{D} = \mathbf{I}_{2M} + \frac{1}{a\rho^2}\mathbf{F}^T\left(\tilde{\mathbf{H}}_j^T\right)^{-1}\left(\mathbf{I}_K \otimes \mathbf{Q} + \mathbf{B} \otimes \mathbf{I}_2\right)^{-1}\left(\tilde{\mathbf{H}}_j\right)^{-1}\mathbf{F} \tag{B.13}$$

$$= \mathbf{I}_{2M} + \frac{1}{a\rho^2}\mathbf{C}^T\left(\mathbf{I}_K \otimes \mathbf{Q} + \mathbf{B} \otimes \mathbf{I}_2\right)^{-1}\mathbf{C} . \tag{B.14}$$

Also note that we can write the eigendecomposition of $\mathbf{Q}$ as $\mathbf{Q} = \mathbf{U}\mathbf{\Lambda}\mathbf{U}^T$, where $\mathbf{U}\mathbf{U}^T = \mathbf{I}_2$ and

$$\mathbf{\Lambda} = \begin{bmatrix} \lambda & 0 \\ 0 & 1-\lambda \end{bmatrix}. \tag{B.15}$$

Now let's take the derivative of $\mathrm{Tr}\{\mathbf{D}^{-1}\}$ with respect to λ:

$$\begin{aligned}
&\frac{d}{d\lambda}\,\mathrm{Tr}\{\mathbf{D}^{-1}\} && \text{(B.16)}\\
&= -\,\mathrm{Tr}\left\{\mathbf{D}^{-1}\left(\frac{d}{d\lambda}\mathbf{D}\right)\mathbf{D}^{-1}\right\} && \text{(B.17)}\\
&= -\frac{1}{a\rho^2}\,\mathrm{Tr}\left\{\mathbf{D}^{-1}\mathbf{C}^T\left(\frac{d}{d\lambda}(\mathbf{I}_K\otimes\mathbf{Q}+\mathbf{B}\otimes\mathbf{I}_2)^{-1}\right)\mathbf{C}\mathbf{D}^{-1}\right\} && \text{(B.18)}\\
&= \frac{1}{a\rho^2}\,\mathrm{Tr}\left\{\mathbf{A}\left(\frac{d}{d\lambda}(\mathbf{I}_K\otimes\mathbf{Q})\right)\mathbf{A}^T\right\} && \text{(B.19)}\\
&= \frac{1}{a\rho^2}\,\mathrm{Tr}\left\{\left(\mathbf{I}_K\otimes\left(\mathbf{U}\begin{bmatrix}1 & 0\\ 0 & -1\end{bmatrix}\mathbf{U}^T\right)\right)\mathbf{A}^T\mathbf{A}\right\}
\end{aligned}$$

where $\mathbf{A} = \mathbf{D}^{-1}\mathbf{C}^T(\mathbf{I}_K\otimes\mathbf{Q}+\mathbf{B}\otimes\mathbf{I}_2)^{-1}$. We can write

$$\mathbf{U}\begin{bmatrix}1 & 0\\ 0 & -1\end{bmatrix}\mathbf{U}^T = \tilde{\mathbf{U}}\begin{bmatrix}-1 & 0\\ 0 & 1\end{bmatrix}\tilde{\mathbf{U}}^T, \tag{B.20}$$

where $\mathbf{U}$ is unitary, symmetric and improper, while $\tilde{\mathbf{U}}$ is unitary, not symmetric but proper. Thus

$$\begin{aligned}
&\frac{d}{d\lambda}\,\mathrm{Tr}\{\mathbf{D}^{-1}\} && \text{(B.21)}\\
&= \frac{1}{a\rho^2}\,\mathrm{Tr}\left\{\left(\mathbf{I}_K\otimes\begin{bmatrix}-1 & 0\\ 0 & 1\end{bmatrix}\right)(\mathbf{I}_K\otimes\tilde{\mathbf{U}}^T)\mathbf{A}^T\mathbf{A}(\mathbf{I}_K\otimes\tilde{\mathbf{U}})\right\} && \text{(B.22)}
\end{aligned}$$

Note that $\mathbf{\Gamma} \triangleq (\mathbf{I}_K \otimes \tilde{\mathbf{U}}^T)\mathbf{A}^T\mathbf{A}(\mathbf{I}_K \otimes \tilde{\mathbf{U}})$ is a proper matrix when $\mathbf{Q} = \frac{1}{2}\mathbf{I}_2$, which means it can be written such that it is composed of 2×2 blocks $\mathbf{\Gamma}_{i,j}$ each of which is proper:

$$\mathbf{\Gamma} = \begin{bmatrix} \mathbf{\Gamma}_{1,1} & \mathbf{\Gamma}_{1,2} & \cdots & \mathbf{\Gamma}_{1,K} \\ \mathbf{\Gamma}_{2,1} & \mathbf{\Gamma}_{2,2} & \cdots & \mathbf{\Gamma}_{2,K} \\ & & \vdots & \\ \mathbf{\Gamma}_{K,1} & \mathbf{\Gamma}_{K,2} & \cdots & \mathbf{\Gamma}_{K,K} \end{bmatrix} . \tag{B.23}$$

Since each block term on the diagonal satisfies

$$\mathbf{\Gamma}_{k,k} = \begin{bmatrix} \mathcal{R}(\gamma_k) & -\mathcal{I}(\gamma_k) \\ \mathcal{I}(\gamma_k) & \mathcal{R}(\gamma_k) \end{bmatrix} , \tag{B.24}$$

it is clear that

$$\frac{d}{d\lambda} \operatorname{Tr}\{\mathbf{D}^{-1}\} \tag{B.25}$$

$$= \frac{1}{a\rho^2} \operatorname{Tr}\left\{ \left(\mathbf{I}_K \otimes \begin{bmatrix} -1 & 0 \\ 0 & 1 \end{bmatrix} \right) (\mathbf{I}_K \otimes \tilde{\mathbf{U}}^T)\mathbf{A}^T\mathbf{A}(\mathbf{I}_K \otimes \tilde{\mathbf{U}}) \right\} \tag{B.26}$$

$$= 0 ,$$

when evaluated at $\mathbf{Q} = \frac{1}{2}\mathbf{I}_2$, which is thus a stationary point for $\operatorname{Tr}\{\mathbf{D}^{-1}\}$ where it is maximized.